Universitat Autònoma de Barcelona

Non-Coherent Acquisition Techniques for High-Sensitivity GNSS Receivers

David Gomez Casco

UAB

Ph.D. Dissertation

Non-Coherent Acquisition Techniques for High-Sensitivity GNSS Receivers

Author: David Gómez Casco

Thesis Advisors: Gonzalo Seco-Granados and José A. López-Salcedo

Department of Telecommunications and Systems Engineering

Ph.D. programme in Electronic and Telecommunication Engineering

Universitat Autònoma de Barcelona

Bellaterra, September 2018

Abstract

Global Navigation Satellite Systems (GNSSs) have become an indispensable tool of daily life, since they offer us the possibility of accurately knowing our location in real time and in open-sky environments. Since the advent of these systems, a large number of successful GNSS applications have emerged. Some examples of these applications are: car navigation, flight tracking, sport activity tracking and augmented reality games. Due to the success achieved by GNSS, a great interest is emerging to extend its services to harsher environments such as urban canyons and indoor scenarios. However, in these environments GNSS receivers face great difficulties to detect the signals received from the satellites, which are very weak since they suffer from severe attenuation due to the presence of obstacles in the propagation path between satellites and the receiver.

This thesis addresses several problems of processing weak GNSS signals, such as the detection at the acquisition stage, the determination of their signal quality and the time delay and Doppler frequency estimations. To do so, detection and estimation tools are used, which are based on the probability theory and statistics. In order to use these tools, it is necessary to understand the architecture and the signals that GNSSs transmit. For this reason, the first part of the thesis focuses on describing the main features of two of the best-known GNSSs, the American GPS and the European Galileo. In addition, we describe the fundamentals of the receivers and analyze the signals that are implemented in these systems. After that, we explain the required fundamentals of detection theory, namely the Neyman-pearson criterion, the Generalized Likelihood Ratio Test and the Bayesian approach. Then, a review of the state of the art in the detection of GNSS signals is carried out.

The main contribution of this thesis is provided in the second part, which tackles the problem of deriving optimal detectors to acquire weak GNSS signals. We have found that the optimal detector depends on the characteristics of the signal transmitted by the satellite, which is different depending on the selected constellation. The theoretical and

simulated results show that the detectors proposed in this thesis clearly outperform the detectors currently used in practice. In addition, we conclude when it is better to apply each detector. Moreover, this thesis addresses the problem of estimating the carrier-to-noise ratio of weak GNSS signals. This parameter provides essential information since it is used in all stages of GNSS receivers. In this thesis, we propose new estimators of the carrier-to-noise ratio, which are very simple to implement in high-sensitivity GNSS receivers and offer an enhanced accuracy with respect to the estimators proposed in the literature. Finally, the last part of the thesis focuses on the so-called high-order binary offset carrier (BOC) signals, a kind of signal that is implemented in the Galileo system. More precisely, this part is devoted to proposing accurate estimators of time delay and Doppler frequency. These estimators improve the accuracy of the method usually applied in practice to estimate these parameters.

Resumen

Los sistemas de radionavegación por satélite (GNSSs) se han convertido en una herramienta indispensable de la vida diaria, ya que nos ofrecen la posibilidad de conocer de manera precisa nuestra ubicación en tiempo real y en entornos al aire libre. Desde la aparición de estos sistemas, han surgido una gran cantidad de exitosas aplicaciones de GNSS. Algunos ejemplos de estas aplicaciones son los siguientes: navegación para automóviles, rastreo de vuelos, seguimiento de actividad deportiva y juegos de realidad aumentada. Debido al éxito alcanzado por los sistemas de GNSS, un gran interés está surgiendo para extender sus servicios a entornos más complicados tales como cañones urbanos e interiores. No obstante, en estos entornos los receptores de GNSS tienen grandes dificultades para poder detectar las señales recibidas desde los satélites, las cuales son muy débiles ya que sufren una severa atenuación a causa de la presencia de obstáculos en el camino de propagación entre los satélites y el receptor.

Esta tesis aborda varios problemas del procesamiento de señales de GNSS débiles como la detección en la etapa de adquisición, la determinación de la calidad de la señal y las estimaciones de la frecuencia Doppler y el tiempo de retraso. Para ello, se emplean las herramientas de detección y estimación de la señal, que se basan en teoría de probabilidad y estadística. Para poder emplear estas herramientas es necesario tener un conocimiento sobre la arquitectura y las señales que transmiten los sistemas de GNSS. Por este motivo, la primera parte de la tesis se centra en describir las principales características de dos de los sistemas de GNSS más conocidos el americano GPS y el europeo Galileo. Además, tratamos los fundamentos de los receptores y analizamos las señales que están implementadas actualmente en estos sistemas. Después, se explican los fundamentos de teoría de detección requeridos, que son el *Neyman-pearson criterion*, el *Generalized likelihood Ratio Test* y el *Bayesian approach*. Más adelante, se realiza una revisión del estado del arte sobre la detección de señales de GNSS.

Las principales contribuciones de esta tesis ocupan lugar en la segunda parte, las cuales

tratan de derivar los detectores óptimos para adquirir las señales de GNSS débiles. Hemos encontrado que el detector óptimo depende de las características de la señal trasmitida por el satélite, que puede variar dependiendo de la constelación seleccionada. Los resultados teóricos y simulados demuestran que los detectores propuestos en esta tesis superan claramente el rendimiento de los detectores utilizados en la práctica actualmente. Además, se concluye en qué condiciones es mejor utilizar un detector u otro. También, en esta tesis se aborda el problema de estimar la relación portadora a ruido de las señales de GNSS débiles. Esta relación aporta información esencial ya que se utiliza en todas las etapas de los receptores de GNSS. En esta tesis proponemos nuevos estimadores de la relación portadora a ruido, que son muy sencillos de implementar en receptores de alta sensibilidad de GNSS y ofrecen una mejora de precisión con respecto a los estimadores propuestos en la literatura. Finalmente, la última parte de la tesis se centra en las *binary offset carrier* (BOC) de alto orden, un tipo de señal que está implementada en el sistema Galileo. Más precisamente, esta parte está dedicada a proponer estimadores precisos de tiempo de retardo y frecuencia Doppler. Estos estimadores mejoran la precisión del método generalmente aplicado en la práctica para estimar estos parámetros.

Dedicated to my family,

Agradecimientos

En primer lugar me gustaría agradecer a Gonzalo Seco-Granados por todo el apoyo, los consejos y las correcciones que me ha dado estos años. Siempre ha tenido tiempo para debatir los resultados y las dudas que han surgido a lo largo de este ciclo de 4 años. Me ha brindado una gran cantidad de conocimiento que de bien seguro me será de utilidad en un futuro próximo. También me gustaría agradecer a José A. López-Salcedo, quien siempre ha estado allí para ayudarme. Él fue la persona que me introdujo en el mundo del procesado de la señal dirigiéndome los dos proyectos finales de carrera. Durante estos años he sido capaz de aprender un sinfín de conceptos gracias a la capacidad que tiene de explicar las cosas que son muy complicadas de manera muy sencilla.

Tampoco me puedo olvidar de mis compañeros de despacho que he tenido durante el transcurso de la tesis: Dani, Sergi, José, Vicente y Toni. Quiero agradecerles toda la ayuda que me han dado y todos los interesantes debates que hemos tenido. Mi agradecimiento también a José A. García-Molina por la dedicación que tuvo durante mi estancia en la Agencia Espacial Europea.

Finalmente, quisiera mostrar mi agradecimiento a mi familia, mi novia y mis amigos, por todo el apoyo que me han ofrecido y por ayudarme a superar los momentos complicados.

Contents

List of Figures

List of Tables

Acronyms

APDI	Average Post Detection Integration
AWGN	Additive White Gaussian Noise
BAPDI	Bayesian Approach Post Detection Integration
BOC	Binary Offset Carrier
C/N_0	Carrier-to-Noise Ratio
CLT	Central Limit Theorem
CSAC	Chip Scale Atomic Clock
CBOC	Composite Binary Offset Carrier
CDMA	Code-Division Multiple Access
CRB	Cramér-Rao Bound
CAF	Cross Ambiguity Function
cdf	Cumulative density function
DLL	Delay Lock Loop
DPDI	Differential Post Detection Integration
GLRT	Generalized Likelihood Ratio Test
GPDI	Generalized Post Detection Integration
GNSS	Global Navigation Satellite System
GPS	Global Positioning System
HS-GNSS	High Sensitivity GNSS
KL	Kullback-Leibler
LS	Least Square

LRT	Likelihood Ratio Test
MBAPDI	Maximum Bayesian Approach Post Detection Integration
MSE	Mean Square Error
MLS	Multilag Least Squares
MBOC	Multiplexed BOC
NWPR	Narrow-band Wide-band Power Ratio
NPDI	Non-Coherent Post Detection Integration
NQ-NPDI	Non-Quadratic Non-Coherent Post Detection Integration
OCXO	Oven-controlled Crystal Oscillator
PLL	Phase Lock Loop
PDI	Post Detection Integration
PSD	Power Spectral Density
pdf	Probability density function
P_d	Probability of detection
P_{fa}	Probability of false alarm
P_{md}	Probability of miss detection
ROC	Receiver Operating Characteristic
SD	Squaring Detector
SNPR	Signal-to-Noise Power Ratio
SNR	Signal-to-Noise Ratio
TCXO	Temperature Compensated Crystal Oscillator
APDIT	Truncated Average Post Detection Integration
GPDIT	Truncated Generalized Post Detection Integration

Chapter 1

Introduction

Nowadays, Global Navigation Satellite Systems (GNSSs) have become an indispensable tool, which is able to provide the position of any user at any time under line-of-sight conditions. Since the emergence of GNSSs, there have appeared many positioning services in the commercial market. Car navigation, commercial aircraft and sport activity tracking are some examples of the most successful GNSS applications. The most popular GNSS corresponds to the Global Positioning System (GPS), which is used by all, or almost all, GNSS receivers. However, the increase of people's needs for positioning has led to the development of new GNSSs, such as GLONASS, Galileo or Compass, in recent years.

The modernization of GNSSs, and particularly of Galileo, has led to the use of Binary Offset Carrier (BOC) signals, which can give a more precise estimation of the user's position than the conventional BPKS modulation in moderately good conditions. However, one of the drawbacks of BOC modulations is that their correlation function is ambiguous since it consists of several peaks. These modulations allow the receiver to obtain an extremely accurate position estimation as long as the main correlation peak is detected. Nevertheless, this peak is really difficult to be tracked, especially in harsh environments due to the strong attenuation of the received signal.

The combination of several GNSSs and the use of BOC signals can offer an accurate location estimation of the receiver, achieving the positioning accuracy that most applications demand in outdoor environments. The excellent performance provided by GNSS outdoors is attracting the interest in extending their applications to harsh environments, such as urban canyons, building indoors and forested areas. Nonetheless, in these environments, the presence of obstacles in the propagation path between the transmitter and the receiver causes a high attenuation of the received signal, making the acquisition and

tracking of weak GNSS signals a challenge. In this situation, conventional GNSS receivers are not able to provide the position of the user since they are designed to work in open-sky scenarios where the power of the received signal is reasonably high.

This fact has led to develop High-Sensitivity GNSS (HS-GNSS) receivers. These receivers usually acquire weak signals by coherently accumulating signals for a long period of time, which provides an additional gain in signal detection. However, this duration cannot be increased without bounds mainly due to the presence of residual frequency offset, data bits and phase noise. If reliable signal detection requires a longer signal accumulation than what is possible in a coherent manner, the receiver has to accumulate the signal in a non-coherent way. This non-coherent accumulation is usually carried out by the use of Post-Detection Integration (PDI) techniques, which overcome the limitations of the coherent accumulation, and they allow the receiver to acquire satellites with very low carrier-to-noise ratio.

Different PDI techniques have been proposed in order to improve the sensitivity of non-coherent integrations. Nonetheless, the question about which is the best technique to perform the non-coherent accumulation under practical conditions remains open. This question does not necessarily has a unique answer, since depending on the characteristics of the received signal the answer can differ. This motivates the application of advanced signal processing algorithms and detection theory tools in order to find promising techniques to acquire weak GNSS signals.

1.1 Motivation and objectives

Weak signals are certainly a dramatic problem for conventional GNSS receivers, which have a critical impact on their performance. The strong attenuation suffered by the received signal causes the signal level to be below the noise level after the correlation process, thus making the acquisition of the signal a tremendous challenge. Hence, advanced detection techniques, which are usually referred to as PDI techniques, must be proposed in order to counteract the effect of the noise and to be able to acquire weak GNSS signals. In light of this, the main purpose of this thesis is to investigate new PDI techniques, which will allow the GNSS receiver to acquire these signals under practical conditions, using the minimum amount of received signal. These detection techniques intend to improve the overall performance of conventional GNSS receivers. The objectives of the research carried out in this dissertation are the following:

1. Performing a detection analysis of existing PDI techniques in conditions of weak GNSS signal acquisition, including the presence of effects that are usually ignored in the literature such as the presence of phase noise.

2. Derivation of new PDI techniques to detect weak GNSS signals, which provide a signal detection gain with respect to the techniques proposed in the literature. This derivation will be performed considering different impairments in the received signal. To do so, several detection strategies such as the Bayesian approach and the Generalized Likelihood Ratio Test (GLRT) will be applied.

3. Design of an accurate signal detection threshold for the new PDI techniques presented in this work. This design requires the knowledge about the distribution of the metric of a PDI technique, which is usually unknown. The objective is to find a closed-form expression of the distribution in order to be able to set a detection threshold for each relevant PDI technique. This threshold permits the receiver to distinguish whether the GNSS satellite is in view or not for a given probability of false alarm.

4. Derivation of Carrier-to-Noise Ratio (C/N_0) estimators in very weak reception conditions, which are required by many applications of HS-GNSS receivers. These estimators will be designed for only using the output of a relevant PDI technique to carry out the estimation.

5. Mitigate the acquisition problems of high-order BOC modulations, especially for low signal to noise regime. The objective of this part is focused on circumventing the probability that the main correlation peak is not acquired, also referred to as false lock probability, under conditions of weak signal reception. In addition to this, exploiting the energy of the secondary peaks of the high-order BOC correlation to obtain accurate estimates of the code-delay and Doppler frequency.

1.2 Thesis outline

This section provides a summary of the content of each chapter included in this thesis. The work in this thesis has been presented in several publications, such as international conference papers and journals, which are listed below the summary of each chapter.

Chapter 2

This chapter provides a general overview of GNSS and the fundamentals of signal detection. First of all, a brief historical review of GNSS is carried out. We also explain the architecture of the system and the characteristics of the signals transmitted by the satellites. After that, the main stages of the GNSS receivers are described. Finally, we provide a background on detection theory, which includes the main approaches used to derive signal detectors for binary hypothesis testing problems.

Chapter 3

This chapter analyses the state of the art about PDI techniques proposed to detect weak GNSS signals. The advantages and disadvantages of each technique are described and we specify that PDI techniques have a closed-form expression for their detection and false alarm probabilities. Moreover, we discuss which is the best option to acquire GNSS signals whether the use of PDI techniques that combine pilot and data components or PDI techniques that only use a pilot component. Finally, the most relevant techniques are benchmarked in the GNSS domain for low C/N_0 levels in presence of phase noise in the receiver clock and frequency offset. The results of this chapter have been published in the following international conference papers:

- E. Domínguez, A. Pousinho, P. Boto, D. Gomez-Casco, S. Locubiche, G. Seco-Granados, J. A. Lopez-Salcedo, H. Fragner, F. Zangerl, O. Peña, D. Jimenez-Baños, "Performance Evaluation of High Sensitivity GNSS Techniques in Indoor, Urban and Space Environments", *Proc. ION GNSS+*, Sep. 12 2016.
- D. Gomez-Casco, J. A. Lopez-Salcedo, G. Seco-Granados, "Generalized Integration Techniques for High-Sensitivity GNSS Receivers Affected by Oscillator Phase Noise", *Proc. IEEE Statistical Signal Processing Workshop (SSP)*, Jun. 27 2016.

Chapter 4

This chapter tackles the problem of finding the optimal PDI technique to detect weak signals with time-varying phase. The first part of the chapter derives promising detectors that are robust against the presence of data bits and variations in the carrier phase by using the GLRT and the Bayesian approach. From these results, we perform a statistical

characterization of the two most relevant proposed techniques, which leads to a closed-form expression of their detection and false alarm probabilities. Finally, simulation results present a performance comparison between the PDI techniques proposed in the literature and those presented in this chapter for signals with time-varying phase. The results of this chapter are summarized in the following papers:

- D. Gomez-Casco, J. A. Lopez-Salcedo, G. Seco-Granados, "Statistical Characterization of the Optimal Detector for a Signal with Time-Varying Phase Based on the Edgeworth Series", *Proc. IEEE Statistical Signal Processing Workshop (SSP)*, Jun. 2018.
- D. Gomez-Casco, J. A. Lopez-Salcedo, G. Seco-Granados, "Optimal Fractional Non-Coherent Detector for High-Sensitivity GNSS Receivers Robust against Residual Frequency Offset and Unknown Bits", *Proc. IEEE Workshop on Positioning, Navigation and Communications (WPNC)*, Oct. 25 2017.

Chapter 5

This chapter aims at deriving the optimal non-coherent detector for the reacquisition of weak GNSS signals in the presence of bits and phase uncertainty. Two solutions are derived based on the use of two detection frameworks: the Bayesian approach and the GLRT. We also derive approximate detectors of reduced computation complexity and without noticeable performance degradation. Simulation results reveal a clear improvement of the detection probability for the proposed techniques with respect to the conventional detectors implemented in HS-GNSS receivers to acquire weak GNSS signals. Finally, the chapter draws conclusions on which is the best technique to reacquire weak GNSS signals in practice considering a trade-off between performance and complexity. The results of this chapter are summarized in one submitted journal paper:

- D. Gomez-Casco, J. A. Lopez-Salcedo, G. Seco-Granados,"Optimal Post-Detection Integration Technique for the Reacquisition of Weak GNSS Signals", *submitted to IEEE Transactions on Aerospace and Electronic Systems* , May 2018.

Chapter 6

This chapter addresses the problem of estimating the C/N_0 in weak signal conditions. There are several environments, such as forested areas, indoor buildings and urban canyons, where HS-GNSS receivers are expected to work under these reception conditions. The acquisition of weak signals from the satellites requires the use of PDI techniques to accumulate enough energy to detect them. However, due to the attenuation suffered by these signals, estimating their C/N_0 becomes a challenge. Measurements of C/N_0 are really important in many applications of HS-GNSS receivers, such as the determination of a detection threshold or the mitigation of near-far problems. For this reason, different techniques have been proposed in the literature to estimate the C/N_0, but they only work properly in the high C/N_0 region where the coherent integration is enough to acquire the satellites. In this chapter, we derive four C/N_0 estimators that are specially designed for HS-GNSS snapshot receivers and only use the output of a PDI technique to perform the estimation. We consider four PDI techniques and we obtain the corresponding C/N_0 estimator for each one of them. Our performance analysis shows a significant advantage of the proposed estimators with respect to other C/N_0 estimators available in the literature in terms of estimation accuracy and computational resources. The results of this chapter are summarized in one journal paper:

- D. Gomez-Casco, J. A. Lopez-Salcedo, G. Seco-Granados, "C/N_0 Estimators for High-Sensitivity Snapshot GNSS receivers", *GPS solutions*, (accepted for publication on Sep. 2018).

Chapter 7

This chapter deals with the analysis of two different problems of high-order BOC signals. Firstly, we tackle the one of mitigating the false lock probability of weak high-order BOC signals in the acquisition stage. To do so, we propose to use a PDI technique to acquire the weak GNSS signal and after that, applying two code-delay estimators to solve the ambiguity of the secondary peaks of BOC signals. Secondly, we address the problem of refining the Doppler frequency estimation provided in the acquisition stage for high-order BOC signals. In this part, we propose a new technique, referred to as multilag least squares estimator, which improves the performance of a conventional least squares estimator by exploiting the autocorrelation shape of high-order BOC signals. The results of this chapter are summarized in the following papers:

- S. Locubiche, D. Gomez-Casco, A. Gusi, J. A. Lopez-Salcedo, G. Seco-Granados, J. A. Garcia-Molina, "Positioning Performance Analysis of High-Order BOC Signals in Advanced Multi-constellation High-Sensitivity GNSS Receivers", *Proc. 6th International Colloquium on Scientific and Fundamental Aspects of GNSS / Galileo*, Oct. 2017

- D. Gomez-Casco, E. S. Lohan, J. A. Lopez-Salcedo, G. Seco-Granados,"Multilag Frequency Estimation for High-Order BOC Signals in the Acquisition Stage", *Proc. 8th ESA Workshop on Satellite Navigation User Equipment Technologies (NAVITEC)*, Dec. 15 2016

- D. Gomez-Casco, J. A. Garcia-Molina, A. Gusi-Amigo, M. Crisci, J. A. Lopez-Salcedo, G. Seco-Granados, "Mitigation of False Locks in the Acquisition of High-Order BOC Signals in HS-GNSS Receivers",*Proc. International Conference on Localization and GNSS (ICL-GNSS)*, Jun. 28 2016

Chapter 2

Fundamentals of detection and GNSS

2.1 Fundamentals of GNSS

2.1.1 Introduction

Positioning is defined as the process of determining the geographical position of a device such as a mobile phone, laptop or tablet computer, or tracking equipment. Nowadays, positioning has become an indispensable tool for society. Positioning systems based on satellite transmissions are the ones that have an important role at the present time [SG12].

By far, the most popular GNSS is the GPS. The GPS satellite radionavigation system is certainly one of the most widespread and currently used systems. Its origin comes from the interest that arose among several governmental organizations in the United States in the 1960s to develop a positioning system with high precision and global coverage.

The success achieved by GPS to get the user's location in outdoor environments has inspired European or Asian institutions to develop similar GNSSs [Mis06, Kap05]. The first of these systems was GLONASS, which was developed in the late 1970s. Later, Europe proposed the Galileo system, which was planned to be a global system fully compatible with GPS, but independent from it. This system is implementing the so-called BOC signals, which could offer better accuracy to estimate the user's position than the BPSK signal implemented in the GPS system. Other new systems such as Compass/Beidou [Bei12] or the Indian Regional satellite system [Har15] are being developed nowadays in

China and India, respectively. These systems are implementing signals quite similar to the Galileo and GPS systems. Despite the fact that there are several GNSSs, we only focus on the Galileo and GPS, which are two of the most representative systems and they allow us to address all of the problems analysed in this thesis.

The aim of these GNSSs is to allow users to obtain an accurate estimate of their Position, Velocity and Time (PVT) anytime, anywhere under line-of-sight conditions. This estimation is carried out by using the received signals from the different satellites orbiting around the Earth. In the following subsections, we explain the basic GNSS concepts, which deal with the architecture, different kind signals and the stages of a HS-GNSS receiver.

2.1.2 GNSS architecture

The architecture of the GNSS is divided into three different segments as follows [Mis06]:

- The GNSS space segment: consists of the system constellation of satellites, which is a group of similar satellites that are synchronized to orbit the Earth. These satellites are in charge of broadcasting radionavigation signals. Table 2.1 shows characteristic parameters of the GPS and Galileo space segments.

	GPS	Galileo
Country	United States	Europe
Number of satellites	24	30
Orbital planes	6	3
Altitude (Km)	20200	23222

Table 2.1: Space segment of GPS and Galileo systems.

- The ground control segment is focused on monitoring and controlling the satellite constellation. More precisely, the main functionalities of this segment are the following: monitoring the navigation signals of the satellites, resolving anomalies of the satellites and update navigation messages including the satellite clock corrections and ephemerides.

- The user segment deals with the set of GNSS receivers, which can be divided into civilian and military users. On the one hand, the civilian users have only access to

the open service signals that broadcast the different satellites. On the other hand, the military users can utilize the open service signals and restricted-access signals that are though to provide a more accurate estimation of the user's position.

2.1.3 GNSS signals

Galileo and GPS satellites broadcast the GNSS signals using different signal modulation and carrier frequencies: E1/L1 (1575.42 MHz), L2 (1227.60 MHz), E5a/L5 (1176.45 MHz) and E6 (1278.75 MHz). More details about the frequency bands and the transmitted signals are included in [Nav14b].

In this thesis, we are only focused on three signals that are used in the E1/L1 frequency band since they are a representative case of different kinds of GNSS modulations. These modulations correspond to the BPSK, which is implemented in the GPS L1 signal, the Composite Binary Offset Carrier (CBOC), which introduced in the Galileo E1BC signal, and a high-order BOC signal that is included in the Galileo system.

2.1.3.1 GPS L1 signal

The open service signal implemented in the GPS L1 band utilizes a simple BPSK modulation, which uses a series of carriers with binary amplitudes 1 and -1. This signal transmitted by the pth satellite, is given by the following expression [Bor07]:

$$s_{L1}(t) = \sqrt{P_p} b_p(t) c_p(t) \cos(2\pi f_{L1} t + \theta), \tag{2.1}$$

where P_p is the signal power, $b_p(t)$ are the navigation data bits, $c_p(t)$ is the pseudo random noise code and $\cos(2\pi f_{L1} t + \theta)$ is the carrier that modulates the GPS signal in the L1 frequency band. The $c_p(t)$ codes are often referred to as spreading codes. These codes consist of bit sequences, which are usually called chips to denote that they do not carry any information. The chip period (T_c) is much smaller than the bit period of the navigation message $b_p(t)$. More precisely, for the case of the former it is 1 / 1.023 ms, whereas the latter has a period of 20 ms.

Each satellite has a specific $c_p(t)$ code that is different of the rest of the codes transmitted by the other satellites. All of these codes consist of 1023 chips, which are formed from a binary sequence that can take values of 1 or -1. They are transmitted periodically so that a complete sequence has a time period of 1 ms. Taking into account that the

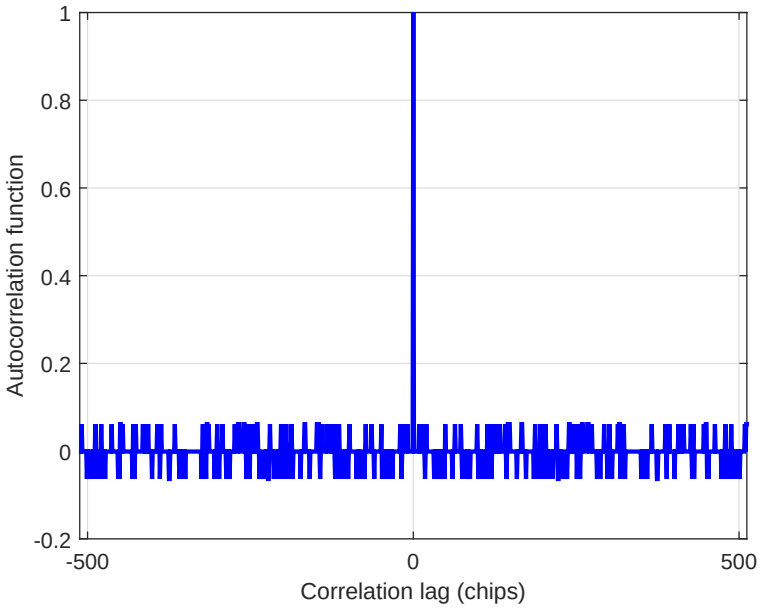

Figure 2.1: Autocorrelation function of a $c_p(t)$ code.

transmitted bits in the navigation message $b_p(t)$ have a duration of 20 ms, a navigation bit contains 20 consecutive periods of the code.

The $c_p(t)$ codes are deterministic sequences based on Gold codes, which have similar correlation properties to the white noise. These properties cause that the autocorrelation function of one of these codes, denoted by $R_{c_p(t)}(\tau)$, presents a maximum value, when the two codes are synchronized, whereas for the rest of values the magnitudes of the autocorrelation are really small. Specifically, the maximum value of the normalized autocorrelation function, that is, $R_{c_p(t)}(0)$ corresponds to 1 and the other correlation lags can have a maximum magnitude of $\pm 65/1023$. An example of the autocorrelation of a $c_p(t)$ code is illustrated in Figure 2.1. It is worth mentioning that the autocorrelation $R_{c_p(t)}(\tau)$ is unambiguous in the range between -1 and 1 chip, since it consists of a simple triangle. However, when the cross-correlation between two different $c_p(t)$ codes is computed, small values of correlation are obtained, which do not surpass the magnitude of $\pm 65/1023$. Figure 2.2 illustrates this phenomenon.

The GPS technology is known as Code-Division Multiple Access (CDMA), which exploits the properties of the autocorrelation function of the pseudo-random sequences $c_p(t)$ codes. These codes permit the receiver to obtain good accuracy in the estimates of the distances between the satellites and the users. This occurs because the $c_p(t)$ codes

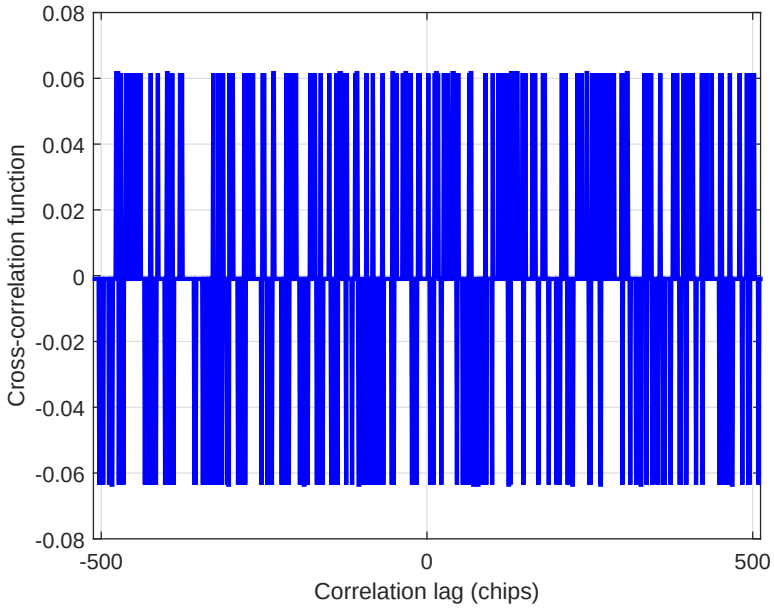

Figure 2.2: Cross-correlation function between two $c_p(t)$ codes.

are almost orthogonal to each other, thus allowing the receiver to distinguish different satellites simultaneously, even though they use the same carrier frequency.

The navigation message $b_p(t)$ contains the required information so that one user can know the position of the different satellites and the transmission times of the received signal. In addition, it provides useful information to make the acquisition of the satellites easier. This information is broadcast each 50 bits per second, which corresponds to the inverse of the bit period that is 20 ms.

The Power Spectral Density (PSD) of this open service signal considering that its autocorrelation function is only a triangle can be expressed by following expression:

$$\mathrm{PSD}_{L1}(f) = T_c \mathrm{sinc}(T_c f)^2, \tag{2.2}$$

where $\mathrm{sinc}(x) = \sin(\pi x)/(\pi x)$. Much of the power of this signal is concentrated between $-1/T_c$ and $1/T_c$, as it is shown in Figure 2.3. The BPSK modulation concentrates practically all of the energy at baseband. This is in contrast to the BOC signals that we will see in the next subsection, which are intended to improve the accuracy that BPSK signals can obtain in terms of positioning accuracy.

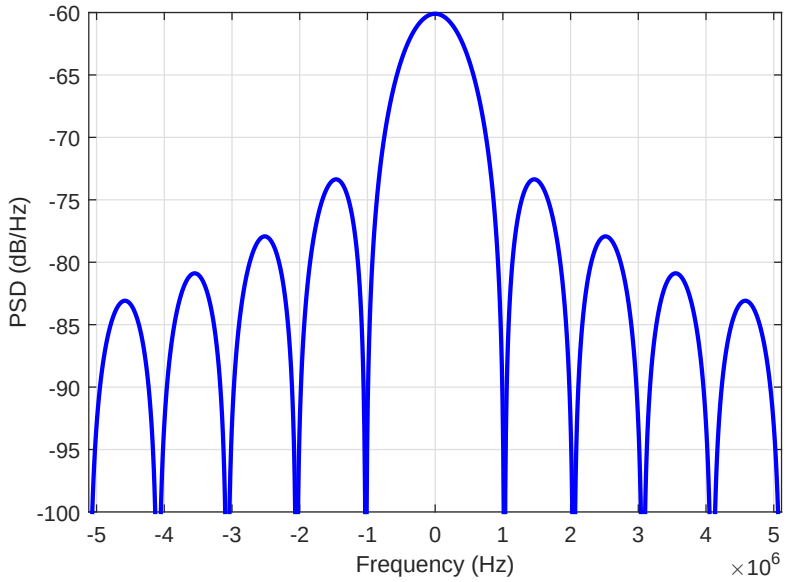

Figure 2.3: Power Density Spectral of the GPS L1 signal.

2.1.3.2 Fundamentals of BOC signals

BOC signals are based on multiplying a pseudo-random code with a sub-carrier, which is formed by the sign of a cosine or sine function. This multiplication leads to the so-called cosine-phased BOC or sine-phased signals, denoted by $\mathrm{BOC}_{\cos}(m_B, n_B)$ or $\mathrm{BOC}_{\sin}(m_B, n_B)$, respectively, as

$$\begin{aligned} \mathrm{BOC}_{\cos}(m_B, n_B) &= c_p(t)\mathrm{sign}[\cos(2\pi f_{sub} t)] \\ \mathrm{BOC}_{\sin}(m_B, n_B) &= c_p(t)\mathrm{sign}[\sin(2\pi f_{sub} t)], \end{aligned} \tag{2.3}$$

where the sign[ ] is a function that returns a sign of its argument, f_{sub} is the sub-carrier frequency, $m_B = f_{sub}/1.023e6$, $n_B = f_c/1.023e6$, and f_c is the chip frequency. Although there are two kind of BOC signals, the same advantages and inconveniences apply to both of them. The main advantage of the BOC signals with respect to BPSK signals is that they can provide a significant enhancement in terms of positioning accuracy. This enhancement is due to the increase of the Gabor bandwidth, which leads to a reduction of the Cramér-Rao bound (CRB) of the time-delay estimation. The CRB of the time-delay can be expressed as [Kay98, Nur16]:

$$\sigma_\tau^2 \geqslant \frac{1}{\mathrm{SNR} \cdot \mathrm{GB}^2}, \tag{2.4}$$

Spreading modulation	Number of positive and negative peaks
$\mathrm{BOC}_{\sin}(m_B, n_B)$	$2K_{\mathrm{BOC}} - 1$
$\mathrm{BOC}_{\cos}(m_B, n_B)$	$2K_{\mathrm{BOC}} + 1$

Table 2.2: Number of peaks of the autocorrelation function of BOC signals.

where SNR corresponds to the Signal-to-Noise Ratio and GB represents the Gabor bandwidth as

$$\mathrm{GB}^2 = \frac{\int_{-\infty}^{\infty}(2\pi f)^2 \mathrm{PSD}(f)df}{\int_{-\infty}^{\infty}\mathrm{PSD}(f)df}, \tag{2.5}$$

where $\mathrm{PSD}(f)$ is the power spectral density of the signal. The Gabor bandwidth is inversely proportional to the CRB. Hence, the larger the Gabor bandwidth, the more accurate the estimation of the time-delay between the receiver and the satellite can be. This is the phenomenon that BOC signals exploit. The idea of these signals is to spread the spectrum so that the signal power is concentrated on the sides of the spectrum to obtain a large Gabor bandwidth.

Nevertheless, BOC signals present some drawbacks. The most important one is the presence of secondary peaks in the autocorrelation function in the range of -1 and 1 chip. This causes that the autocorrelation of BOC signals is ambiguous. The existence of secondary peaks is usually an important concern since they hamper the identification of the main peak of the correlation function, particularly in scenarios with low C/N_0 such as deep urban canyons. The detection of a secondary peak, also referred to as a false lock, must be circumvented since a positioning bias of some meters appears when the time-delay is estimated from a secondary peak.

The number of peaks of a BOC autocorrelation function depends basically on the parameters m_B, n_B, and if the signal is $\mathrm{BOC}_{\cos}$ or $\mathrm{BOC}_{\sin}$ [Bet15]. This number is directly proportional to the BOC modulation order, which is defined as:

$$K_{\mathrm{BOC}} = \frac{2m_B}{n_B}. \tag{2.6}$$

Table 2.2 indicates the number of positive and negative peaks of BOC signals. The $\mathrm{BOC}_{\cos}$ autocorrelation contains two more peaks than the $\mathrm{BOC}_{\sin}$ for the same values of m_B and n_B. The normalized PSD of BOC signals are also affected by the BOC modulation order K_{BOC} and the kind of BOC used. The PSD of a $\mathrm{BOC}_{\sin}(m_B, n_B)$ modulation for an even

K_{BOC} is

$$\mathrm{PSD}_{\sin}(f) = \frac{\mathrm{sinc}^2\left(\frac{\pi f}{f_c}\right)\tan^2\left(\frac{\pi f}{2f_s}\right)}{f_c}, \tag{2.7}$$

and for an odd K_{BOC} it is

$$\mathrm{PSD}_{\sin}(f) = \frac{f_c\cos^2\left(\frac{\pi f}{f_c}\right)\tan^2\left(\frac{\pi f}{2f_s}\right)}{(\pi f)^2}. \tag{2.8}$$

The PSD of a $\mathrm{BOC}_{\cos}(m_B, n_B)$ modulation for an even K_{BOC} is given by

$$\mathrm{PSD}_{\cos}(f) = \frac{4\mathrm{sinc}^2\left(\frac{\pi f}{f_c}\right)\sin^4\left(\frac{\pi f}{4f_s}\right)}{\cos^2\left(\frac{\pi f}{2f_s}\right)f_c}, \tag{2.9}$$

and for an odd K_{BOC} it is defined as

$$\mathrm{PSD}_{\cos}(f) = \frac{4f_c\cos^2\left(\frac{\pi f}{f_c}\right)\sin^4\left(\frac{\pi f}{4f_s}\right)}{(\pi f)^2\cos^2\left(\frac{\pi f}{2f_s}\right)}. \tag{2.10}$$

2.1.3.3 Galileo E1BC signal

The E1 open service signal uses a CBOC modulation, which is a particular implementation of the MBOC (Multiplexed BOC) modulation [Nav14a, Com11, AR08]. Specifically, this signal utilizes a MBOC(6,1,1/11), which is the result of combining a narrowband signal $\mathrm{BOC}_{\sin}(1,1)$ with a wideband signal $\mathrm{BOC}_{\sin}(6,1)$ using a different power for each signal.

The whole broadcasted Galileo E1BC signal consists of two different signal components: the data component E1B and the pilot component E1C. On the one hand, the E1C signal is in charge of transmitting the signal that allows the receiver to obtain the estimation of the time-delay between the satellite and the receiver. On the other hand, the E1B signal contains the navigation message. The Galileo E1BC signal can be defined in baseband for one satellite by the following expression:

$$\begin{aligned} S_{E1BC}(t) = \frac{1}{\sqrt{2}}\,(&E1B(t)(\alpha_{E1}\mathrm{sign}[\sin(2\pi f_a t)] + \beta_{E1}\mathrm{sign}[\sin(2\pi f_b t)]) \\ &- E1C(t)(\alpha_{E1}\mathrm{sign}[\sin(2\pi f_a t)] - \beta_{E1}\mathrm{sign}[\sin(2\pi f_b t)]))\,, \end{aligned} \tag{2.11}$$

where $f_a = 1.023$ MHz and $f_b = 6.138$ MHz being the subcarrier frequencies, $\alpha_{E1} = \sqrt{\frac{10}{11}}$ and $\beta_{E1} = \sqrt{\frac{1}{11}}$. The $E1C(t)$ and $E1B(t)$ are different codes, both being deterministic

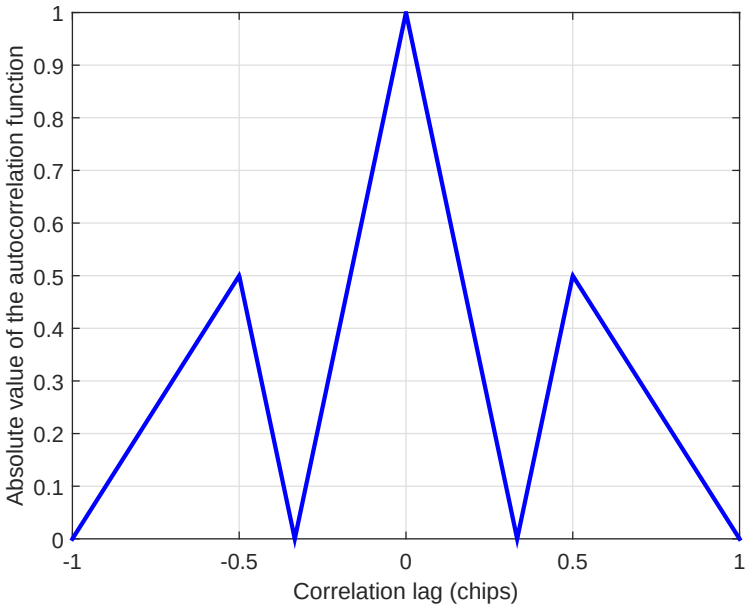

Figure 2.4: Absolute value of the autocorrelation of a $\text{BOC}_{\text{sin}}(1,1)$.

sequences that provide good correlation properties to estimate the time-delay of the received signal, similarly to the PRN codes of the GPS L1 signal. Both $E1B(t)$ and $E1C(t)$ codes have a period of 4 ms and a chip frequency of $f_c = 1.023$ MHz. Each $E1C(t)$ code is multiplied by one bit of a secondary code. The secondary code consists of 25 known bits that are periodically transmitted taking a total duration of 100 ms. The advantage of using a known secondary code is that the receiver can easily increase the coherent integration time beyond the duration of the pilot bit by using a data-aided technique [SG12], which is very beneficial to obtain a gain in signal detection. This is in contrast to the GPS L1 signal where the navigation data bits are transmitted together with the PRN used to estimate the time-delay and each 20 ms there are unknown bits, which limits the coherent integration duration.

As previously said, the $S_{E1BC}(t)$ expressed in (2.11) is a MBOC(6,1,1/11) modulation, which combines the $\text{BOC}_{\text{sin}}(1,1)$ and $\text{BOC}_{\text{sin}}(6,1)$ modulations. However, much of the energy of this signal is concentrated in the $\text{BOC}_{\text{sin}}(1,1)$. The autocorrelation of this signal is ambiguous since it consists of three peaks in the range from -1 chip to 1 chip as it is shown in Figure 2.4. Although the Galileo E1BC signal contains two BOC modulations, they are independent from each other, which means that it is not necessary to use the combination of BOC signals to acquire the received signal. For instance, to avoid the complexity of generating two BOC signals in the local replica, the signal is often acquired

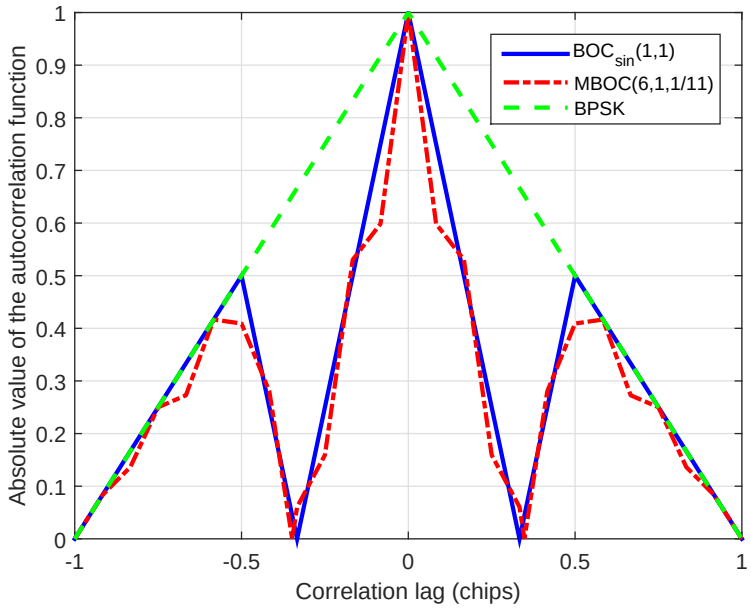

Figure 2.5: Comparison among the absolute value of the autocorrelation of the MBOC(6,1,1/11), BOC$_{\text{sin}}$(1,1), and BPSK modulations.

only using the BOC$_{\text{sin}}$(1,1) signal. The fundamental idea of the MBOC signal is to make the main correlation peak narrower so that the time-delay estimation was more accurate without increasing the number of secondary peaks of the autocorrelation function. This effect can be seen in Figure 2.5, which illustrates a comparison among the absolute value of the autocorrelation of the MBOC(6,1,1/11), BOC$_{\text{sin}}$(1,1), and BPSK modulations. The disadvantages of the MBOC signal are that they require a larger sampling frequency value to guarantee the Nyquist criterion, and that the local replica generated to acquire the satellite signal is more complex. This signal is often implemented at the tracking stage, whose aim is to get an accurate estimation of the time-delay.

The PSD of MBOC(6,1,1/11), BOC$_{\text{sin}}$(1,1), and BPSK modulations are illustrated in Figure 2.6. As anticipated, the BOC and MBOC signals utilize a wider spectrum than the BPSK modulation. The former ones split the spectrum of the signal, dividing the power between lower and upper side lobes. This causes that the magnitude of the Gabor bandwidth of these signals is larger, which leads to a reduction of the CRB of the time-delay with respect to the conventional BPSK modulation. This is the reason why the BOC and MBOC signals can exhibit quite good accuracy in estimating the user's position, outperforming the accuracy offered by the GPS L1 signal.

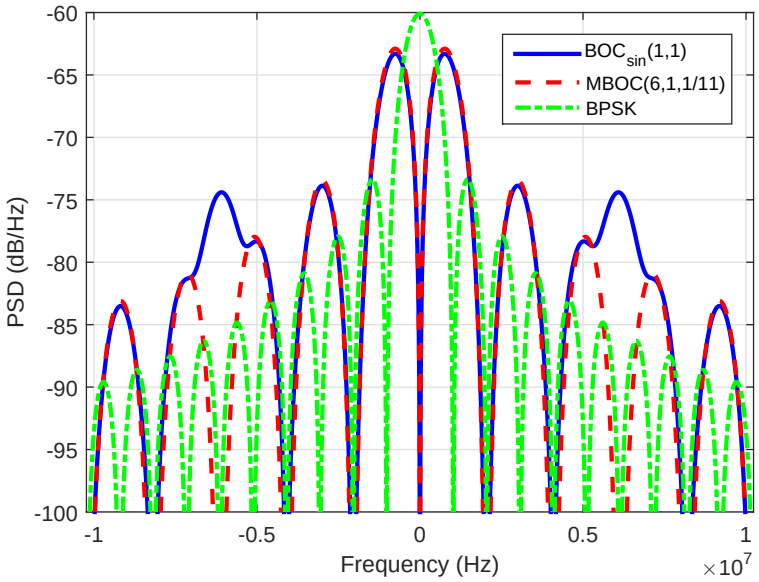

Figure 2.6: Comparison among the PSD of the autocorrelation of MBOC(6,1,1/11), $\text{BOC}_{\text{sin}}(1,1)$, and BPSK modulations.

2.1.3.4 High-order BOC signals

High-order BOC signals are a particular case of BOC signals, which have a relative large BOC modulation order K_{BOC} [Wu14]. An example of high-order BOC signal is the $\text{BOC}_{\text{cos}}(15, 2.5)$, which is being implemented in the E1 band of Galileo. The details of this Galileo signal are unknown for civilian users since it is restricted to military users. For this reason, in this section, we are going to focus only on the high-level properties of the $\text{BOC}_{\text{cos}}(15, 2.5)$ modulation.

The autocorrelation of this signal, illustrated in Figures 2.7 and 2.8, includes a very multi-peaked characteristic, which some of these peaks present a similar magnitude with one another. More precisely, the correlation of these signal contains 25 peaks taking into account the positive and negative peaks. Since many peaks are of similar amplitude and are very close one another in time domain, it is very easy to erroneously track a secondary peak, and therefore provide a bias position. However, when the main correlation peak is tracked, this estimation is extraordinary accurate since the main peak of this signal is much narrower than the correlation peak of a BPSK signal. The problem of tracking a secondary peak is known in the literature as a false lock. The false lock problem can easily be circumvented in good conditions of signal reception. Nonetheless, it becomes

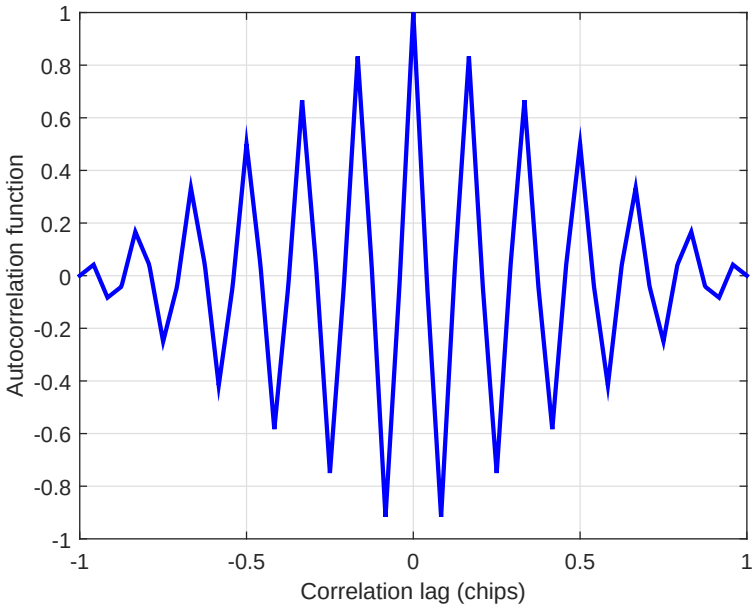

Figure 2.7: Autocorrelation of a $\mathrm{BOC}_{\cos}(15,2.5)$.

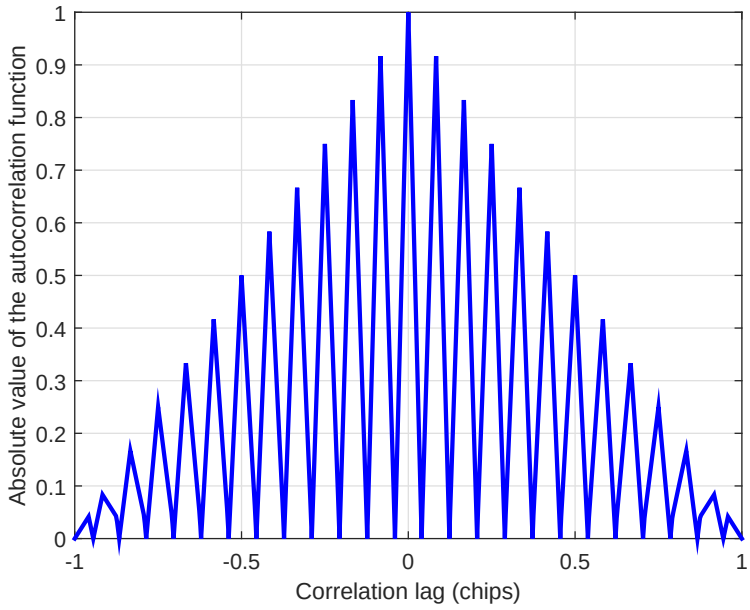

Figure 2.8: Absolute value of the autocorrelation of a $\mathrm{BOC}_{\cos}(15,2.5)$.

much more difficult to solve in harsh environments such as indoor or urban canyons due to the strong attenuation of the received signal.

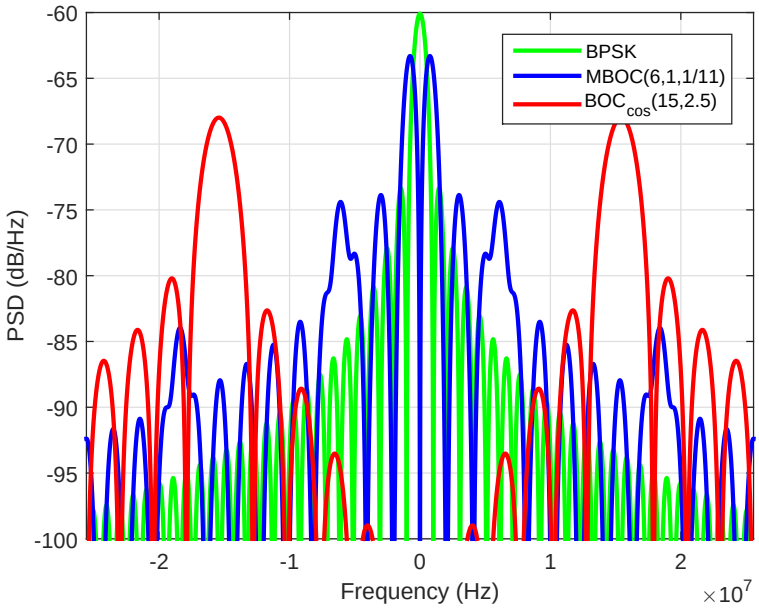

Figure 2.9: Comparison among the PSD of the BPSK, MBOC$(6, 1, 1/11)$ and $\text{BOC}_{\cos}(15, 2.5)$ signals.

Figure 2.9 shows the comparison among the PSD of the BPSK, MBOC$(6, 1, 1/11)$ and $\text{BOC}_{\cos}(15, 2.5)$ signals. The $\text{BOC}_{\cos}(15, 2.5)$ signal concentrates practically all of the energy on the carrier of 15 MHz. This signal has by far the widest spectrum. It is for this reason that the estimation of the time-delay can be very accurate. Nevertheless, apart from the disadvantage of the false locks, this kind of signals requires using a large frequency sampling to accomplish the Nyquist theorem. Typical values of sampling frequencies for this signal are usually between 40 and 60 MHz [Blu07b, O'D09]. These values of sampling frequency are an impairment for HS-GNSS receivers since they have to process a larger number of samples to obtain the position of the user, which leads to a greater complexity in terms of computational load.

2.1.4 GNSS receiver

GNSS receivers are mainly in charge of determining the user's location based on the different received signals coming from the satellites in view. The main stages of a standard GNSS receiver are illustrated in Figure 2.10, which consists of 4 stages: the front-end, acquisition, tracking and PVT module. Next subsections explain with more detail these stages.

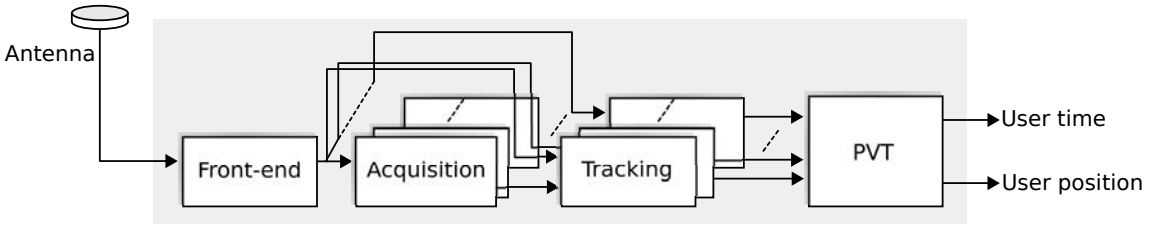

Figure 2.10: General architecture of standard GNSS receivers.

2.1.4.1 Front-end

The front-end module carries out the baseband conversion process of the band-pass signal captured by the antenna. Basically, it consists of a low-noise amplification, one or several intermediate frequency conversion stages, and an analog-to-digital conversion.

Once the received GNSS signal has been properly conditioned by the front-end, it can be generically expressed in baseband form, assuming that there is only one subcarrier, in discrete time as follows [Jay13, Wei06]:

$$r(nT_s) = \sum_{h=1}^{Q} \sqrt{P_h} b_h(nT_s - \tau_h) c_h(nT_s - \tau_h) s_h(nT_s - \tau_h) \times e^{j(2\pi f_{d,h} nT_s + \tilde{\theta}_h)} + \tilde{\omega}(nTs), \tag{2.12}$$

where Q is the number of broadcasting satellites, $T_s = 1/f_s$ is the sampling time, f_s is the sampling frequency, P_h is the received signal power of the hth satellite, $c_h(nT_s - \tau_h)$ is the pseudo random noise code, $b_h(nT_s - \tau_h)$ is the unknown navigation data message, $s_h(nT_s - \tau_h)$ is the subcarrier (if $s_h(nT_s - \tau_h) = 1$, there is no subcarrier and the received signal is a simple BPSK signal), τ_h is the time-delay from the hth satellite to the receiver, $f_{d,h}$ is the Doppler frequency because of the movement of the satellite and the clock receiver, $\tilde{\theta}_h$ is the phase of the received signal and $\tilde{\omega}(nT_s)$ is the complex Additive White Gaussian Noise (AWGN).

2.1.4.2 Acquisition stage

The acquisition stage is the part that is explained in more detail since most of the content of this thesis is focused on this stage. The main purpose of the acquisition stage is to detect the different satellites currently in view and providing a coarse estimation of the time-delay and Doppler frequency of the detected satellites. This process is carried out by correlating the received signal $r(nT_s)$ with all of the Q local replicas of the transmitted signals with

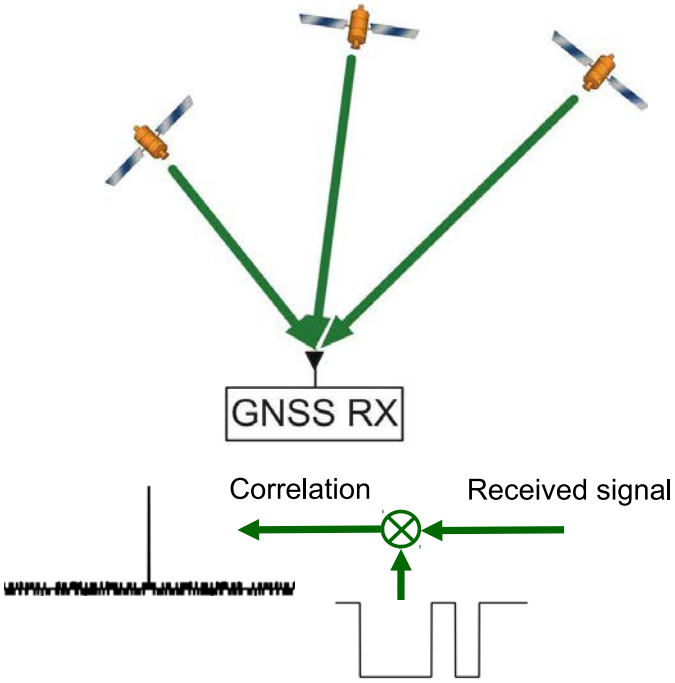

Figure 2.11: Acquisition process of GNSS receivers.

trial values of Doppler frequency and time-delay. However, in this work, we perform this process only for the qth satellite because it is enough to analyze the performance of detection problems. As there is no risk of confusion, we remove this subscript to simplify the notation. Figure 2.11 represents the acquisition process of GNSS receivers. The local replica of the qth satellite with different trial values of the time-delay τ and the Doppler frequency f_d as $\tilde{\tau}$ and $\tilde{f}_d$, respectively, is written as

$$g(nT_s) = s(nT_s - \tilde{\tau})c(nT_s - \tilde{\tau})e^{j(2\pi \tilde{f}_d nT_s)}. \tag{2.13}$$

The trial values $\tilde{f}_d$ and $\tilde{\tau}$ evaluate all the possible values of Doppler frequency and time-delay performing a bidimensional search in order try to acquire the satellites. The circular correlation between $g(nT_s)$ and $r(nT_s)$ is called CAF [Pre09], which assuming that there no exist bit transition is given by

$$\begin{aligned} x(\tilde{\tau}, \tilde{f}_d) &= \sum_{n=1}^{M_{ch}} r(nT_s)c(nT_s - \tilde{\tau}_k)s(nT_s - \tilde{\tau})b(nT_s - \tilde{\tau}_q)e^{j(2\pi \tilde{f}_d nT_s)} \\ &= d\tilde{A}e^{j\phi}\text{sinc}(\Delta f T_{\text{coh}})B(\Delta\tau) + \omega = Ade^{j\phi} + \omega, \end{aligned} \tag{2.14}$$

where A is the amplitude obtained from computing the CAF with phase ϕ, d is the value of the data navigation bits taking value of 1 or -1, $\Delta\tau = \tau - \tilde{\tau}$ is the time-delay offset between

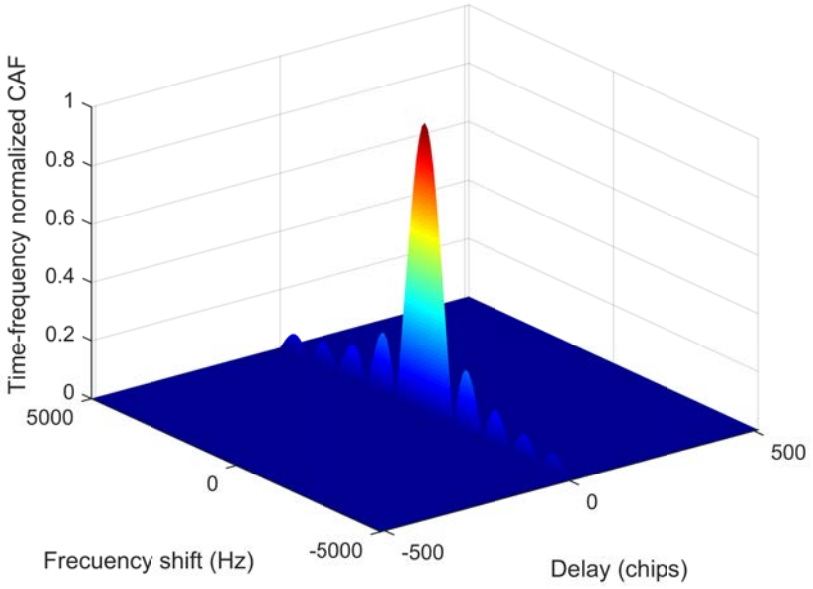

Figure 2.12: Illustrative bi-dimensional search space of frequency and time-delay in absence of noise.

the local replica and the received GNSS signal, $\Delta f = f_d - \tilde{f}_d$ is the residual frequency offset, T_{coh} is the coherent integration time, $B(\Delta\tau)$ is the circular autocorrelation function of a GNSS signal, M_{ch} is the number of samples integrated coherently and ω is AWGN after computing the CAF with zero-mean and variance σ^2. The $\text{sinc}(\Delta f T_{\text{coh}})$ term provides the losses of coherent integration because of the residual Doppler frequency between the received signal and the local replica.

The range of the bi-dimensional search depends on if the receiver has assisted data about the uncertainties of Doppler frequency and the time-delay. Conventional GNSS receivers without any a priori information about these uncertainties must perform a bi-dimensional search from -5 KHz to 5 KHz in the frequency domain and check all the different chips of the code. An example of the absolute value of a CAF in absence of noise and without any assisted data is illustrated in Figure 2.12. However, if the receiver has assisted data about the Doppler of the satellites in view, the search can be reduced to 1 kHz around this information [VD09].

The CAF is mainly affected by the signal transmitted by the satellite and the T_{coh}. In time domain, the CAF is given by the shape of the autocorrelation of the received signal. In frequency domain, the CAF is always a sinc function, but its width depends

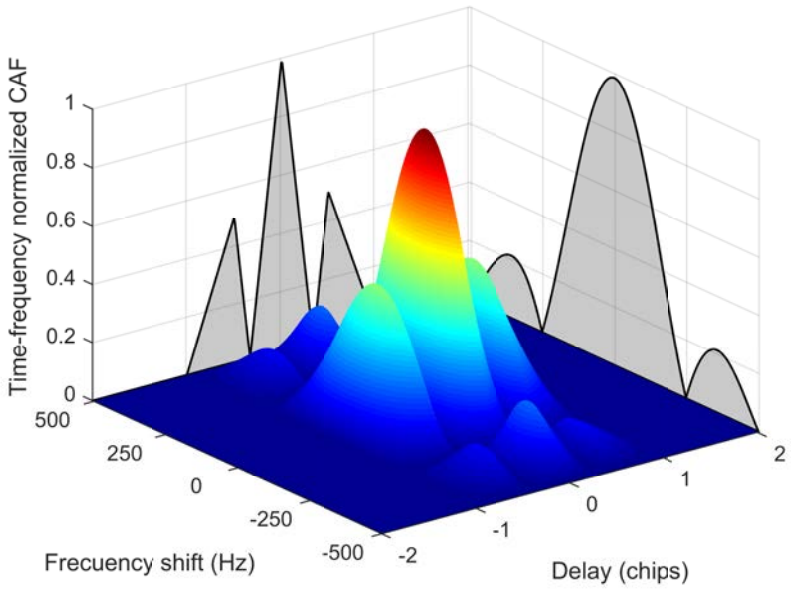

Figure 2.13: Illustrative CAF of a $\mathrm{BOC}_{\sin}(1,1)$ signal.

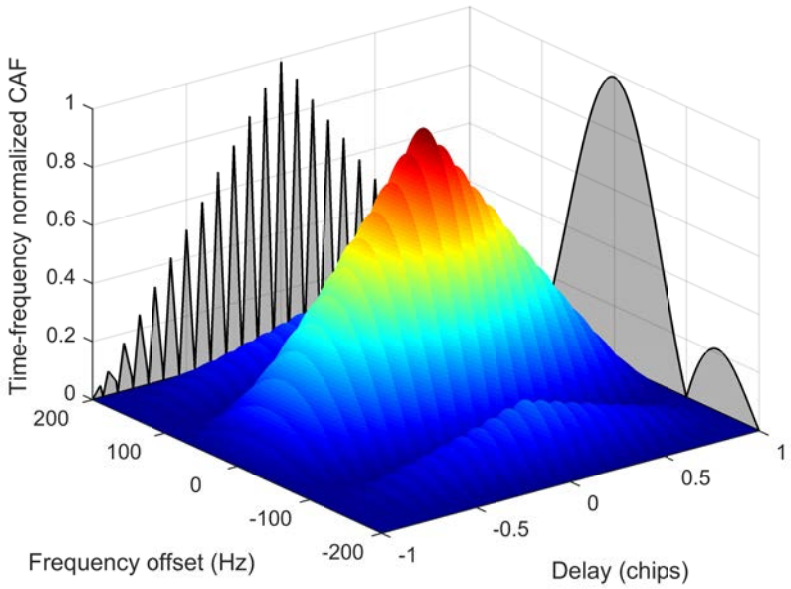

Figure 2.14: Illustrative CAF of a $\mathrm{BOC}_{\cos}(15,2.5)$ signal.

on the T_{coh} as shown in (2.14). This effect can be seen in Figures 2.13 and 2.14, which shows the CAF of a $\mathrm{BOC}_{\sin}(1,1)$ and $\mathrm{BOC}_{\cos}(15,2.5)$ using a T_{coh} of 4 ms and 10 ms, respectively. In any case, the process to acquire the satellite is always based on computing

the CAF independently from the modulation employed. After performing the CAF, its absolute value is computed to remove the phase information. In order to detect whether the satellite is in view or not, the maximum of the absolute CAF value is compared to a signal detection threshold. The satellite is considered absent if the CAF does not exceed the detection threshold. On the contrary, if the CAF surpasses the signal detection threshold the satellite is considered in view and a coarse estimation of the time-delay and Doppler frequency are provided.

In general, independently from the signal to be acquired, the objective is to find the tentative values where the correlation peak is located in the CAF. To do so, there are three main acquisition strategies to compare the CAF with the detection threshold:

- Serial search: Each trial value of time-delay and Doppler frequency is compared individually to a detection threshold.
- Hybrid search: A group of trial values of time-delay and Doppler frequency (e.g. a row/column of the CAF) are compared to a given detection threshold.
- Parallel search: The maximum value of all of the tentative values is compared to a given detection threshold.

Most HS-GNSS receivers compute the CAF in the frequency domain by applying FFT-based techniques, since it is more efficient in terms of computational load. The most common way to carry out this process is by computing several circular correlations in the frequency domain. One correlation is computed for each tentative value of Doppler frequency. The result of each circular correlation gives all CAF values for the tested Doppler frequency. This fact leads most HS-GNSS receivers to use the hybrid or the parallel acquisition. Typically, in both acquisition searches, the accuracy of the time-delay estimation is usually given by the sampling frequency used at the receiver. The error of the estimation of Doppler frequency is comprised between the range $[-f_{st}/2, f_{st}/2]$, where f_{st} is the search step of Doppler frequency used in the local replica to compute the CAF. The step f_{st} is chosen taking into account a trade-off between complexity in terms of computational burden at the receiver and accuracy in the estimation of Doppler frequency. A typical value of f_{st} to mitigate the coherent integration losses is $1/(2T_{\text{coh}})$.

The CAF usually allows the receiver to acquire the satellites in view in good conditions of signal reception such as open sky environments. Nevertheless, it is not usually enough to detect the presence of satellites in harsh environments such as indoor or urban since the received signal arrives too attenuated. This degradation is due to the presence of obstacles

in the working environment such as trees, walls and glass causing that the signal level after computing the CAF is below the noise level. The optimal way to obtain some benefit in terms of signal detection consists in extending T_{coh}, which boils down to summing several CAFs computed in consecutive time instants. The main reason why the coherent integration provides a great gain is because the signal component of a few CAFs is strongly correlated, while the thermal noise component is completely uncorrelated. Thus, the sum of several CAFs allows the receiver to accumulate enough energy to detect the signal.

Despite the fact that the coherent integration offers a considerable gain in terms of signal detection, it cannot be extended without bounds since several impairments that affect the carrier phase of the received signal limit its length. These impairments are mainly the frequency offset, the navigation data bits and the phase noise. If long coherent integration times are implemented, the impairments reduce or cancel the improvement obtained by the coherent integration. This is because the signal component suffers some variations in the carrier phase causing an attenuation of the signal component in the CAF. The existence of these impairments has originated the need to use a different strategy to be able to detect weak signals surpassing the limitations of the coherent integration. This strategy is based on combining several consecutive CAFs using a non-linear function as

$$Z_x(\mathbf{x}) = f\left(\sum_{k=1}^{N_{nc}} x_k(\tilde{\tau}, \tilde{f}_d)\right) \tag{2.15}$$

where f is some non-linear function, the sub-index k indicates the time instant where the CAF has been calculated, N_{nc} is the number of non-coherent correlation and $\mathbf{x}$ is a column vector containing the different CAFs. The non-linear combination of several CAFs is typically called non-coherent correlation or PDI technique. The main advantage of PDI techniques is that they are robust against most of the impairments that limit the duration of the coherent integration. Therefore, they have the capability of lengthening the total integration time beyond the limits of the coherent integration time. The price to be paid for using the PDI techniques is some losses in terms of signal detection with respect to the use of coherent integration in ideal conditions (in absence of frequency offsets, phase noise and data bits). Nevertheless, PDI techniques become the only choice that HS-GNSS receivers have to detect weak GNSS signals. The approach used by HS-GNSS receivers to acquire weak GNSS signals usually involves combining a long T_{coh} with few N_{nc} using a PDI technique. By doing so, HS-GNSS receivers can detect weak signals using the minimum total integration time, by combining the sum of the time used for coherent and non-coherent integration. When PDI techniques are required to perform the acquisition of the satellite signal, the output of the PDI technique is compared to

the detection threshold to decide if the satellite is present or not. More details about the definition of a detection threshold can be found in Section 2.2.2.

However, the problem of determining the best PDI technique to acquire weak GNSS signals under real-life working conditions still remains open. As a matter of fact, this is the main point that this thesis intends to address. Moreover, this question may have several answers, which depend on the characteristics of the transmitted signal. For instance, the optimal PDI technique would be different if the transmitted signal contains unknown data bits or not, or whether the CAF contains a frequency offset or not. As will be shown later, several theoretical derivations are carried out in this thesis in order to determine the best PDI technique in each case.

The process of acquiring weak GNSS signals in HS-GNSS receivers can require a large amount of computational load, though assisted data is exploited. This occurs because an extremely long signal (of hundreds of milliseconds or even several seconds) must be processed to detect these signals in harsh environments such as indoor or urban. This process involves the computation of the CAF for different parts of the signal with many tentative values of f_d since the duration of the T_{coh} can extend up to 1 or 2 seconds [Mus14]. One way to circumvent this huge computational load is by the use of cloud computing services. In recent years, the emergence of cloud computing services has become an exceptional opportunity to carry out the procedure of acquiring weak GNSS signals. The user would only need to collect the samples of the received signal and transmit them to the cloud service where the tasks of the GNSS receiver can remotely be performed [LS16d, LS16c].

2.1.4.3 Tracking stage

The main task of the tracking stage consists in refining the coarse estimation of the time-delay and Doppler frequency of the satellites declared in view in the acquisition stage. These estimates are tracked to accurately follow any possible variation of time and frequency either in the receiver or the satellite [Kap05]. There are mainly two approaches to carry out this refinement, the so-called closed-loop and open-loop architectures [Tah12].

On the one hand, conventional GNSS receivers usually implement a closed-loop architecture to perform this refinement. This consists essentially of two architectures in parallel: one focused on tracking the time-delay, known as Delay Lock Loop (DLL), and another dedicated to the track of the frequency, referred to as Phase Lock Loop (PLL). Both architectures obtain an accurate estimate of the parameter of interest based on

comparing the received signal to a local replica. This comparison is used to correct the estimates of the parameters that have been used to generate the local replica, so that the alignment with the received signal is achieved as accurate as possible.

These architectures are basically formed by three components: the discriminator, the numerical controlled oscillator and the loop filter. The process of the tracking stage is the following. In both architectures, the local replica is correlated with the received signal and the result is introduced to a discriminator, which provides an error signal that is proportional to the parameter of interest. The output of the discriminator in the PLL is obtained from using one correlator known as prompt and focused on the time-delay of interest. The output of the discriminator in the DLL is obtained by using three correlators: the prompt and two correlators symmetrically located before and after the prompt, which are referred to as early and late correlators, respectively. The output of the both discriminators is subsequently smoothed through the loop filter, whose output is then fed to the numerical controlled oscillator. The output of the numerical controlled oscillator is used to generate a new local replica, thus closing the loop.

Closed-loop architectures have extensively been studied in the literature during last decades, which has generated several contributions regarding the loop filters and the discriminators. Recently, new tracking architectures are emerging, which implement adaptive Kalman filter-based techniques. These techniques are more robust than the classic PLL/DLL allowing the receiver to track the signal in harsher conditions, that is, under high dynamics or even in the presence of ionospheric scintillation disturbances [LS16b, Pou15].

On the other hand, in contrast to conventional GNSS receivers, HS-GNSS receivers usually implement an open–loop architecture or often so-called snapshot-based architecture. This architecture is based on computing one CAF from time to time with a narrow search for the Doppler frequency. This narrow search is performed around the coarse Doppler frequency estimation obtained from the first CAF. Open-loop architectures provide some advantages over closed-loop architecture. For instance, it is a well-known fact that PLLs suffer from fading effects, particularly associated with harsh scenarios such as urban or indoor, and cycle slips [Rib98]. In addition, the closed loop structures require long signal time before giving a refinement of the estimation of time-delay and Doppler frequency, and this might be an important disadvantage when the Doppler frequency rapidly changes within this signal time. These problems can be circumvented by implementing an open-loop architecture. However, the estimates of time-delay and Doppler frequency offered by the CAF obtained in the open-loop architecture are not precise enough to

provide an accurate estimation of the user's position.

For this reason, a fine acquisition stage is usually implemented after computing each CAF [SG12]. The aim of this stage is to enhance the accuracy of the estimates of interest only using the CAF generated in one determined time. One way to refine the time-delay estimation is by performing an interpolation of the main correlation peak that has the shape of a triangle. More precisely, this method deals with finding the position of the vertex of this triangle by making a linear interpolation of each side slope of the main correlation peak. The refinement of the Doppler frequency can be carried out by minimizing a cost function, which compares the received CAF in frequency domain to the ideal expected sinc function [Tan13].

In the tracking stage, apart from refining the estimation of the parameters of interest, HS-GNSS receivers are capable of obtaining highly desirable information about the quality of the signal. For instance, these receivers can estimate the C/N_0, which indicates the accuracy that we can obtain in the estimation of parameters. Moreover, they detect and mitigate near-far interferences given in scenarios with strong and weak signals. Some techniques to carry out this task are included in [LS16a, LR05]. In addition, these receivers are also able to detect the presence of multipath effects abounding in urban canyon or indoor environments. A relevant approach to detect quickly this effect has been proposed recently, which is based on applying quickest detection theory. More details about this technique can be found in [ER17, ER15].

2.1.4.4 Position, velocity, timing module

Even though the tracking stage aims at filtering noise, the time-delay estimates obtained from this stage will still contain some residual noise. In addition, the presence of impairments such as clock errors or multipath may also introduce some bias in the measurements of the distance between the satellites and the GNSS receiver. In this sense, the goal of the PVT module is to provide the most accurate estimate of the user's position by using these measurements.

One approach to estimate the PVT of the receiver is by the use of an iterative algorithm. The most common method based on this approach deals with applying an iterative least square estimator. This method boils down to solving a system of linear equations, which contains several unknowns, the three coordinates of the receiver and the time instant of the satellite transmission. The algorithm starts by considering an initial position of the receiver. Once the position of the receiver is estimated the initial position is up-

dated for this estimation [Kap05]. By doing this procedure, the position of the receiver is refined and tracked accurately.

Another approach consists in finding a closed-form solution of the position of the receiver. The most representative method following this approach is based on the Bancroft algorithm [Ban85]. This method contains the same unknowns as the iterative least square estimator, but it presents the advantage of not requiring a tentative value of the initial position of the receiver. However, this kind of methods usually offer a worse performance than the ones obtained from an iterative algorithm. This occurs because this kind of algorithms usually have to use a squared operation to solve the problem, which leads to increase the noise in the time-delay estimates.

2.2 Detection theory

Signal detection theory is a branch of probability theory widely applied in different electronics signal processing systems, such as radar, communications, speech and sonar. This theory allows us to make decisions in the presence of uncertainty. Basically, simple detection problems deal with distinguishing whether some signal embedded in the noise is present or absent. The objective is to use the received signal as efficiently as possible to perform a correct decision. This kind of problems are usually referred to as binary hypothesis testing since only two hypotheses are involved: H_0 and H_1. Traditionally, the hypothesis H_1 is called the alternative hypothesis and the hypothesis H_0 corresponds to the null hypothesis.

2.2.1 GNSS signal detection as hypothesis testing

The binary hypothesis testing can tackle the problem of GNSS signal detection because this problem can be broken down into two hypotheses: under H_0 the signal from the satellite is absent and under H_1 the signal from the satellite is present. One of the two hypotheses is considered to be true for any tested GNSS signal. Since GNSS signals are described as a random variable, the decision between the two hypotheses is carried out using statistical detection theory. The analysis of the problem starts with the characterization of the probability density function (pdf) that defines the received GNSS signal

under each hypothesis. Rewriting the CAF[1] $x(\tilde{\tau}, \tilde{f}_d)$ obtained from the acquisition stage as simply x to avoid the complexity of the notation, the two following pdfs can be defined as

$$p(x|H_0) = \text{pdf of } x \text{ given that the signal from satellite is absent.}$$

$$p(x|H_1) = \text{pdf of } x \text{ given that the signal from satellite is present.}$$

Detection problems also require finding appropriate models of these two distributions. Generally, the detection process is based on using N samples of the data x_k forming a vector as $\mathbf{x} \doteq [x_1, ..., x_k, ..., x_N]^T$. To do so, the N-dimensional joint pdfs $p(\mathbf{x}|H_1)$ and $p(\mathbf{x}|H_0)$ are usually utilized. Taking into account the two joint distributions, several required probabilities are described to characterize these problems [Ric05, McD95, Kay98]:

- Probability of false alarm (P_{fa}): is the probability of considering the satellite to be present (H_1 is chosen) when the satellite is absent.
- Probability of detection (P_d): is the probability that the satellite is declared (H_1 is chosen) when the satellite is present.
- Probability of miss detection (P_{md}): is the probability that the satellite is considered to be absent (H_0 is chosen) when the satellite is indeed present.

It is worth noticing that $P_{md} = 1 - P_d$. Therefore, the P_d and P_{fa} are enough to specify the probabilities of the detection problem. Moreover, since this is a statistical problem, there is a certain probability that the assumed decision is wrong. The P_{fa} and P_d can be defined by the following expressions, which depend on the signal detection threshold:

$$P_{fa} = \text{prob}(f(\mathbf{x}) \geqslant \gamma|H_0) = 1 - \text{cdf}_f(\gamma|H_0), \tag{2.16}$$

$$P_d = \text{prob}(f(\mathbf{x}) > \gamma|H_1) = 1 - \text{cdf}_f(\gamma|H_1), \tag{2.17}$$

where $f(\mathbf{x})$ is a function of $\mathbf{x}$, cdf_f is the cumulative density function of the $f(\mathbf{x})$ and γ is the detection threshold.

An illustrative plot of a binary hypotheses test problem is illustrated in Figure 2.15. This figure shows the two pdfs under each hypothesis H_0 and H_1. The pdf under H_0 is zero-mean since there is no presence of the satellite signal, while the pdf under H_1

[1]The CAF is a process used in the acquisition stage of the GNSS receiver to acquire the satellites. More details can be found in Section 2.1.4.2

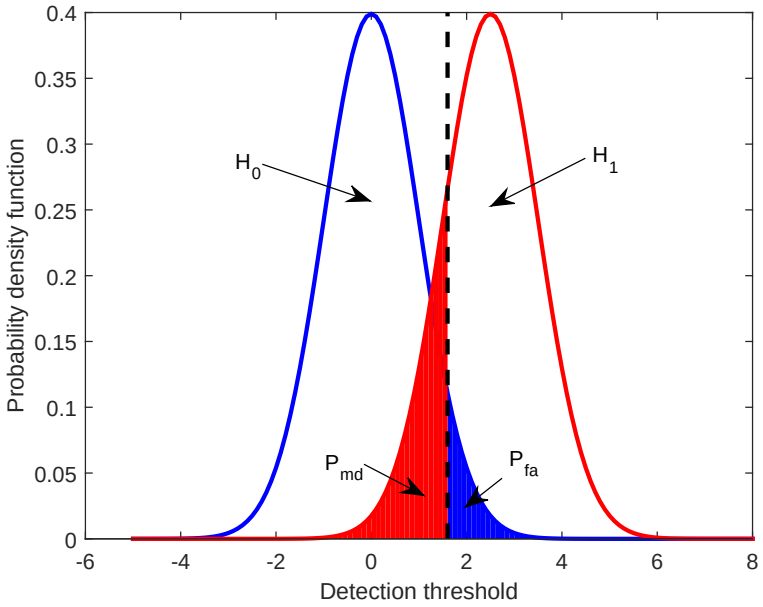

Figure 2.15: Illustrative plot of binary hypotheses problem for a given $p(x|H_0)$ and $p(x|H_1)$.

contains a non-zero mean owing to the presence of the satellite signal. The difference of means between the two pdfs causes that the pdf under H_1 is shifted to the right side. Then, a detection threshold is defined in order to discriminate between the two hypotheses. This threshold is usually established for a small value of P_{fa}, in order not to suffer a larger number of incorrect detected satellites. The definition of an appropriate detection threshold involves the knowledge of the cdf of the metric of interest under the null hypothesis or a good approximation of this cdf. The probability of false alarm represents the blue area of the H_0 distribution. This area contains the values under H_0 that exceed the detection threshold. The probability of miss detection corresponds to the red area of the distribution of the H_1 hypothesis, which consist of the values of this distribution that do not surpass the detection threshold.

2.2.2 Detection threshold for the acquisition of weak GNSS signals

The detection of a weak signal deals with the comparison between the maximum magnitude of a PDI technique, denoted as Z_x in Section 2.1.4.2, and an appropriate detection threshold to determine whether the satellite is considered to be in view or not. If the

detection threshold is surpassed, the satellite is assumed present and then, the process moves forward to tracking. If the detection threshold is not exceeded, the satellite is considered not to be in view and the acquisition process is finished. The detection threshold is affected by the P_{fa} to which we refer from now on as individual probability of false alarm as

$$P_{fa} = 1 - \mathrm{cdf}_Z(\gamma|H_0), \tag{2.18}$$

where $\mathrm{cdf}_Z(\gamma|H_0)$ is the cumulative density function of the metric of a PDI technique under the condition H_0. However, the definition of the detection threshold is usually set by fixing a value of global probability of false alarm (P_{FA}). The P_{FA} depends on P_{fa} as

$$P_{FA} = 1 - (1 - P_{fa})^L, \tag{2.19}$$

where L is the number of independent trial points of Doppler frequency and time-delay. The difference between P_{fa} and P_{FA} is that P_{fa} is the probability that one individual tentative value of time-delay and Doppler frequency surpasses the detection threshold when the satellite is not present. In contrast, P_{FA} is the probability that the maximum magnitude of the L independent tentative values exceeds the detection threshold when the signal satellite is absent. After setting a small value of P_{FA}, P_{fa} is computed from (2.19). Then, the detection threshold can be computed from (2.18) as

$$\gamma = 1 - \mathrm{cdf}_Z^{-1}(1 - P_{fa}|H_0), \tag{2.20}$$

where cdf_Z^{-1} is the inverse cumulative density function of the metric of the PDI technique.

2.2.3 Neyman-Pearson rule

This section consists in finding the optimal rule to decide between two hypotheses, provided that the parameters of both hypotheses are known. The Neyman-Pearson rule is one of the most extended optimality criterion used for binary hypothesis testing. The objective of the Neyman-Pearson rule is to maximize P_d while guaranteeing that P_{fa} does not surpass an established value fixed by a detection threshold. This is a detection problem, which can be solved by using the Lagrange multipliers methods. The result of this problem is well-known in the literature as the Likelihood Ratio Rest (LRT) [Kay98]

$$\Lambda(\mathbf{x}) = \frac{p(\mathbf{x}|H_1)}{p(\mathbf{x}|H_0)} \lessgtr \gamma. \tag{2.21}$$

The LRT establishes that the ratio between two pdfs, one under H_0 and the other under H_1, must be compared with a detection threshold. If the LRT exceeds the detection threshold the condition under H_1 is considered to be correct, in our case meaning that the signal from the satellite is present. Nonetheless, when the LRT does not surpass the detection threshold, the condition under H_0 is assumed to be true, in our problem meaning that the signal from the satellite is absent. Since the decision depends only on whether the LRT surpasses the detection threshold or not, a monotonic function can be applied on both sides of (2.21) without affecting the performance of the detector obtained from the LRT. A common monotonic function widely used is the logarithm function, which usually decreases the computational cost required to calculate the LRT. Taking the logarithm function in (2.21), we obtain the log-likelihood ratio test as

$$\ln \Lambda(\mathbf{x}) \lessgtr \ln \gamma. \tag{2.22}$$

The result of the LRT is the optimal detector, or also sometimes referred to as PDI technique in GNSS, to discriminate between the two hypotheses under the Neyman-Pearson criterion. It is worth noting that models of the two pdfs are needed in order to compute the LRT. Moreover, the pdf under each hypothesis must not contain unknown parameters, otherwise we cannot calculate the LRT to compare to the detection threshold. Finally, it should be added that the Neyman-Pearson rule does not require assuming any knowledge about the a priori probability of the two hypotheses.

2.2.4 ROC curves

The Receiver Operative Characteristic (ROC) curve is a graphical plot that illustrates the P_d versus P_{fa} of one or several detectors or PDI techniques. These curves allow us to compare the performance of several PDI techniques and predict their performances [VT04, Poo13, Lev08]. An illustrative ROC plot of a common detector used in GNSS and radar is shown in Figures 2.16 and 2.17. This detector corresponds to the absolute value of the CAF, defined previously in Section 2.1.4.2. In this example, the relationship between the detection and false alarm probabilities, denoted as P_d^{CAF} and P_{fa}^{CAF}, is given by the following expression:

$$P_d^{\mathrm{CAF}} = Q_1\left(\sqrt{2\mathrm{SNR}}, \sqrt{-2\ln\left(P_{fa}^{\mathrm{CAF}}\right)}\right), \tag{2.23}$$

where Q_1 is known as Marcum's Q function. This example serves to describe the general characteristics of the ROC curves of any detector. These curves contain all of the values

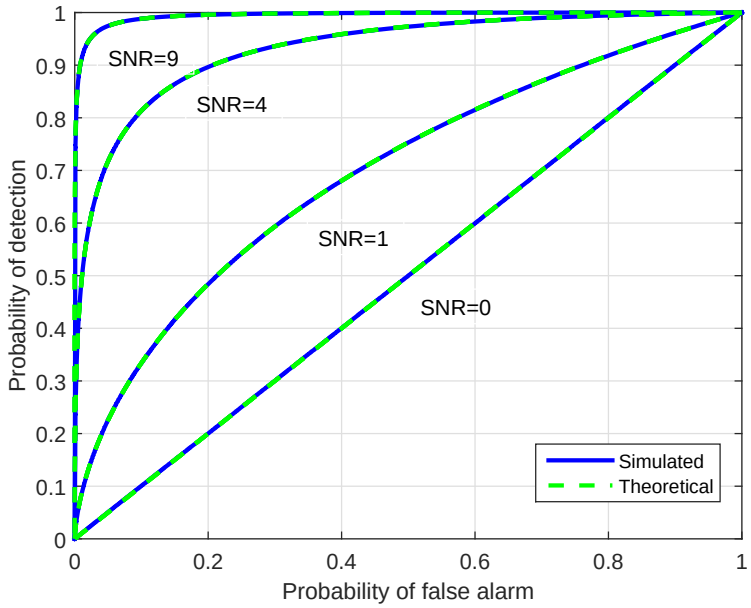

Figure 2.16: Theoretical and simulated ROCs curves for a CAF displayed on a linear P_{fa} scale. The SNR is in linear scale.

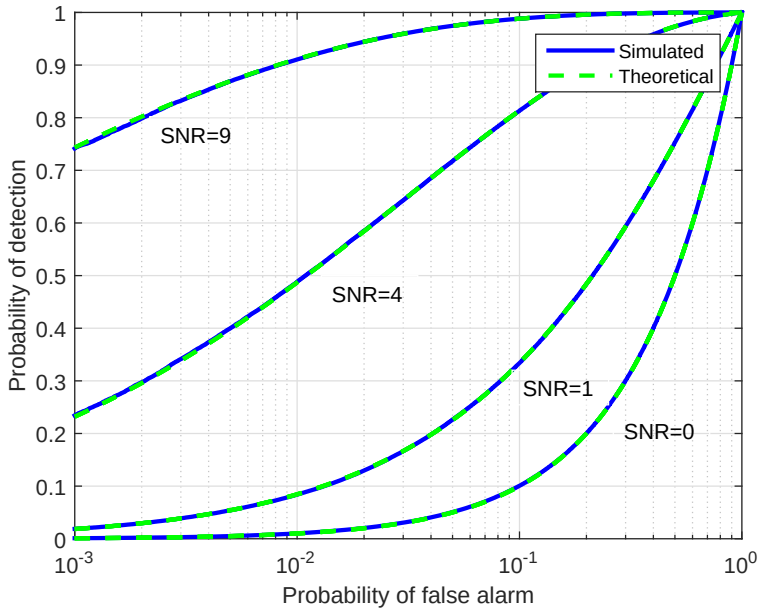

Figure 2.17: Theoretical and simulated ROCs curves for a CAF displayed on a logarithmic P_{fa} scale. The SNR is in linear scale.

in the square [0, 1] x [0, 1] since they are the ones that the probabilities can take. Each point on the curve corresponds to a value of P_{fa} and P_d for a given detection threshold. We can obtain any value of the curves changing the value of the threshold. If the detection threshold increases, the P_d and P_{fa} decreases but whether the threshold decreases, the two probabilities increase. All points on the ROC curve satisfy $P_d \geqslant P_{fa}$. The comparison among several detectors can be carried out fixing a value of P_{fa}. Then, the best detector is chosen as the one that maximizes the P_d.

Moreover, these curves allow us to predict the performance of our detector for given conditions as in the case of the Figures 2.16 and 2.17. For instance, we can find out the detector performance for different values of SNR. For the case of SNR=0 (not dB), we obtain that the $P_{fa} = P_d$. This fact is expected because the pdf under H_0 and H_1 is the same. For a given value of P_{fa}, the P_d increases if the SNR increases since there is more distance between the two distributions under each hypothesis. It should be added that these curves are often illustrated using a semi-log scale for the P_{fa} to show the detector performance in this region.

ROC curves can be obtained by using Monte-Carlo simulations or theoretically. Unlike the example described above, closed-form expressions for P_{fa} and P_d are usually difficult to obtain owing to the complexity of the metrics of many detectors. This is a fundamental problem because having access to such closed-form expressions allows us to know the detector performance even for small values of P_{fa}, which are the ones typically implemented in the receiver. These values of P_{fa} are difficult to find through simulations because they require a huge number of Monte-Carlo iterations, involving many computational resources and simulation time. In fact, this is precisely one of the problems that this thesis aims to address in Chapter 4 for some relevant PDI techniques.

2.2.5 Bayesian approach

The Bayesian approach is a detection tool that is applied when the LRT contains unknown parameters, for which some a-priori knowledge is available. Under H_0, we consider that the vector $\boldsymbol{\theta_0}$ is unknown while under H_1, the vector $\boldsymbol{\theta_1}$ is unknown. The outcome of the Bayesian approach is certainly the optimal detector under the assumed conditions. This approach consists in computing the LRT and using a priori information about the vectors $\boldsymbol{\theta_0}$ and $\boldsymbol{\theta_1}$. The impairment of the unknown parameters is circumvented by averaging the conditional pdfs to obtain the unconditional pdfs, which are not affected by $\boldsymbol{\theta_0}$ and $\boldsymbol{\theta_1}$

any more. The Bayesian approach is based on a ratio of pdfs as [Kay98, Sim95]

$$\Lambda_B(\mathbf{x}) = \frac{\int p(\mathbf{x}|H_1, \boldsymbol{\theta_1}) p(\boldsymbol{\theta_1}) d\boldsymbol{\theta_1}}{\int p(\mathbf{x}|H_0, \boldsymbol{\theta_0}) p(\boldsymbol{\theta_0}) d\boldsymbol{\theta_0}} = \frac{p(\mathbf{x}|H_1)}{p(\mathbf{x}|H_0)} \lessgtr \gamma, \tag{2.24}$$

where $p(\mathbf{x}|H_i, \boldsymbol{\theta_i})$ is the pdf of $\mathbf{x}$ conditioned on $\boldsymbol{\theta_i}$ and $p(\boldsymbol{\theta_i})$ corresponds to the prior pdf of $\boldsymbol{\theta_i}$. Nonetheless, the hypothesis H_0 does not usually contain unknown parameters in GNSS problems. Therefore, the Bayesian approach can be rewritten as

$$\Lambda_B(\mathbf{x}) = \frac{\int p(\mathbf{x}|H_1, \boldsymbol{\theta_1}) p(\boldsymbol{\theta_1}) d\boldsymbol{\theta_1}}{p(\mathbf{x}|H_0, \boldsymbol{\theta_0})} = \frac{p(\mathbf{x}|H_1)}{p(\mathbf{x}|H_0)} \lessgtr \gamma. \tag{2.25}$$

The drawback of the Bayesian approach is that the unknown parameters must be modelled accurately with a certain prior distribution, whose knowledge is required. In addition, it needs to compute a multidimensional integral, which does not usually admit a closed-form solution or often provides a very complex solution in terms of computational load.

2.2.6 Generalized likelihood ratio test

The Generalized Likelihood Ratio Test (GLRT) is a general procedure for binary hypotheses testing problems. This test is the best well-known joint estimation and detection approach for finding promising detectors, which consists of two steps. First, the Maximum Likelihood (ML) estimates of the unknown parameters are obtained for the different hypotheses. Second, these parameters are replaced by their ML estimates under each hypothesis and the LRT is computed as if the estimation of the unknown parameters were in fact the correct values. The GLRT can be defined as follows [Lev08]:

$$\Lambda_G(\mathbf{x}) = \frac{p(\mathbf{x}|H_1, \hat{\boldsymbol{\theta}}_\mathbf{1})}{p(\mathbf{x}|H_0, \hat{\boldsymbol{\theta}}_\mathbf{0})} \lessgtr \gamma, \tag{2.26}$$

where $\hat{\boldsymbol{\theta}}_\mathbf{0}$ and $\hat{\boldsymbol{\theta}}_\mathbf{1}$ are the ML estimates of $\boldsymbol{\theta_0}$ and $\boldsymbol{\theta_1}$, respectively. Nevertheless, in GNSS detection problems, the hypothesis H_0 does not usually depend on unknown parameters, thus leading the GLRT to reduce to

$$\Lambda_G(\mathbf{x}) = \frac{p(\mathbf{x}|H_1, \hat{\boldsymbol{\theta}}_\mathbf{1})}{p(\mathbf{x}|H_0)} \lessgtr \gamma. \tag{2.27}$$

Although the GLRT approach makes no claims about the optimality of its result in general, it is widely implemented in practice since it usually provides good performance and needs less restrictive assumptions than the Bayesian approach. Furthermore, the GLRT result often gives an easier expression than the Bayesian approach since the latter is

composed by the integral of products of several PDFs. This occurs because ML estimation equations usually allow a closed-form solution, which can be easily introduced in the LRT. However, the performance exhibited by the GLRT can be the same or worse than the one obtained from the Bayesian approach, but it is never better as long as the conditions assumed in the Bayesian approach were true.

Chapter 3

State of the art and performance analysis of PDI techniques under the presence of frequency offset and phase noise

This chapter provides a review of the state of the art about PDI techniques applied in the context of CDMA. This review serves to identify the existing PDI techniques, which will be used as a benchmark to compare their performance with the PDI techniques derived in the following chapters. Moreover, a performance comparison of the most relevant PDI techniques described in this chapter is carried out in a scenario that the received signal includes the impairments of frequency offset and severe or mild phase noise. This analysis allows us to establish which is the best technique under the presence of these impairments. In addition to this, we indicate the coherent integration time that can be implemented in practice when the receiver clock is affected by severe or mild phase noise.

3.1 PDI techniques for the acquisition with pilot component

This part analyses the different PDI techniques that have been proposed in the literature, which make use of the pilot component only, while at the same time providing a critical review of their advantages and disadvantages. These techniques can be used to acquire

any GNSS signal either GPS or Galileo.

3.1.1 Non-coherent PDI technique

The Non-coherent PDI (NPDI) is the most common technique implemented in HS-GNSS receivers to detect weak signals. This technique dates back to the early days of signal detection problems in radar theory [Mar60]. The NPDI is an approximation of the result of applying a Bayesian approach for a low SNR regime. This Bayesian approach is derived for a received signal with a constant amplitude and unknown time-varying phase following a uniform distribution [McD95]. The expression of the NPDI technique is given by [EB04],

$$Z_{\mathrm{NPDI}}(\mathbf{x}) = \sum_{k=1}^{N_{nc}} |x_k(\tilde{\tau}, \tilde{f}_d)|^2. \tag{3.1}$$

By considering an unknown time-varying phase, it removes the carrier impairments that limit the T_{coh} duration such as the data bits and the frequency offset by combining N_{nc} consecutive CAFs using the squared absolute value. The disadvantage of the NPDI technique is that it suffers from the squaring loss effect [Str07]. That is, the mean of the noise is increased with respect to the coherent integration under ideal conditions (assuming that there is no presence of variations in the carrier phase and the only disturbance is AWGN). Thereby, the NPDI technique requires a total integration time longer than the coherent integration to detect the signal. The metric of the NPDI technique involves the sum of central and non-central Chi-square distributions with $2N_{nc}$ when the signal is absent and present, respectively. The probability of detection and false alarm of this detector are well-know in the literature and are defined as [Sim07, Bor09a]

$$P_{fa}^{\mathrm{NPDI}} = \exp\left(-\frac{\gamma}{\sigma^2}\right) \sum_{i=0}^{N_{nc}-1} \frac{1}{i!} \left(\frac{\gamma}{\sigma^2}\right)^i \tag{3.2}$$

$$P_{d}^{\mathrm{NPDI}} = Q_{N_{nc}}\left(\sqrt{\frac{2\lambda}{\sigma^2}}, \sqrt{\frac{2\gamma}{\sigma^2}}\right), \tag{3.3}$$

where γ is the detection threshold, $\lambda = N_{nc}(A\mathrm{sinc}(\Delta f T_{\mathrm{coh}})B(\Delta\tau))^2$ and $Q_{N_{nc}}$ is the generalized (N_{nc}th-order) Marcum Q-function [Mar50].

3.1.2 Differential PDI technique

The Differential PDI (DPDI) is a useful technique to acquire weak GNSS signals. The origin of the this technique comes from radar detection theory to detect signals with

unknown constant phase and unknown Doppler frequency [Sel65]. The metric of the DPDI consists in multiplying one CAF $x_k(\tilde{\tau}, \tilde{f}_d)$ with a delayed and conjugated version of itself as $x_{k-1}(\tilde{\tau}, \tilde{f}_d)$. Then, sum $N_{nc}-1$ of these multiplications and finally it takes the absolute value as [Sch05b, Vil07]

$$Z_{\text{DPDI}}(\mathbf{x}) = \left| \sum_{k=2}^{N_{nc}} x_k(\tilde{\tau}, \tilde{f}_d) x_{k-1}^*(\tilde{\tau}, \tilde{f}_d) \right|, \tag{3.4}$$

The DPDI technique is fully robust against the presence of frequency offsets, but it suffers a strong degradation in presence of data bits [Cha11]. This technique may provide better performance than the NPDI technique in the absence of data bits since it is not affected by the squaring loss problem. The idea behind the DPDI technique is to exploit that the signal components of two consecutive CAFs are highly correlated, while the noise components are completely uncorrelated.

The exact distribution of the DPDI metric is not known in closed-form. However, a closed-form approximation of the detection and false alarm probabilities of this metric can be obtained using the Central Limit Theorem (CLT). According to this theorem, for large number of N_{nc}, the pdf of the DPDI metric tends to be Rayleigh or Rician distribution under H_0 and H_1, respectively. Then, the approximations of the probabilities of this detector can be expressed as [Lan73]

$$P_{fa}^{\text{DPDI}} \approx 1 - \text{cdf}_{Z_{\text{DPDI}}}\left(\sqrt{(N_{nc}-1)\sigma^4} | H_0\right) \tag{3.5}$$

$$P_{d}^{\text{DPDI}} \approx 1 - \text{cdf}_{Z_{\text{DPDI}}}\left((N_{nc}-1)A^2, \sqrt{(N_{nc}-1)\sigma^4} | H_1\right). \tag{3.6}$$

where $\text{cdf}_{Z_{\text{DPDI}}}\left(\sqrt{(N_{nc}-1)\sigma^4} | H_0\right)$ and $\text{cdf}_{Z_{\text{DPDI}}}\left((N_{nc}-1)A^2, \sqrt{(N_{nc}-1)\sigma^4} | H_1\right)$ corresponds to the Rayleigh and Rayleigh and Rician and distribution, respectively.

3.1.3 Enhanced differential PDI technique

Another alternative was introduced in [Paj06], which is an improvement of the DPDI technique. This alternative, which is given by (3.7), was found empirically by the use of simulations based on Galileo signals.

$$Z_{\text{EDPDI}}(\mathbf{x}) = \left| \sum_{k=3}^{N_{nc}} x_k^*(\tilde{\tau}, \tilde{f}_d) x_{k-1}(\tilde{\tau}, \tilde{f}_d) + x_k^*(\tilde{\tau}, \tilde{f}_d) x_{k-2}(\tilde{\tau}, \tilde{f}_d) \right|^2. \tag{3.7}$$

This technique can offer better performance than the NPDI and DPDI techniques in terms of the probability of acquisition in fading channels. The drawback of this technique is

that the computational complexity is greater than the ones implemented in the NPDI and DPDI techniques because it requires more memory to save three consecutive CAFs. Moreover, this technique is susceptible to suffer a performance degradation in presence of data bits since it does not apply any non-linear operation that removes the bit information. An analysis of the statistical characterization of this metric is not found in literature. Intuitively, the metric of the enhanced DPDI technique does not seem to follow any known pdf. However, according to the CLT, this metric may tend to have a non-central chi square distribution if the signal is present or central chi-square if the signal is absent for large N_{nc} values.

3.1.4 Non-linear Teager-Kaiser technique

The non-linear Teager-Kaiser technique has also been proposed to detect weak GNSS signals. It consists of the sum and multiplication of the different delayed CAFs as follows [Ham03],

$$Z_{\mathrm{TK}}(\mathbf{x}) = \left| \sum_{k=3}^{N_{nc}} |x_{k-1}(\tilde{\tau}, \tilde{f}_d)|^2 + \frac{1}{2} \left(x_k^*(\tilde{\tau}, \tilde{f}_d) x_{k-2}(\tilde{\tau}, \tilde{f}_d) + x_k(\tilde{\tau}, \tilde{f}_d) x_{k-2}^*(\tilde{\tau}, \tilde{f}_d) \right) \right|. \quad (3.8)$$

The Teager-Kaiser technique can slightly outperform the NPDI technique, but the former requires a computational load much more larger than the latter [Loh13]. In addition, this technique might not be robust against the data bits because only one term of this metric removes the information of the bits. The statistical distribution of the metric of the non-linear Teager-Kaiser technique is completely unknown neither H_0 nor H_1 hypotheses.

3.1.5 Generalized and average PDI techniques

An interesting approach was presented in [Cor03] and later extended in [Cor07] for CDMA signals. This paper derives the quasi-optimal PDI schemes through a theoretical approach taking into account the presence of two uncertainties: a constant phase during the whole integration time and frequency offset. To do this task, the LRT is computed from the pdfs under the null and alternative hypotheses. The uncertainty of the constant phase is removed by applying the Bayesian approach assuming that this phase is a uniform random variable from 0 to 2π. After that, two different approaches are considered to eliminate the frequency offset uncertainty: the GLRT and Bayesian approach.

On the one hand, the approach used in the GLRT supposes that frequency offset is

an unknown deterministic parameter. The resulting expression is known as a Generalized PDI (GPDI) technique, which consists of the sum of several terms as follows,

$$\begin{aligned} Z_{\mathrm{GPDI}}(\mathbf{x}) &= \sum_{k=1}^{N_{nc}} |x_k(\tilde{\tau}, \tilde{f}_d)|^2 + 2\left| \sum_{d=1}^{N_{nc}-1} \sum_{k=1+d}^{N_{nc}} x_k(\tilde{\tau}, \tilde{f}_d) x_{k-d}^*(\tilde{\tau}, \tilde{f}_d) \right| \\ &= \sum_{k=1}^{N_{nc}} |x_k(\tilde{\tau}, \tilde{f}_d)|^2 + 2\left| \sum_{k=2}^{N_{nc}} x_k(\tilde{\tau}, \tilde{f}_d) x_{k-1}^*(\tilde{\tau}, \tilde{f}_d) \right| + \cdots + 2|x_{N_{nc}}(\tilde{\tau}, \tilde{f}_d) x_1^*(\tilde{\tau}, \tilde{f}_d)|, \end{aligned} \tag{3.9}$$

where $d = 1, \ldots, N_{nc} - 1$. The fundamental of the GPDI technique is that it naturally encompasses several PDI techniques. This technique includes the conventional NPDI and DPDI techniques and beside all possible differential combination among the distinct CAFs. The performance of the GPDI technique depends on the number of terms introduced. The larger the number of terms used, the better the performance of the GPDI. However, the incremental enhancement becomes smaller as more terms are introduced.

On the other hand, when the Bayesian approach is applied the frequency offset is assumed to be a uniform random variable that can take values between $-\Delta f_{max}$ and Δf_{max}. The resulting expression is referred to as the Average PDI (APDI) technique, which also consists of the sum of several terms, and it can be expressed as

$$Z_{\mathrm{APDI}}(\mathbf{x}) = \sum_{k=1}^{N_{nc}} |x_k(\tilde{\tau}, \tilde{f}_d)|^2 + 2\mathrm{Re}\left\{ \sum_{d=1}^{N_{nc}-1} \sum_{k=1+d}^{N_{nc}} \mathrm{sinc}(2d\Delta f_{max} T_{\mathrm{coh}}) x_k(\tilde{\tau}, \tilde{f}_d) x_{k-d}^*(\tilde{\tau}, \tilde{f}_d) \right\}. \tag{3.10}$$

In the same way as the GPDI technique, the APDI technique encompasses various PDI techniques. More precisely, it contains the sum of the NPDI technique with a kind of the differential PDI technique. This differential technique takes the real part instead of the absolute value and moreover multiplies each term by $\mathrm{sinc}(2d\Delta f_{max} T_{\mathrm{coh}})$.

The larger the number of terms of the APDI technique to perform the detection, the better the results are obtained. However, the incremental enhancement becomes smaller when APDI uses more terms until a saturation in the performance occurs.

There exist a trade-off between the GPDI and APDI techniques. If very small values of frequency offset are present, the APDI technique offers the best performance, while the GPDI becomes the best option for large values of the frequency offset. This happens because the sinc terms used in the APDI become very small and possibly negative. For the case of acquisition of weak GNSS signal, we often have a uncertainty of frequency offset that cause that most of the terms in the APDI technique are close to zero. For this reason, the GPDI technique should be more adequate to acquire weak GNSS signals.

Both the GPDI and APDI techniques have an important drawback. They require a significant amount of computational load since they both consist of many terms. As a consequence, practical and efficient solutions with good performance are sought. For the case of the GPDI, a practical solution is to combine the terms corresponding to NPDI with DPDI. This solution is so-called Truncated Generalized Post Detection Integration (GPDIT) technique can be expressed as the following equation

$$Z_{\mathrm{GPDIT}}(\mathbf{x}) = \sum_{k=1}^{N_{nc}} |x_k(\tilde{\tau}, \tilde{f}_d)|^2 + 2 \left| \sum_{k=2}^{N_{nc}} x_k(\tilde{\tau}, \tilde{f}_d) x_{k-1}^*(\tilde{\tau}, \tilde{f}_d) \right|. \tag{3.11}$$

Notice the weighting factor 2 applied to the differential correlation in the summation. The solution proposed in (3.11) outperforms the conventional NPDI and the DPDI as long as the present uncertainties are a constant phase and frequency offset. The same truncation of terms can be applied for the case of the APDI, which leads to Truncated Average Post Detection Integration (APDIT) technique and it results in:

$$Z_{\mathrm{APDIT}}(\mathbf{x}) = \sum_{k=1}^{N_{nc}} |x_k(\tilde{\tau}, \tilde{f}_d)|^2 + 2\mathrm{Re} \left\{ \sum_{k=2}^{N_{nc}} \mathrm{sinc}(2\Delta f_{max} T_{\mathrm{coh}}) x_k(\tilde{\tau}, \tilde{f}_d) x_{k-1}^*(\tilde{\tau}, \tilde{f}_d) \right\}. \tag{3.12}$$

The practical solution of APDI technique exhibits better performance than the NPDI and DPDI techniques when there is no large frequency offset.

The disadvantage of the GPDIT and APDIT techniques is that they are not robust against the data bits. This occurs because they contain the differential PDI technique, which suffers a strong degradation in presence of this impairment. These techniques might be very useful to acquire weak GNSS signals with pilot bits as it is the case of the Galileo E1BC signal, since the impairment of the bits can be circumvented. However, if the received signal contains unknowns bits as it happens in the GPS L1 signal, these techniques may not be the best option to acquire weak GNSS signals.

The overall statistical characterization of the GPDI and APDI techniques is a challenging task and open problem. This occurs because these techniques are composed by the sum of several different PDI techniques, which some of them are correlated with each other. Even though this fact an analysis of the GPDI and APDI techniques excluding the NPDI technique is carried out in [Cor07]. On the one hand, the metric of the GPDI technique is well approximated by a Rayleigh or Ricean distributions in presence or absence of the signal, respectively, if the NPDI term is ignored. On the other hand, the APDI metric omitting the NPDI term is close to a Gaussian distribution with zero-mean if the signal is absent and non-zero mean when the signal is present. However, a statistical analysis of the GPDIT and APDIT techniques, which are the practical solutions of the GPDI and APDI, is not found in the literature.

3.1.6 Combination of the NPDI with the squaring detector

Another method has been proposed recently in [Sat11], which is a new class of improved acquisition technique for weak GNSS signals. Specifically, this technique has been derived from an approximation of the GLRT, considering that the unknown parameter is a constant phase during the whole integration time. The pdfs used to compute the GLRT assume that the received signal contains unknown data bits, which are a random variable and can take values of -1 or 1 with the same probability. The resulting PDI technique from this approach can be defined as

$$Z_{\mathrm{NPDISD}}(\mathbf{x}) = \sum_{k=1}^{N_{nc}} |x_k(\tilde{\tau}, \tilde{f}_d)|^2 + \left| \sum_{k=1}^{N_{nc}} x_k(\tilde{\tau}, \tilde{f}_d)^2 \right|. \tag{3.13}$$

The key point of this proposed technique is that combines the term corresponding to the NPDI with a new term. This new term is referred to as Squaring Detector (SD) and it consists of summing the squared values of the CAFs.

A statistical analysis of this PDI technique is performed in [Bor14b]. Due to the dependence between the NPDI and the SD, it is not feasible to find the exact distribution of the PDI technique expressed in (3.13). For this reason, an approximation of the false alarm probability of this PDI technique is carried out, which uses a non-linear transformation to accelerate the convergence speed of the distribution of this metric to a Gaussian distribution.

3.1.7 Combination of the GPDIT and the squaring detector

The last method that we introduce is referred to as GPDITSD. This technique is proposed in this thesis and it results from putting together terms of the GPDIT with the SD terms as

$$Z_{\mathrm{GPDITSD}}(\mathbf{x}) = \sum_{k=1}^{N_{nc}} |x_k(\tilde{\tau}, \tilde{f}_d)|^2 + 2 \left| \sum_{k=1}^{N_{nc}-1} x_k(\tilde{\tau}, \tilde{f}_d) x_{k-1}^*(\tilde{\tau}, \tilde{f}_d) \right| + \left| \sum_{k=1}^{N_{nc}} x_k(\tilde{\tau}, \tilde{f}_d)^2 \right|. \tag{3.14}$$

The key point here is that this method exploits the performance and the low complexity that the both the GPDIT and SD techniques individually have. The combination between the GPDIT and SD techniques can exhibit good performance in terms of acquisition probability in some scenarios, as we will see in Subsection 3.3. However, finding a closed-form expression of the statistical distribution of this technique does not seem to be a simple task to carry out.

3.2 PDI techniques for the acquisition joining data and pilot components

This subsection provides a state of the art of the PDI techniques that exploit the two components the data and pilot to acquire GNSS signals. These techniques seem that some gain in terms of signal detection can be obtained by using both the data and pilot. Nevertheless, this gain can vanish if one takes into consideration the computational load, especially for acquiring very weak signals where extremely long integration times are required. That is to say, given some computational resources available, it is preferable to devote then to process a longer fragment of the pilot component than shorter fragments of the pilot and data. The reason is basically that the pilot allows the receiver to extend much longer coherent correlations. If short coherent correlation of the data component is combined with longer coherent correlations of the pilot, no significant gain is obtained because the former are much nosier than the latter and does not help so much in improving the quality of the coherent correlations.

So far, PDI techniques that have been proposed in the literature are based on combining the data and pilot components using the same coherent integration time for each component, which is limited by the data component. In the following subsections, we describes the most relevant strategies, which can be found in [Ta10, Bor08].

3.2.1 Comparing Combination

The so-called "Comparing Combination" uses a comparator to select the squared absolute value of the two channels, which are obtained combining the data and pilot components. More precisely, the received signal is correlated with the codes of the pilot and data components for different tentative values of time-delay and Doppler frequency. The decision variable is obtained by choosing the maximum between two combinations of these correlations. In particular, the first correlation is the sum of the correlations of the data and pilot components and the second one is subtraction between the correlations of the data and pilot components. This PDI technique can be expressed as follows,

$$Z_{\mathrm{CC}}(\mathbf{x}) = \sum_{k=1}^{N_{nc}} \max\{|x_{k,(P-D)}(\tilde{\tau}, \tilde{f}_d)|^2, |x_{k,(P+D)}(\tilde{\tau}, \tilde{f}_d)|^2\}, \tag{3.15}$$

where $x_{k,(P-D)}(\tilde{\tau}, \tilde{f}_d)$ and $x_{k,(P-D)}(\tilde{\tau}, \tilde{f}_d)$ are the CAF obtained from summing and subtracting the pilot and data components, respectively.

3.2.2 Dual Channel

In the dual channel technique, the conventional NPDI technique is simultaneously performed on both the data and pilot components. Specifically, the received signal is correlated with two codes. The first code is the pilot component and the second one is the data component. Then, the technique consists of summing up the squared absolute of the different CAFs as

$$Z_{\mathrm{DC}}(\mathbf{x}) = \sum_{k=1}^{N_{nc}} |x_{k,(D)}(\tilde{\tau}, \tilde{f}_d)|^2 + |x_{k,(P)}(\tilde{\tau}, \tilde{f}_d)|^2, \tag{3.16}$$

where $x_{k,(P)}(\tilde{\tau}, \tilde{f}_d)$ is the CAF of the pilot component and $x_{k,(D)}(\tilde{\tau}, \tilde{f}_d)$ is the CAF of the data component.

3.2.3 Differential data and pilot

In this technique, the received signal is also correlated with two codes for different trial values of time-delay and Doppler frequency. The first code is the pilot component and the second one corresponds to the data component. After that, the CAF obtained from the data component is multiplied by the conjugate of the CAF computed from the pilot component. Thus, a new equivalent complex correlation value is obtained, and finally the real part of this multiplication is taken as,

$$Z_{\mathrm{DXP}}(\mathbf{x}) = \sum_{k=1}^{N_{nc}} \left| \mathrm{Re}\{x_{k,(D)}(\tilde{\tau}, \tilde{f}_d) x^*_{k,(P)}(\tilde{\tau}, \tilde{f}_d)\} \right|. \tag{3.17}$$

This approach can be seen as a modification of the differential PDI technique. The CAF of one component is multiplied by the conjugated CAF of the other component instead of the delayed copy of itself as in the real differential PDI technique.

3.2.4 Results of joint data and pilot components

According to [Ta10], the best joint data/pilot technique depends on the received signal power. When the received signal has low power $C/N_0 < 24$ dB-Hz, the dual channel strategy has better performance than the other techniques. However, if the power is $C/N_0 \geqslant 24$ dB-Hz, the comparing combination technique is a bit better than the other.

The best joint data/pilot method holds the sensitivity enhancement of 2.8 dB over the NPDI using only one component when one non-coherent integration is performed and for

a coherent integration time quite small as 4 ms. However, the problem of these techniques is that when the number of non-coherent correlation or the coherent integration time is increased, the detection gain of the joint data/pilot methods over pilot methods is reduced using the former a larger amount of memory. For this reason, the use of only the pilot component is the best option to acquire very weak signals, since the HS-GNSS receiver must process several seconds of the received signals to make a reliable decision about the presence of the signal.

3.3 Simulations results of PDI techniques for signals with time-varying phase due to phase noise and frequency offset

In the context of GNSS, this subsection carries out a performance comparison of the most relevant PDI techniques described in Subsection 3.1. The comparison is divided into two parts. The first one deals only with the simulations in presence of AWGN and frequency offset, but not phase noise, while the second one includes the phase noise. The ROC curves are used to analyze the performance of the detection techniques. Moreover, simulations have been performed using the Galileo E1C signal for different values of C/N_0 [Com11]. We remember that the E1C signal includes pilot bits, which makes the maximum T_{coh} is not limited by the duration of the bit. The acquisition of the signal is achieved by the application of a HS-GNSS receiver, which uses the double-FFT algorithm [JB06, SG12]. This algorithm provides an efficient signal acquisition using a long coherent integration time and assuming some assistance information about the Doppler of the satellite.

3.3.1 Simulation without phase noise

Figure 3.1 shows that the proposed GPDITSD defined in (3.14) offers a significant gain in terms of probability of detection when the frequency offset is zero. The key aspect of this method is that it combines the terms corresponding to NPDI with both DPDI and SD. Comparing the performance of the terms that form the GPDITSD, the following conclusions can be drawn:

- SD outperforms NPDI.

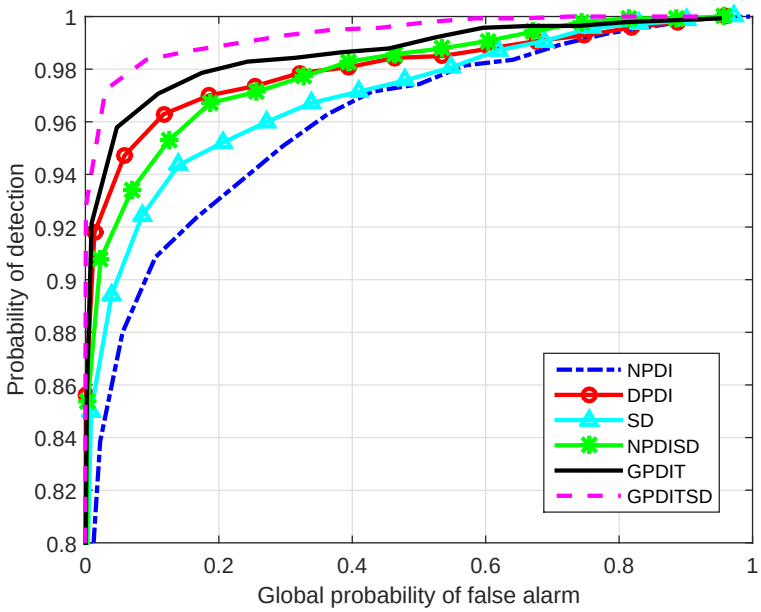

Figure 3.1: ROC curves for C/N_0=20 dB-Hz, coherent integration time=100 ms, N_{nc}=7 and Δf=0 Hz.

- DPDI outperforms NPDI and SD.
- NPDISD outperforms NPDI and SD.
- GPDIT outperforms NPDISD.

In the first simulation, the frequency offset of the incoming signal was set to 0 Hz. The following simulation considers the frequency offset to be a uniform random variable in the range of [-50, 50] Hz. At first glance in Figure 3.2, it can be seen that the SD method suffers significant degradation in presence of frequency offset. Due to this degradation, GPDIT turns out to be the most performing technique, unlike the case with no frequency offset, where GPDITSD outperformed the rest of detectors. The comparison between GPDITSD and GPDIT reveals that there is a certain value of frequency offset below which GPDITSD is advantageous; and above this value, GPDIT is preferable. This is an important result because different applications, depending on the dynamics of the receiver, have different Doppler uncertainty, and hence one technique may be more appropriate than the other. Extensive simulations have shown that this thresholding frequency offset value is 1 Hz for a coherent integration time equal to 100 ms. In general, in the acquisition stage the uncertainty of Doppler frequency is larger than 1 Hz since the Doppler frequency step is

usually given by $1/(2T_{\text{coh}})$. This result suggests that the best technique to acquire weak GNSS signals in presence of Doppler frequency is the GPDIT.

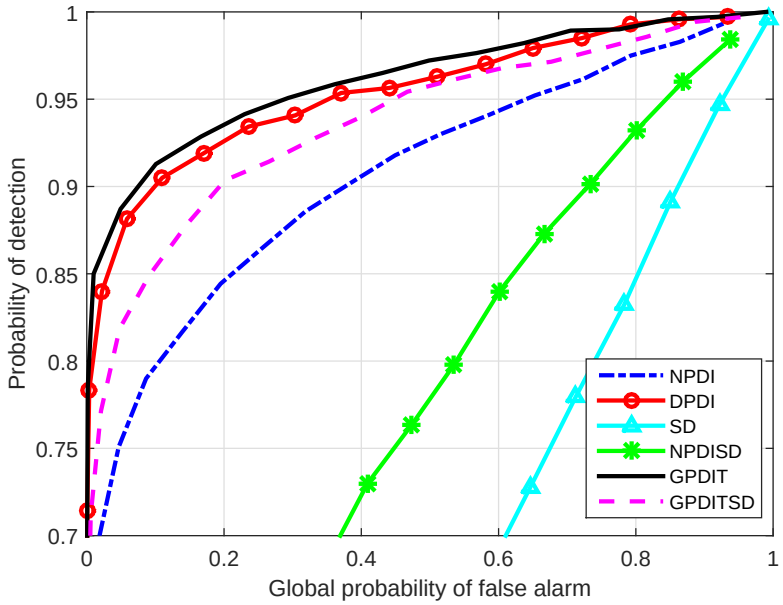

Figure 3.2: ROC curves for C/N_0=20 dB-Hz, coherent integration time=100 ms, N_{nc}=7 and $\Delta f \neq 0$ Hz.

3.3.2 Simulation with phase noise

One of the main limitations of HS-GNSS receivers is caused by clock instabilities, which translate into random deviations of the instantaneous phase, often referred to as *phase noise* [PS10]. As a result, the coherent integration time cannot be increased without bound and must be restricted to a limited time period.

More details about the generation of the phase noise can be found in Subsection 6.1.1. In our simulations, we have used two clocks, namely, a Temperature Compensated Crystal Oscillator (TCXO) and an Oven-controlled Crystal Oscillator (OCXO). The power of phase noise introduced by a TCXO clock is larger than the power of phase noise introduced by an OCXO clock. More precisely, the parameters used for the TCXO and OCXO clocks are given by [Cur12] and they are shown in the Table 3.1.

The phase noise caused by TXCO clock is introduced in the simulation, as shown in Figure 3.3. The ROC of the methods is obviously degraded with respect to the case

	h_0 $[s]$	h_{-2} $[1/s]$
TCXO	9.43e-20	3.8e-21
OCXO	3.4e-22	1.3-24

Table 3.1: Clock parameters.

without phase noise. Nevertheless, it is still possible to use a relatively long integration time (*i.e.* 100 ms) with this TCXO.

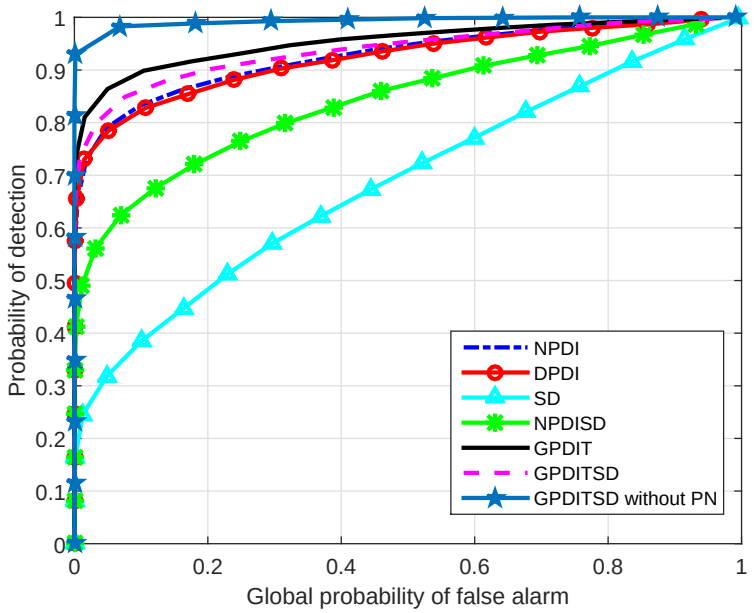

Figure 3.3: ROC curves for C/N_0=20 dB-Hz, coherent integration time=100 ms, N_{nc}=7, Δf=0 Hz and using a TCXO. In the legend, 'without PN" means 'without phase noise".

We recall that, when the frequency offset is null, the method that has the best performance is the GPDITSD in absence of phase noise. However, when phase noise is added to a large extent (as it is the case with a TCXO), the GPDIT turns out to be the best method even when the frequency offset is zero. This occurs because the SD term suffers a severe degradation. Moreover, the DPDI method also experiences a breakdown due to the phase noise because, unlike the case without phase noise (Figure 3.1), it has a very similar ROC to the standard NPDI. As a consequence, given the marginal advantage of GPDIT with respect to NPDI, but its higher complexity, we can conclude that NPDI is the most

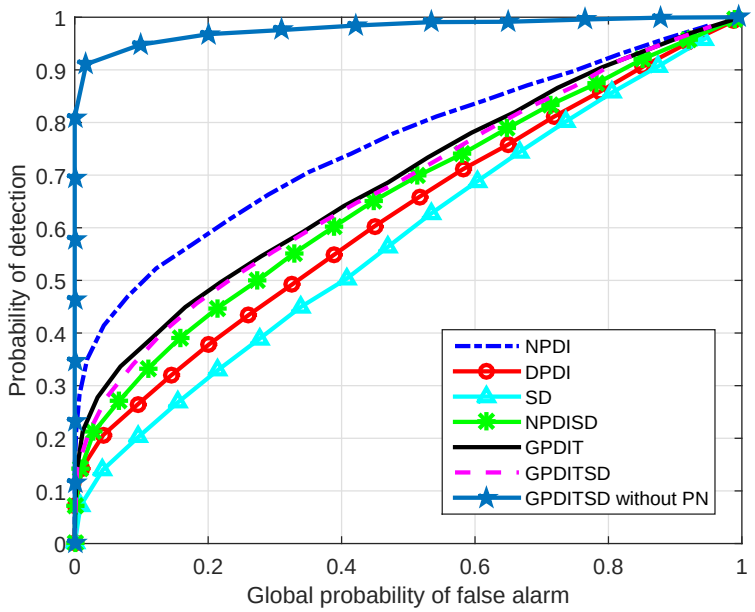

Figure 3.4: ROC curves for C/N_0=15 dB-Hz, coherent integration time=500 ms, N_{nc}=4, Δf=0 Hz and using a TCXO.

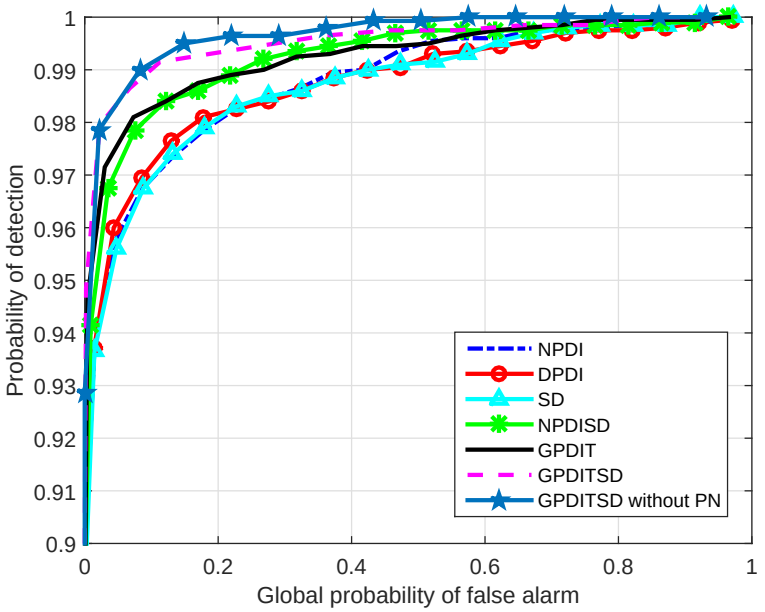

Figure 3.5: ROC curves for C/N_0=12 dB-Hz, coherent integration time=1000 ms, N_{nc}=4, Δf =0 Hz and using an OCXO.

robust method in case of large phase noise. Furthermore, the results in Figure 3.4 confirm that a coherent time of 500 ms is not feasible with a TCXO; and in any case, the NPDI would be the method providing the least degraded ROC.

An OCXO is used for the results in Figure 3.5. In this case, the coherent integration is increased to 1 second. The results show that coherent integrations of 1 second are perfectly feasible with this type of clock. As the phase noise is small, the GPDITSD offers the best performance, and very similar to the case without phase noise. Actually, the SD term is almost not degraded using this clock unlike the case with TCXO, which is the reason why the GPDITSD maintains its advantage.

3.4 Conclusions

This chapter has provided the state of the art of PDI techniques. We have concluded that the best option to detect weak GNSS signals is based only on using the pilot component. Moreover, we have analysed the performance of several detectors under several conditions of frequency offset and assuming receivers with a standard TCXO or with an average-to-good OCXO quality clocks. When there is no presence of phase noise, but we have the presence of frequency offset the best technique is the GPDIT technique. In general, the TCXO limits the coherent correlation interval to about 100 ms, and the large phase noise wipes outs the advantage of all differential and squaring detectors, leaving the standard NPDI as the best option. However, the OCXO permits the receiver to use coherent integration times as long as 1 second, and the GPDIT behave much better than the conventional NPDI.

Chapter 4

Weak GNSS signal acquisition in presence of data bits

Weak signal conditions are certainly the main obstacle for HS-GNSS receivers since the severe attenuation of the received signal makes difficult to reliably detect it [SG12]. In this situation, the increase of the coherent integration time is the optimal way to reduce the effect of noise so that the signal can be detected more easily. Nonetheless, as previously discussed, the coherent integration time is limited in practice by the presence of residual frequency offset, data bits, and phase noise.

The way to circumvent this limitation is to adopt PDI techniques or non-coherent accumulations, which are more robust against frequency offset, data bits, and phase noise than the coherent integration. Although PDI techniques suffer some degradation in the signal detection performance with respect to the ideal coherent integration (without taking into account the impairments that limit the coherent integration duration), the use of PDI techniques is the only choice we have if long integration times need to be implemented [Yan07]. Thereby, PDI techniques have become an indispensable tool to acquire weak signals in the context of HS-GNSS receivers [Sch05b, Mus14].

Different authors have proposed several PDI techniques to detect weak GNSS signals. The PDI technique most commonly used in GNSS is the NPDI, which is robust frequency offset and data bits. Another alternative is the DPDI technique, which leads to better detection probability than the NPDI technique in absence of data bits. Nevertheless, it suffers a significant degradation in presence of data bits. Others alternatives that combine two PDI techniques are the GPDIT, which uses the NPDI and DPDI, and the combination of the NPDI with the squaring detector. These combinations can provide some gain in

signal detection with respect to the NPDI technique. However, although several PDI techniques have been proposed, the question about what is the optimal PDI technique to acquire weak signals, which include data bits, is still unknown.

In Chapter 3, we have benchmarked the techniques used in the literature and propose a new technique based on the observations that are extracted from existing techniques in presence of frequency offset and phase noise. In this chapter, we derive the GLRT and the Bayesian approach considering signals with phase changes owing to the presence of frequency offsets, phase noise and also data bits. The resulting optimal detectors are difficult to implement in practice because the amplitude of the signal must be known a priori and it is not often possible to known. Then, two approximations of the both optimal detectors (obtained from the GLRT and the Bayesian approach) are performed leading in both cases to the NPDI technique for low SNR region and the Non-Quadratic PDI (NQ-NPDI) technique for high SNR region.

Moreover, this chapter provides some statistical characterizations of metrics such as the NQ-NPDI technique and the resulting detector obtained from the Bayesian approach. These statistical characterizations allow us to find closed-form expressions for the detection and false alarm probabilities of these techniques by using some approximations. These probabilities are of paramount importance because they permit us to predict the performance of the PDI technique of interest in any SNR region and set a detection threshold from a false alarm probability value.

Finally, a performance comparison among the different PDI techniques proposed in this chapter and found in the literature is carried out. Simulations results reveal a clear gain in favour of the proposed techniques in terms of signal detection.

4.1 Signal model

As introduced in Chapter 3, HS-GNSS receivers use long correlation intervals to detect weak signals in two steps. First, the CAF is calculated by performing the correlation between the local replica and the received signal using an integration time as long as possible. Second, several CAFs are combined non-coherently by the application of a PDI technique to avoid the cancellation of the signal due to the residual frequency offset and data bits. This process is usually done for all the satellites, but in this thesis, we focus on acquiring only a satellite because it is enough to analyse the detection problem. The

result of this process is the output detection metric, which can be expressed as

$$Z_x(\mathbf{x}) = f\left(\sum_{k=1}^{N_{nc}} x_k\right), \tag{4.1}$$

where $\mathbf{x} \doteq [x_1, ..., x_{N_{nc}}]^T$, $k = 1, ..., N_{nc}$ and N_{nc} is the number of non-coherent combinations, x_k is the CAF, defined in (2.14), in the instant k evaluated for a value of time-delay and Doppler frequency. In this chapter, we omit the dependence of the time-delay and Doppler frequency to simplify the notation. The problem of detecting signals can be modelled under two hypotheses H_0 and H_1 since the satellite can be in view or not.

- Under H_0: $x_k = \omega_k$ is a complex Gaussian noise with mean zero and variance σ^2 (the signal from the satellite is absent).
- Under H_1: $x_k = Ad_k e^{j\phi_k} + \omega_k$ is the signal plus complex Gaussian noise (the signal from the satellite is present).

where d_k is a random variable that contains the unknown data bits taking values -1 or 1 and A is a constant amplitude affected by an unknown time-varying phase ϕ_k. We assume that the phase of the signal can change every time instant since it is affected by frequency offset and phase noise. We introduce the rectangular form of the CAF $x_k = I_k + jQ_k$, which will be used later on, being $I_k = \mathbb{R}(x_k)$, $Q_k = \Im(x_k)$.

4.2 Generalized likelihood ratio test

In this subsection, we derive the GLRT assuming that the incoming signal contains data bits of the GNSS signal and that the phase of the signal can change for different time instants. To do so, we have to calculate the LRT and replacing the unknown phase by its ML estimate [Kay98]. A related approach was used in [Sat11], but they used a ML estimator assuming that the phase of the received signal does not change during the whole observation interval. This causes that the detector in [Sat11] is not robust against the frequency offset and variations in the carrier phase. However, in this chapter, we want to find the optimal detector being robust against any variation in the carrier phase.

The pdf of the CAF x_k, assuming that it is affected by data bits taking equiprobable

values 1 and -1, is expressed under H_1 as

$$p(\mathbf{x}|H_1,\phi_k) = \frac{1}{(\pi\sigma^2)^{N_{nc}}}\exp\left(-\sum_{k=1}^{N_{nc}}\frac{1}{\sigma^2}(I_k^2+Q_k^2+A^2)\right) \prod_{k=1}^{N_{nc}}\cosh\left(\frac{2A}{\sigma^2}(I_k\cos(\phi_k)+Q_k\sin(\phi_k))\right). \tag{4.2}$$

Under H_0, the pdf can be written as

$$p(\mathbf{x}|H_0) = \frac{1}{(\pi\sigma^2)^{N_{nc}}}\exp\left(-\sum_{k=1}^{N_{nc}}\frac{1}{\sigma^2}(I_k^2+Q_k^2)\right). \tag{4.3}$$

The detector is derived by invoking the GLRT, which consists in applying the LRT and replacing the unknown parameter with its ML estimate as follows,

$$\Lambda(\mathbf{x}) = \frac{p(\mathbf{x}|H_1,\hat{\phi}_k)}{p(\mathbf{x}|H_0)} \lessgtr \tilde{\gamma}, \tag{4.4}$$

where $\tilde{\gamma}$ is the detection threshold, $\Lambda(\mathbf{x})$ is the GLRT and $\hat{\phi}_k$ is the ML estimate of ϕ_k. Substituting (4.2) and (4.3) into (4.4) and including the constants terms in a new threshold γ', the LRT can be rewritten as

$$\Lambda'(\mathbf{x}) = \prod_{k=1}^{N_{nc}}\cosh\left(\frac{2A}{\sigma^2}(I_k\cos(\hat{\phi}_k)+Q_k\sin(\hat{\phi}_k))\right) \lessgtr \gamma'. \tag{4.5}$$

Taking the logarithm operation on both sides of (4.5), we get the log-LRT as

$$L(\mathbf{x}) = \sum_{k=1}^{N_{nc}}\ln\left(\cosh\left(\frac{2A}{\sigma^2}(I_k\cos(\hat{\phi}_k)+Q_k\sin(\hat{\phi}_k))\right)\right), \tag{4.6}$$

where $L(\mathbf{x}) = \ln(\Lambda'(\mathbf{x}))$. Now, we substitute the ML estimate of the phase assuming that ϕ_k can take different values at each time instant. In this case, the ML estimate is the arctangent discriminator as $\hat{\phi}_k = \operatorname{atan}(Q_k/I_k)$ [Bor09b, Kap05]. By replacing the unknown phase and making some simplifications, the resulting detector is expressed as follows,

$$L(\mathbf{x}) = \sum_{k=1}^{N_{nc}}\left[\ln\left(\cosh\left(\frac{2A|x_k|}{\sigma^2}\right)\right)\right] \lessgtr \gamma, \tag{4.7}$$

where $\gamma = \ln(\gamma')$. Nevertheless, it is not desirable to use this detector because the relationship between the amplitude A and the noise power σ^2 must be known a priori and, in practice, this is normally not possible. To circumvent this impairment, some approximations can be made to the function $\ln(\cosh(x))$.

On the one hand, using the Taylor's series, an approximation of $\cosh(x)$ for small values of x is $1 + x^2/2$. Moreover, the Taylor series expansion of the logarithm function is $\ln(x+1) \approx x$. Combining the two expressions, we obtain $\ln(\cosh(x)) \approx x^2/2$. Thus, for small values of x and including all of the constant terms in the threshold, the resulting detector is well approximated by the conventional NPDI technique as

$$Z_{\text{NPDI}}(\mathbf{x}) = \sum_{k=1}^{N_{nc}} |x_k|^2 \lessgtr \gamma_{Z_{\text{NPDI}}}. \tag{4.8}$$

On the other hand, for large values of x, the $\cosh(x)$ can be approximated by $e^{|x|}/2$. Taking the logarithm function, the approximation of the function $\ln(\cosh(x))$ is $|x| - \ln(2)$. Thereby, if x is large, the approximation of the resulting detector leads to another technique, referred to as Non-Quadratic PDI (NQ-NPDI), since the constant terms can be incorporated into the threshold as

$$Z_{\text{NQ-NPDI}}(\mathbf{x}) = \sum_{k=1}^{N_{nc}} |x_k| \lessgtr \gamma_{Z_{\text{NQ-NPDI}}}. \tag{4.9}$$

It is worth noticing that even though the NQ-NPDI can be found in radar systems, this technique is practically unknown in GNSS systems. To date, most HS-GNSS receivers implement the NPDI technique.

Figure 4.1 shows the fit among the function $\ln(\cosh(x))$ and its approximations for small and large values of x as $x^2/2$ and $|x| - \ln(2)$, respectively. We can see that the NPDI detector fits very well for small values of x and the NQ-NPDI detector has an excellent fit for large values of x. From Figure 4.1, we obtain the trade-off between the NPDI and NQ-NPDI techniques. For $x > 1.2$, it is better to apply the NQ-NPDI detector and whether $x < 1.2$ it is preferable to use the NPDI technique. As we will see later on, the implementation of the NQ-NPDI detector provides a gain over the NPDI detector in HS-GNSS receivers. This occurs because HS-GNSS receivers adopt a long T_{coh} and a small N_{nc} value to detect the signal using the minimum total integration time (taking into account coherent and the non-coherent integration time). Moreover, the signal must be discriminated among a large amount of samples of noise, which causes that SNR at the output of the CAF cannot be small since performing a small N_{nc} value the signal is acquired. This SNR value is different from the C/N_0 of the received signal since the former depends on T_{coh} used in the CAF. The longer the T_{coh} used to compute the CAF, the larger the magnitude of the SNR at the output of the CAF. If long T_{coh} is used, the term $\frac{2A|x_k|}{\sigma^2}$ is usually a relative large number and for this reason, the resulting detector is better approximated by the NQ-NPDI technique.

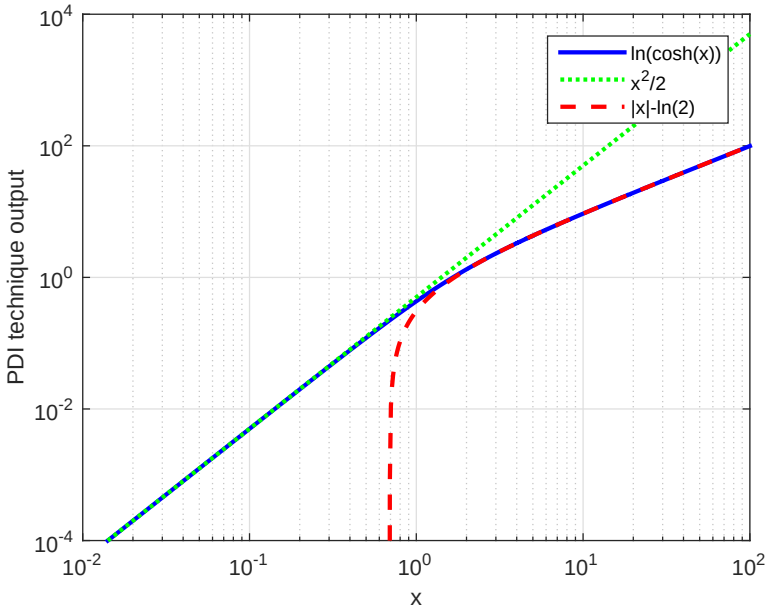

Figure 4.1: Approximation of $\ln(\cosh(x))$ for small and large values of x.

4.3 Bayesian approach

The Bayesian approach is based on using a priori information about the unknown parameter (in this case phase of the incoming signal) to obtain unconditional pdf, which no longer depends on the unknown parameter, and thus the LRT can be assessed without problems. This approach is based on a ratio of pdfs and in this case it can be written as

$$\Lambda_B(\mathbf{x}) = \frac{\int p(\mathbf{x}|H_1,\phi_k)p(\phi_k)d\phi_k}{p(\mathbf{x}|H_0)} = \frac{p(\mathbf{x}|H_1)}{p(\mathbf{x}|H_0)} \lessgtr \tilde{\gamma}_B, \tag{4.10}$$

where $p(\mathbf{x}|H_1)$ is the unconditional pdf, $p(\phi_k)$ is so-called the prior pdf and the pdfs $p(\mathbf{x}|H_0)$ and $p(\mathbf{x}|H_1,\phi_k)$ are defined in (4.2) and (4.3), respectively. To apply the Bayesian approach, let us start to calculate the ratio between $p(\mathbf{x}|H_1,\phi_k)$ and $p(\mathbf{x}|H_0)$. This result neglecting some irrelevant constants leads to the following expression

$$\prod_{k=1}^{N_{nc}} \cosh\left(\frac{2A}{\sigma^2}(I_k\cos(\phi_k) + Q_k\sin(\phi_k))\right). \tag{4.11}$$

Now, we calculate the Bayesian approach by removing the dependence on the phase information by averaging (4.11). To do so, we assume that ϕ_k is a random variable, which follows a uniform distribution from $-\pi$ to π. Proceeding in this way, the resulting

Bayesian approach is

$$\Lambda'_B(\mathbf{x}) = \frac{1}{(2\pi)^{N_{nc}}} \int_{-\pi}^{\pi} \prod_{k=1}^{N_{nc}} \cosh\left(\frac{2A}{\sigma^2}\xi(I_k, Q_k, \phi_k)\right) d\phi_k \tag{4.12}$$

being

$$\xi(I_k, Q_k, \phi_k) = I_k \cos(\phi_k) + Q_k \sin(\phi_k). \tag{4.13}$$

To solve the integral in (4.12), we make a transformation of (4.13) as

$$\xi(I_k, Q_k, \phi_k) = \sqrt{I_k^2 + Q_k^2}\cos(\phi_k - \operatorname{atan}(Q_k/I_k)) = |x_k|\cos(\phi_k - \operatorname{atan}(Q_k/I_k)). \tag{4.14}$$

By doing so, (4.12) can be expressed as follows:

$$\begin{aligned}
\Lambda'_B(\mathbf{x}) &= \frac{1}{(2\pi)^{N_{nc}}} \int_{-\pi}^{\pi} \prod_{k=1}^{N_{nc}} \frac{\mathrm{e}^{\left(\frac{2A}{\sigma^2}|x_k|\cos(\phi_k - \operatorname{atan}(Q_k/I_k))\right)} + \mathrm{e}^{-\left(\frac{2A}{\sigma^2}|x_k|\cos(\phi_k - \operatorname{atan}(Q_k/I_k))\right)}}{2} d\phi_k \\
&= \frac{1}{(2\pi)^{N_{nc}}} \left(\int_{-\pi}^{\pi} \frac{\mathrm{e}^{\left(\frac{2A}{\sigma^2}|x_1|\cos(\phi_1)\right)}}{2} d\phi_1 + \int_{-\pi}^{\pi} \frac{\mathrm{e}^{-\left(\frac{2A}{\sigma^2}|x_1|\cos(\phi_1)\right)}}{2} d\phi_1) \right) \\
&\cdots \left(\int_{-\pi}^{\pi} \frac{\mathrm{e}^{\left(\frac{2A}{\sigma^2}|x_2|\cos(\phi_2)\right)}}{2} d\phi_2 + \int_{-\pi}^{\pi} \frac{\mathrm{e}^{-\left(\frac{2A}{\sigma^2}|x_2|\cos(\phi_2)\right)}}{2} d\phi_2 \right) \\
&\cdots \left(\int_{-\pi}^{\pi} \frac{\mathrm{e}^{\left(\frac{2A}{\sigma^2}|x_{N_{nc}}|\cos(\phi_{N_{nc}})\right)}}{2} d\phi_{N_{nc}} + \int_{-\pi}^{\pi} \frac{\mathrm{e}^{-\left(\frac{2A}{\sigma^2}|x_{N_{nc}}|\cos(\phi_{N_{nc}})\right)}}{2} d\phi_{N_{nc}} \right) \\
&= I_0\left(\frac{2A}{\sigma^2}|x_1|\right) \cdots I_0\left(\frac{2A}{\sigma^2}|x_2|\right) \cdots I_0\left(\frac{2A}{\sigma^2}|x_{N_{nc}}|\right) \\
&= \prod_{k=1}^{N_{nc}} I_0\left(\frac{2A}{\sigma^2}|x_k|\right),
\end{aligned} \tag{4.15}$$

where I_0 is the modified Bessel function of the first kind and order 0. Finally, applying the logarithm on both sides, we get

$$L'_B(\mathbf{x}) = \sum_{k=1}^{N_{nc}} \ln\left(I_0\left(\frac{2A}{\sigma^2}|x_k|\right)\right) \lessgtr \gamma_B. \tag{4.16}$$

The optimal detector to acquire GNSS signals assuming that ϕ_k is a random variable with uniform distribution is shown in (4.16). Nonetheless, this detector is difficult to implement in practice since the amplitude A and the noise power σ^2 must be known a priori and it is not usually possible. For this reason, to avoid this obstacle two useful approximations of the function $\ln(I_0(x))$ are applied. On the one hand, the function $\ln(I_0(x))$ can be approximated by $x^2/4$ for small values of x. On the other hand, a good

approximation of the function $\ln(I_0(x))$ is $x - \ln\left(\sqrt{2\pi x}\right)$ for large values of x. However, this approximation has the same problem as the $\ln(I_0(x))$ function, which is the amplitude A and the noise power σ must be known a priori. Then, the function $x - \ln\left(\sqrt{2\pi x}\right)$ is approximated by x for larger values of x. By using these approximations, the optimal detector defined in (4.16) leads to the implementation of the NPDI detector for a low SNR region in (4.8) and the NQ-NPDI detector for a high SNR region as in (4.9), reproduced here for the sake of clarity:

$$Z_{\text{NPDI}}(\mathbf{x}) = \sum_{k=1}^{N_{nc}} |x_k|^2 \lessgtr \gamma_{Z_{\text{NPDI}}} \tag{4.17}$$

$$Z_{\text{NQ-NPDI}}(\mathbf{x}) = \sum_{k=1}^{N_{nc}} |x_k| \lessgtr \gamma_{Z_{\text{NQ-NPDI}}}. \tag{4.18}$$

Figure 4.2 shows the comparison among the functions $\ln(I_0(x))$, $x^2/4$, $x - \ln\left(\sqrt{2\pi x}\right)$, and $x - \ln\left(\sqrt{2\pi}\right)$. The function $\ln(I_0(x))$ is well approximated by $x^2/4$ if x is lower than 2. However, the function $x - \ln\left(\sqrt{2\pi}\right)$ is a good fit of $\ln(I_0(x))$ for $x > 2$. This result is quite similar to the one obtained in Figure 4.1, which was performed for the GLRT approach.

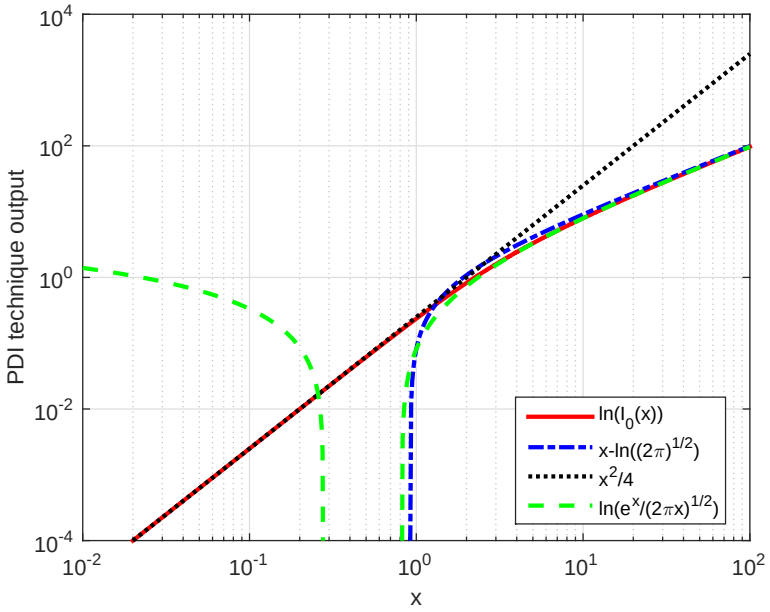

Figure 4.2: Approximation of $\ln(I_0(x))$ for small and large values of x.

4.4 Discussion between the GLRT and the Bayesian approach

In the two previous subsections, we have applied the Bayesian approach and the GLRT to find the optimal technique to detect weak GNSS signals using a pdf that take into account unknown data bits and phase changes of the received signal. In Section 4.2, we have assumed that the phase of the received signal is unknown. The outcome of this approach is shown in (4.7), which leads to the use of $\ln(\cosh(x))$ function. However, in Section 4.3, we have applied the Bayesian approach considering that the phase information of the received signal is a uniform random variable. The resulting detector expressed in (4.16) leads to the use of the $\ln(I_0(x))$ function. Although the outcome from the two approaches is different, the resulting detectors in both cases are well approximated by the NPDI technique for small values of x and if x is large, the detectors have an excellent fit using the NQ-NPDI technique.

Despite the fact that the $\ln(\cosh(x))$ and $\ln(I_0(x))$ functions can be approximated by a quadratic term if x is small or by a linear term for large values of x, they are different functions. The computational load of $I_0(x)$ is much larger than the one obtained from the $\cosh(x)$ because the former needs to be evaluated numerically and the latter can be obtained from a simple formula. This is an interesting point since if these two techniques provide similar performance and one has to choose between these techniques, the result obtained from the GLRT approach would be a detector more useful to be applied in practice owing to its computational load.

Moreover, another interesting issue is that it is not clear where is exactly the trade-off between the NQ-NPDI and NPDI techniques in terms of SNR at the output of the CAF. We have shown that approximately the turning point of using the NQ-NPDI or the NPDI is when the term $\frac{2A}{\sigma^2}|x_k|$ is close to 1.2 and 2 according to the GLRT and the Bayesian approach, respectively. However, the term $\frac{2A}{\sigma^2}|x_k|$ is not exactly the SNR, which is a parameter of interest to characterize where is the compromise between the NQ-NPDI and NPDI techniques. For this reason, in Section 4.6, we try to find the region of SNR values that indicate when the NQ-NPDI technique works better than NPDI technique and vice versa.

4.5 Statistical characterization of PDI techniques

This section provides the statistical characterization of the NQ-NPDI technique and the resulting detector from the Bayesian approach, which the latter must offer the optimal performance under the assumed conditions. The literature still lacks a theoretical analysis of these PDI techniques. The analysis involves obtaining closed-form expressions of the detection and false alarm probabilities of these detectors. We do not make a statistical characterization of the NPDI technique since its false alarm and detection probabilities are well-known in the literature and were defined in (3.3) and (3.2), respectively.

Closed-form expressions of the detection and false alarm probabilities become necessary to set an appropriate detection threshold or to be able to predict the performance of a detector. These probabilities require the knowledge about the cdf of the metrics of the PDI techniques under H_0 and H_1, as it is explained in Section 2.2.1. However, closed-form expressions of these cdfs are not known owing to the complexity introduced by the sum of N_{nc} independent random variables, which use the modified Bessel function and the absolute value, for the result from the Bayesian approach and the NQ-NPDI technique, respectively.

In this situation, approximations of the cdfs of the metric of these techniques are needed to be able to compute the probabilities of interest. A simple approximation of the sum of distributions involves the use of the CLT theorem because the metric of these techniques asymptotically converges to a Gaussian distribution for large values of N_{nc}. However, if the N_{nc} value is not large enough, the CLT does not offer an acceptable approximation, particularly at the tail region, where the probabilities of interest are often calculated.

One way to reduce the error introduced by the CLT approximation is by exploiting the Edgeworth series, which use some coefficients that depend on the moments of the variable of the metric of the technique [Pap02, Ken68, Cra46]. Another approach consists in applying the saddle-point approximation, which could offer even better accuracy than the Edgeworth series. Nevertheless, the saddle-point approximation requires the prior knowledge about the moment-generating function for the distribution of interest [Dan54]. Unfortunately, this function is not always known or it is very complex to obtain a manipulable expression. An additional interesting approach consists in improving the convergence speed of the distribution of the technique using a fractional exponential, which is very practical in some cases as we will see for the NQ-NPDI technique. For this reason, the best options to estimate the distribution of the techniques is by using the

Edgeworth series or applying a non-linear function to improve its convergence speed to a Gaussian distribution.

4.5.1 Edgeworth series

Edgeworth series are an indispensable tool to obtain an accurate approximation of the pdf and cdf for a random variable, which has been obtained from summing several independent random variables. These series provide some clues to enhance the CLT approximation by introducing some terms that depend on Hermite polynomials and the moments of the random variable. More precisely, Edgeworth series are a particular case of the Gram-Charlier Type A series, which are defined as

$$f_{GC}(\tilde{Z}) = \frac{1}{\sqrt{2\pi}\sigma_Z} e^{-\frac{\tilde{Z}^2}{2}} \left[1 + \sum_{n=3}^{\infty} \frac{C_n}{n!} H_n\left(\tilde{Z}\right) \right], \tag{4.19}$$

$$F_{GC}(\tilde{Z}) = \Phi(\tilde{Z}) - \frac{1}{\sqrt{2\pi}} e^{-\frac{\tilde{Z}^2}{2}} \left[\sum_{n=3}^{\infty} \frac{C_n}{n!} H_{n-1}\left(\tilde{Z}\right) \right], \tag{4.20}$$

where f_{GC} and F_{GC} are the Gram-Charlier Type A series approximation for the pdf and cdf, respectively, $\tilde{Z} \doteq \frac{Z-\mu_Z}{\sigma_Z}$, μ_Z and σ_Z are the mean and the standard deviation of the variable Z, $\Phi(\tilde{Z}) = \int_{-\infty}^{\tilde{Z}} \frac{1}{\sqrt{2\pi}\sigma_Z} e^{-\frac{\lambda^2}{2}} d\lambda$, $H_n(\tilde{Z})$ are the Hermite polynomials, which are given by

$$H_n(\tilde{Z}) = (-1)^n e^{\frac{\tilde{Z}^2}{2}} \frac{\partial^n}{\partial \tilde{Z}^n} e^{\frac{-\tilde{Z}^2}{2}}. \tag{4.21}$$

being

$$
\begin{aligned}
H_0(\tilde{Z}) &= 1 \\
H_1(\tilde{Z}) &= \tilde{Z} \\
H_2(\tilde{Z}) &= \tilde{Z}^2 - 1 \\
H_3(\tilde{Z}) &= \tilde{Z}^3 - 3\tilde{Z} \\
H_4(\tilde{Z}) &= \tilde{Z}^4 - 6\tilde{Z}^2 + 3 \\
H_5(\tilde{Z}) &= \tilde{Z}^5 - 10\tilde{Z}^3 + 15\tilde{Z} \\
H_6(\tilde{Z}) &= \tilde{Z}^6 - 15\tilde{Z}^4 + 45\tilde{Z}^2 - 15 \\
H_7(\tilde{Z}) &= \tilde{Z}^7 - 21\tilde{Z}^5 + 105\tilde{Z}^3 - 105\tilde{Z} \\
H_8(\tilde{Z}) &= \tilde{Z}^8 - 28\tilde{Z}^6 + 210\tilde{Z}^4 - 420\tilde{Z}^2 + 105 \\
H_9(\tilde{Z}) &= \tilde{Z}^9 - 36\tilde{Z}^7 + 378\tilde{Z}^5 - 1260\tilde{Z}^3 + 945\tilde{Z} \\
H_{10}(\tilde{Z}) &= \tilde{Z}^{10} - 45\tilde{Z}^8 + 630\tilde{Z}^6 - 3150\tilde{Z}^4 + 4725\tilde{Z}^2 - 945 \\
H_{11}(\tilde{Z}) &= \tilde{Z}^{11} - 55\tilde{Z}^9 + 990\tilde{Z}^7 - 6930\tilde{Z}^5 + 17325\tilde{Z}^3 - 10395\tilde{Z} \\
H_{12}(\tilde{Z}) &= \tilde{Z}^{12} - 66\tilde{Z}^{10} + 1485\tilde{Z}^8 - 13860\tilde{Z}^6 + 51975\tilde{Z}^4 - 62370\tilde{Z}^2 + 10395.
\end{aligned} \tag{4.22}
$$

The coefficients C_n can be expressed as

$$
C_n = \int_{-\infty}^{\infty} H_n(\tilde{Z}) p_Z(\tilde{Z}) d\tilde{Z}, \tag{4.23}
$$

where $p_Z(\tilde{Z})$ is the pdf of the random variable Z. After some straightforward, but tedious manipulations, it is found that

$$
C_3 = \frac{\mu_{Z,3} - 3\mu_{Z,1}\mu_{Z,2} + 2\mu_{Z,1}^3}{\sigma_Z^3}, \tag{4.24}
$$

$$
C_4 = \frac{\mu_{Z,4} - 4\mu_{Z,1}\mu_{Z,3} + 6\mu_{Z,1}^2\mu_{Z,2} - 3\mu_{Z,1}^4}{\sigma_Z^4} - 3, \tag{4.25}
$$

$$
C_5 = \frac{\mu_{Z,5} - 5\mu_{Z,4}\mu_{Z,1} + 10\mu_{Z,3}\mu_{Z,1}^2 - 10\mu_{Z,2}\mu_{Z,1}^3 + 4\mu_{Z,1}^5}{\sigma_Z^5} - 10\frac{\mu_{Z,3} - 3\mu_{Z,1}\mu_{Z,2} + 2\mu_{Z,1}^3}{\sigma_Z^3}, \tag{4.26}
$$

$$
\begin{aligned}
C_6 = &\frac{\mu_{Z,6} - 6\mu_{Z,5}\mu_{Z,1} + 15\mu_{Z,4}\mu_{Z,1}^2 - 20\mu_{Z,1}^3\mu_{Z,3} + 15\mu_{Z,2}\mu_{Z,1}^4 - 5\mu_{Z,1}^6}{\sigma_Z^6} + 30 \\
&- 15\frac{\mu_{Z,4} - 4\mu_{Z,1}\mu_{Z,3} + 6\mu_{Z,1}^2\mu_{Z,2} - 3\mu_{Z,1}^4}{\sigma_Z^4},
\end{aligned} \tag{4.27}
$$

where $\mu_{Z,p} = \mathrm{E}\left[Z^p\right]$ is the p-th moment of the random variable under analysis, which has been calculated through some tedious manipulations. This result for the first most

commonly used moments is shown as follows,

$$\mu_{Z,1} = N_{nc}\mu_{x,1}, \tag{4.28}$$

$$\mu_{Z,2} = N_{nc}(\mu_{x,2} + (N_{nc}-1)\mu_{x,1}^2), \tag{4.29}$$

$$\mu_{Z,3} = N_{nc}(\mu_{x,3} + (N_{nc}-1)(3\mu_{x,2}\mu_{x,1} + (N_{nc}-2)\mu_{x,1}^3)), \tag{4.30}$$

$$\mu_{Z,4} = N_{nc}(\mu_{x,4} + (N_{nc}-1)(4\mu_{x,3}\mu_{x,1} + 3\mu_{x,2}^2 + (N_{nc}-2)(6\mu_{x,2}\mu_{x,1}^2 + (N_{nc}-3)\mu_{x,1}^4))), \tag{4.31}$$

$$\mu_{Z,5} = N_{nc}\,(\mu_{x,5} + (N_{nc}-1)(5\mu_{x,4}\mu_{x,1} + 10\mu_{x,3}\mu_{x,2} + (N_{nc}-2)(10\mu_{x,3}\mu_{x,1}^2 + 15\mu_{x,2}^2\mu_{x,1} + (N_{nc}-3)(10\mu_{x,1}^3\mu_{x,2} + (N_{nc}-4)\mu_{x,1}^5)))), \tag{4.32}$$

$$\mu_{Z,6} = N_{nc}(\mu_{x,6} + (N_{nc}-1)(6\mu_{x,5}\mu_{x,1} + 10\mu_{x,3}^2 + 15\mu_{x,4}\mu_{x,2} + (N_{nc}-2)(15\mu_{x,4}\,\mu_{x,1}^2 + 15\mu_{x,2}^3 + 60\mu_{x,2}\mu_{x,3}\mu_{x,1} + (N_{nc}-3)(20\mu_{x,3}\mu_{x,1}^3 + 45\mu_{x,1}^2\mu_{x,2}^2 + (N_{nc}-4)(15\mu_{x,2}\mu_{x,1}^4 + (N_{nc}-5)\mu_{x,1}^6))))). \tag{4.33}$$

The $\mu_{Z,p}$ moments depend on the moments of the individual term inside the PDI technique. On the one hand for the result of the Bayesian approach the moments $\mu_{Z,p}$ are affected by the moments of $\ln\left[I_0\left(\frac{2A|x_k|}{\sigma^2}\right)\right]$ variable, which are denote as $\mu_{x,l} = \mathrm{E}\left[\left(\ln\left[I_0\left(\frac{2A|x_k|}{\sigma^2}\right)\right]\right)^l\right]$. Because of the Rayleigh or Rice nature of $|x_k|$ for the hypotheses H_0 and H_1, respectively, the moments can be computed numerically for H_0

$$\mu_{x,l,H_0} = \int_0^\infty \left(\ln\left[I_0\left(\frac{2A|x_k|}{\sigma^2}\right)\right]\right)^l p(|x_k|;H_0)d|x_k|, \tag{4.34}$$

and for H_1

$$\mu_{x,l,H_1} = \int_0^\infty \left(\ln\left[I_0\left(\frac{2A|x_k|}{\sigma^2}\right)\right]\right)^l p(|x_k|;H_1)d|x_k|. \tag{4.35}$$

The mean and variance of these random variable, which are also required for the problem at hand, are also evaluated numerically.

On the other hand, for the NQ-NPDI technique, the moments $\mu_{x,l}$ depend on the absolute value of the received CAF, $\mu_{x,l} = E[|x_k|^l]$. Due to the complex Gaussian nature of received CAF, the moments are given by for H_0 and H_1 as [McD95]

$$\mu_{x,l|H_0} = \sigma^l\Gamma\left(1+\frac{l}{2}\right), \tag{4.36}$$

$$\mu_{x,l|H_1} = \sigma^l\Gamma\left(1+\frac{l}{2}\right)L_{l/2}(-A^2/\sigma^2), \tag{4.37}$$

where $\Gamma(x)$ is the Gamma function and $L_q(x)$ denotes a Laguerre polynomial. The mean and the variance of the NQ-NPDI technique are given by for H_0

$$\mu_{Z_{\text{NQ-NPDI}|H_0}} = N_{nc}\sigma\frac{\sqrt{\pi}}{2}, \tag{4.38}$$

$$\text{Var}(Z_{\text{NQ-NPDI}|H_0}) = N_{nc}\sigma^2(1-\pi/4), \tag{4.39}$$

and for H_1

$$\mu_{Z_{\text{NQ-NPDI}|H_1}} = N_{nc}\sigma\frac{\sqrt{\pi}}{2}L_{1/2}(-A^2/\sigma^2), \tag{4.40}$$

$$\text{Var}(Z_{\text{NQ-NPDI}|H_1}) = N_{nc}(\sigma^2 + A^2 - \pi\sigma^2/4L_{1/2}(-A^2/\sigma^2)^2), \tag{4.41}$$

Figures 4.3 and 4.4 show the comparison between the theoretical formulas of the moments $\mu_{Z,p}$ and the simulated moments using Monte-Carlo iterations for the NQ-NPDI metric under H_0 and H_1, respectively. The outcome shows that the theoretical moments obtained are exactly the same as the one obtained from simulations.

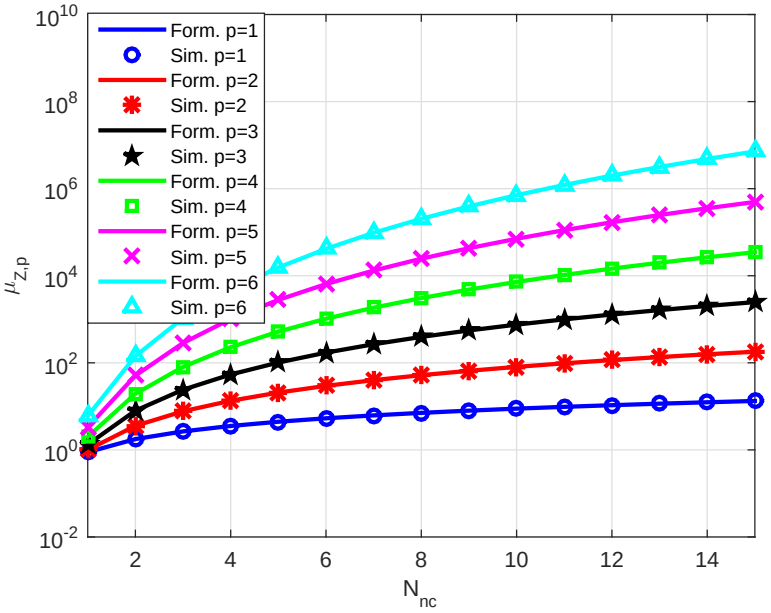

Figure 4.3: Comparison between simulated moments using Monte-carlo iterations and theoretical moments under H_0 for the NQ-NPDI technique.

Although the series in (4.19) and (4.20) decrease as $1/n!$ in the coefficients, they suffer from having poor convergence properties, which can cause an inaccurate estimation of the

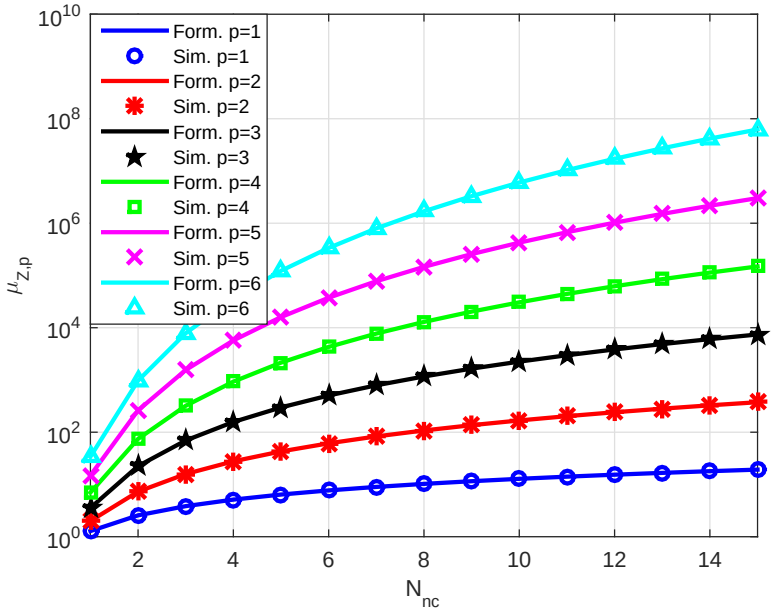

Figure 4.4: Comparison between simulated moments using Monte-carlo iterations and theoretical moments under H_1 for the NQ-NPDI technique.

pdf of interest. This problem is circumvented by taking a specific grouping of terms that guarantees the convergence of the series expansion. These groupings of terms lead to the approximations known as Edgeworth series, which are given by (4.42) and (4.43) [Cra46]

$$f_E(\tilde{Z}) = \frac{1}{\sqrt{2\pi}\sigma_Z} e^{-\frac{\tilde{Z}^2}{2}} \left[1 + \sum_{n \in \mathcal{L}} \frac{C_n^*}{n!} H_n\left(\tilde{Z}\right) \right], \tag{4.42}$$

$$F_E(\tilde{Z}) = \Phi(\tilde{Z}) - \frac{1}{\sqrt{2\pi}} e^{-\frac{\tilde{Z}^2}{2}} \left[\sum_{n \in \mathcal{L}} \frac{C_n^*}{n!} H_{n-1}\left(\tilde{Z}\right) \right], \tag{4.43}$$

where f_E and F_E are the Edgeworth series approximation for the pdf and the cdf, respectively. There are different group terms $\mathcal{L}$ that guarantee the convergence of the series. These group of terms are affected by the coefficients C_n^*. The relationship between the group of terms $\mathcal{L}$ and the coefficients C_n^* is shown in Table 4.1. The more coefficients are included in the Edgeworth series approximation, the more accurate the approximation tends to be. Nevertheless, if no coefficients are added, the Edgeworth series is the same as the CLT approximation.

Taking into account the expressions in (4.42) and (4.43), it is possible to obtain the approximation of the cdf of the PDI techniques of interest depending whether the moments of the variable have been computed for the NQ-NPDI or the result from the Bayesian

Series	$\mathcal{L}$	C_n^*
E. 1	3	C_3
E. 2	3,4,6	$C_3, C_4, 10C_3^2$
E. 3	3,4,6,	$C_3, C_4, 10C_3^2,$
	5,7,9	$C_5, 35C_4C_3, 280C_3^3$
E. 4	3,4,6,	C_3, C_4, C_6
	5,7,9,	$C_5, 35C_4C_3, 280C_3^3$
	8,10,12	$35C_4^2 + 56C_5C_3, 2100C_3^2C_4, 15400C_3^4$

Table 4.1: Relationship between the group of terms $\mathcal{L}$ and the coefficients C_n.

approach and for H_0 or H_1. Finally, from the estimation of the cdfs, we can obtain the false alarm and detection probabilities of the NQ-NPDI and the result from the Bayesian approach using the expressions in (2.16) and (2.17), respectively.

4.5.2 Detection threshold for the NQ-NPDI technique

Although the Edgeworth series provides a closed-form expression of the false alarm probability, it is not possible to isolate the detection threshold. For this reason, in this subsection, we propose another alternative to set the detection threshold for the NQ-NPDI technique.

To do so, a non-linear transformation can be applied to enhance the convergence speed of the NQ-NPDI metric to a Gaussian distribution with respect to N_{nc}. In this case, if this metric is raised to an appropriate fractional exponent, the pdf of the NQ-NPDI metric may converge faster to a Gaussian distribution. To define the detection threshold for the NQ-NPDI technique following this approach, the mean and the variance of the metric of interest raised to a fractional exponent must be calculated. To do this, we suppose that Y is a random variable, which is raised to β as

$$T = Y^{\beta}. \tag{4.44}$$

The mean and the variance of T, denoted by μ_T and $\mathrm{Var}(T)$, can be calculated using a

Taylor series, which results in [Bor14b]

$$\mu_T \approx \mu_Y^{\beta}\left[1+\frac{1}{2}\beta(\beta-1)\frac{\mathrm{Var}(Y)}{\mu_Y^2}\right], \tag{4.45}$$

$$\mathrm{Var}(T) \approx \beta^2\frac{\mathrm{Var}(Y)}{\mu_Y^{2(1-\beta)}}, \tag{4.46}$$

where μ_Y is the mean of Y and $\mathrm{Var}(Y)$ is its variance. Applying (4.45) and (4.46) in our problem, the mean and the variance of the NQ-NPDI metric under H_0 raised to the power of β are given by

$$\mu_{Z^{\beta}_{\text{NQ-NPDI}|H_0}} \approx \mu^{\beta}_{Z_{\text{NQ-NPDI}|H_0}}\left[1+\frac{1}{2}\beta(\beta-1)\frac{\mathrm{Var}(Z_{\text{NQ-NPDI}|H_0})}{\mu^2_{Z_{\text{NQ-NPDI}|H_0}}}\right], \tag{4.47}$$

$$\mathrm{Var}(Z^{\beta}_{\text{NQ-NPDI}|H_0}) \approx \beta^2\frac{\mathrm{Var}(Z_{\text{NQ-NPDI}|H_0})}{\mu^{2(1-\beta)}_{Z_{\text{NQ-NPDI}|H_0}}}, \tag{4.48}$$

where $\mu_{Z_{\text{NQ-NPDI}|H_0}}$ and $\mathrm{Var}(Z_{\text{NQ-NPDI}}|H_0)$ are the mean and the variance of the NQ-NPDI metric defined in (4.38) and (4.39). Finally, the threshold for the NQ-NPDI technique is defined considering that the NQ-NPDI metric raised to β is a Gaussian distribution as

$$\gamma_{Z_{\text{NQ-NPDI}}} \approx \mathrm{cdf}_{\mathrm{N}}^{-1}\left(1-P_{fa}, \mu_{Z^{\beta}_{\text{NQ-NPDI}|H_0}}, \sqrt{\mathrm{Var}(Z^{\beta}_{\text{NQ-NPDI}|H_0})}\right)^{\frac{1}{\beta}}, \tag{4.49}$$

where $\mathrm{cdf}_{\mathrm{N}}^{-1}$ is the inverse cumulative distribution function of a Gaussian distribution. It is worth mentioning that although the metric of the NQ-NPDI is raised to β the detection performance of the NQ-NPDI technique is the same since $\mathrm{prob}(Z_{\text{NQ-NPDI}}(\mathbf{x}) > \gamma_{Z_{\text{NQ-NPDI}}}) = \mathrm{prob}(Z^{\beta}_{\text{NQ-NPDI}}(\mathbf{x}) > \gamma^{\beta}_{Z_{\text{NQ-NPDI}}})$.

Optimum value of β

The problem is to find the optimum fractional exponent to improve the convergence speed of the NQ-NPDI metric to a Gaussian distribution for small values of N_{nc}, which are the typical values used in HS-GNSS receivers to acquire weak signals. In order to determine which is the best value of β to enhance the convergence speed of the NQ-NPDI metric, we use the Kullback-Leibler (KL) distance or divergence. The KL divergence is a measure of the distance between two pdfs as

$$D_{KL}(P||G) = \sum_{i=1}^{M} P(i)\ln\left(\frac{P(i)}{G(i)}\right), \tag{4.50}$$

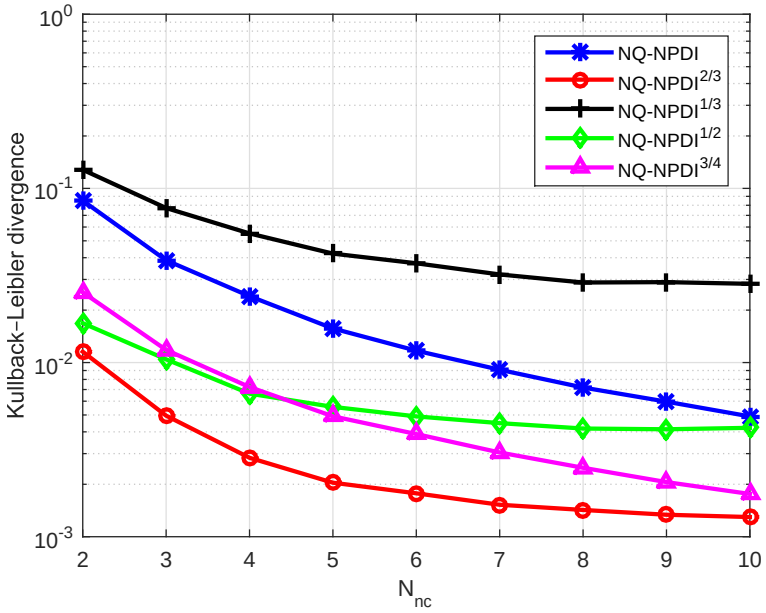

Figure 4.5: Kullback-Leibler divergence between the empirical pdf and the Gaussian approximation for different fractional exponents.

where $i = 1, ..., M$, M is the number of points of the pdf, $P(i)$ is the pdf of the NQ-NPDI metric and $G(i)$ is the Gaussian approximation of the NQ-NPDI metric.

The KL distance is computed by using different fractional exponent values i.e. raising the term NQ-NPDI to $\beta = 1/3, 1/2, 2/3, 3/4$, and 1 in Figure 4.5. The case of $\beta = 1$ corresponds to the CLT approximation. The result shows that the minimum error between the empirical pdf and the Gaussian approximation is obtained for $\beta = 2/3$. As we will see, the use of $\beta = 2/3$ in the NQ-NPDI outperforms the accuracy of the computation of the detection threshold compared to the conventional CLT approximation. We have used the fractional exponent of 2/3 in the simulation on purpose since it is known the convergence speed of a chi-squared random variable to a Gaussian distribution can be improved with respect to N_{nc} using the fractional exponent of 1/3 [Bor14b]. In H_0, the term inside the summation of the NQ-NPDI follows a Rayleigh distribution. If a Rayleigh distribution is squared, this distribution becomes a chi-square with 2 degrees of freedom. Then, intuitively, if the NQ-NPDI metric is raised to 2/3, its convergence to a Gaussian distribution will be faster, as we confirm in Figure 4.5.

4.6 Simulation results

The results are divided into two parts. The first part consists in performing a comparative analysis between the techniques obtained from the Bayesian approach and GLRT herein and the most common detectors proposed in the literature described in Subsection 3.1. The second one shows the comparison between the empirical false alarm and detection probabilities and the approximations of these probabilities presented in this chapter for the NQ-NPDI technique and the result from the Bayesian approach.

4.6.1 Detection performance under phase variations

This subsection consists of two parts. The first one deals with the comparison of the ROC curves, which are obtained from generating several independent CAFs. The second one is focused on comparing the performance of the NQ-NPDI and NPDI techniques using a HS-GNSS receiver.

4.6.1.1 Detection analysis of PDI techniques

The first test presents a performance comparison between the different detectors derived herein and those proposed in the literature, which are described in Section 3.1, by using ROC curves. Simulations are carried out assuming the signal model explained in Section 4.1 and using 1 million of Monte Carlo iterations. This signal model applies to the GPS L1 signal, which includes unknown data bits. The value of σ is 1 for all of the simulations and the value of A and N_{nc} change for the different simulations. It should be noticed that A and σ^2 are the signal amplitude and the noise power at the output of the CAF, respectively, which depend on the C/N_0 of the received signal as $C/N_0 = A^2/(T_{\text{coh}}\sigma^2)$. Thus, the ROC plots illustrated in the first part of this subsection are performed for one value of A and σ, which correspond to a C/N_0 value depending on the T_{coh} considered to compute the CAF. We perform two kind of experiments. Experiment 1: keeping the value of ϕ_k constant for all the integration time. Experiment 2: assuming that ϕ_k is a uniform random variable from 0 to 2π. This assumption is reasonable since the phase of the signal can change randomly due to phase noise, frequency offsets, data bits. It is worth mentioning that we have added in the figures the theoretical ROC curves for the NPDI technique defined in (3.3) and for the coherent integration defined in (2.23) as a benchmark.

Experiment 1

Figure 4.6 shows the ROC curves of the several detectors presented herein and the proposed detector in the literature. In this case, we can also compare the performance of the optimal detectors derived by using the GLRT and the Bayesian approach since we assume to know the value of A and σ. In this figure, we consider ϕ_k constant during all the integration time and do not consider the presence of unknown data bits for $A = 1.8$ and $N_{nc} = 6$. The best detector under these conditions without any uncertainty is the coherent integration, which sums coherently all the CAFs and performs the absolute value. This result was expected since it is well-known that the coherent integration is the optimal detector if there is no presence of change variations in the carrier phase. The worst detector under these conditions is the NPDI technique. The PDI techniques that come from the result of the GLRT and the Bayesian approach exhibit practically the same performance. In this case, these techniques are outperformed by the others proposed in the literature such as the GPDIT, NPDISD and DPDI techniques. This occurs because the phase of the signal remains stable during all the integration time and the proposed techniques herein have been derived assuming a more restrictive condition, which considers that this phase can suffer variations. Finally, we can observe that the NQ-NPDI technique provides a gain over the NPDI technique in terms of signal detection since the SNR at the output of the CAF relatively large.

Experiment 2

Figure 4.7 illustrates the comparison among the different PDI techniques considering ϕ_k as a uniform distribution from 0 to 2π with $A = 1.8$ and $N_{nc} = 6$. In this case, all of the techniques that are not robust against phase variations owing to both data bits and frequency offset such as the coherent integration, GPDIT, DPDI, NPDISD techniques suffer a strong degradation. The best performing detectors are the ones obtained from the Bayesian approach and the GLRT. They provide a performance really similar in terms of signal detection. The NQ-NPDI technique is an excellent approximation of these optimal detectors since the SNR at the output of the CAF is a value quite high approximately 5.1 dB. The approach used in this simulation is the typical one implemented in HS-GNSS receivers to detect weak GNSS signals, where N_{nc} is usually a small number since a long T_{coh} is used to compute the CAF. From this result, we can conclude that the NQ-NPDI technique is the best option to acquire GNSS signals because it provides similar performance as the one obtained from the Bayesian approach and the GLRT, but it does not require the knowledge about the A nor σ values.

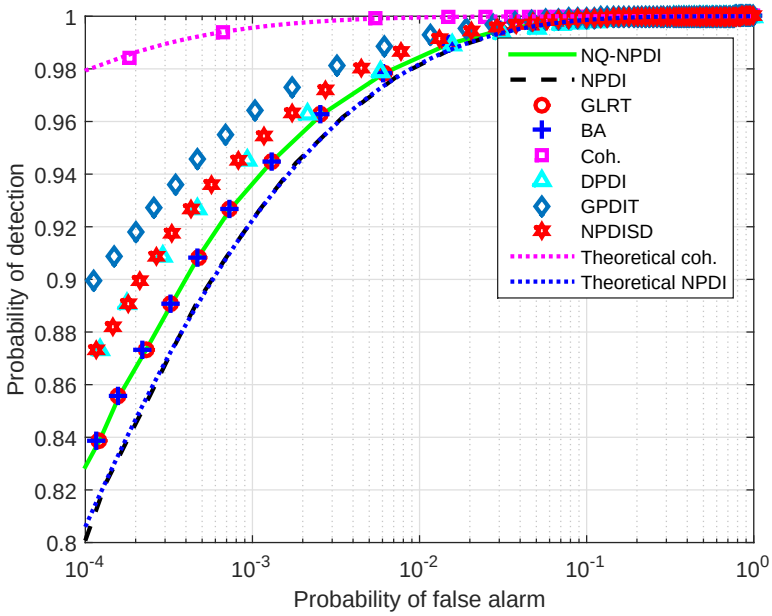

Figure 4.6: Comparison among the different PDI techniques assuming ϕ_k constant during all the integration time and for $A = 1.8$, $N_{nc} = 6$ and $\sigma = 1$. In the legend, BA means Bayesian approach and Coh. refers to coherent integration. Moreover, we have included the theoretical ROC curves for the NPDI technique and for the coherent integration as Theoretical NPDI and Theoretical coh., respectively.

In Figure 4.8, we decrease the value of A in order to find the trade off between the NPDI and NQ-NPDI techniques. The parameters used for the simulations are $A = 0.85$, $N_{nc} = 60$ and ϕ_k is assumed to be a uniform random variable. The outcome shows that the techniques that provide the best performance remain the derived from the GLRT and the Bayesian approach. Comparing the NPDI and NQ-NPDI techniques, we can see that they offer an identical performance. The value of SNR at the output of the CAF that provides the same performance for the NPDI and NQ-NPDI techniques is approximately -1.4 dB. Considering a $T_{\text{coh}} = 20$ ms, the C/N_0 of the received signal would be approximately 15.5 dB-Hz. In this condition, we need a larger N_{nc} value such as 60 to be able to obtain a similar detection probability as in the Figure 4.7. This values of N_{nc} are not often implemented in HS-GNSS receivers, since they try to detect the weak signals extending the T_{coh} as much as possible and using a small number of N_{nc} to use the minimum duration of the signal.

In Figure 4.9, we decrease further the value of A up to 0.45, and perform $N_{nc} = 500$ and ϕ_k is considered to be a uniform random variable. The best techniques remain the

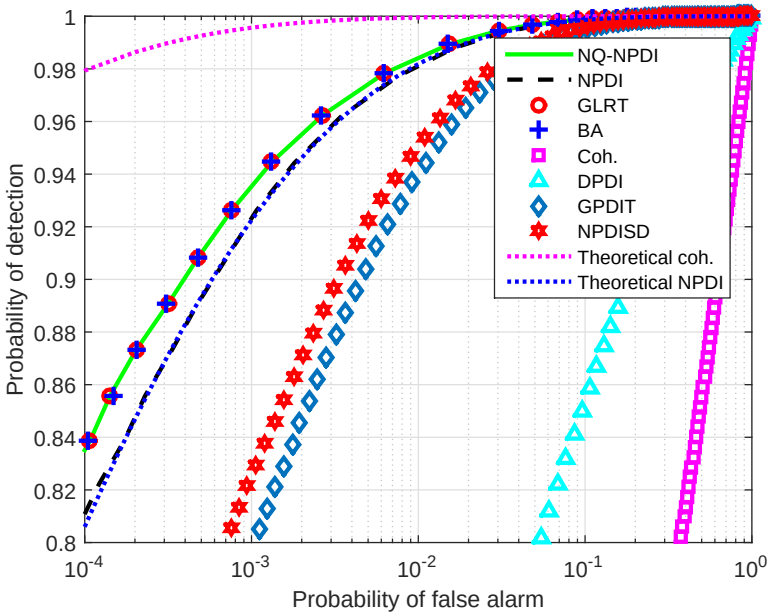

Figure 4.7: Comparison among the different PDI techniques assuming that ϕ_k follows a uniform distribution and for $A = 1.8$, $N_{nc} = 6$ and $\sigma = 1$.

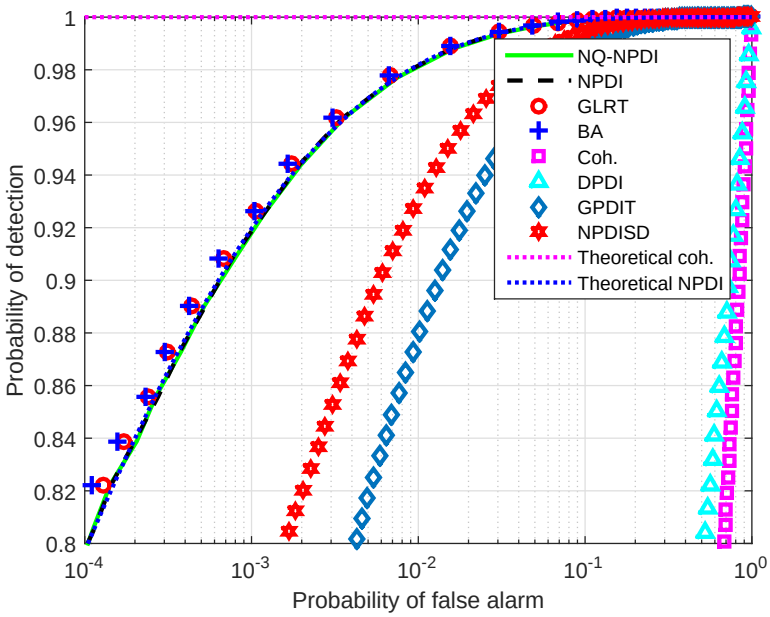

Figure 4.8: Comparison among PDI techniques assuming that ϕ_k follows a uniform distribution and for $A = 0.85$, $N_{nc} = 60$ and $\sigma = 1$.

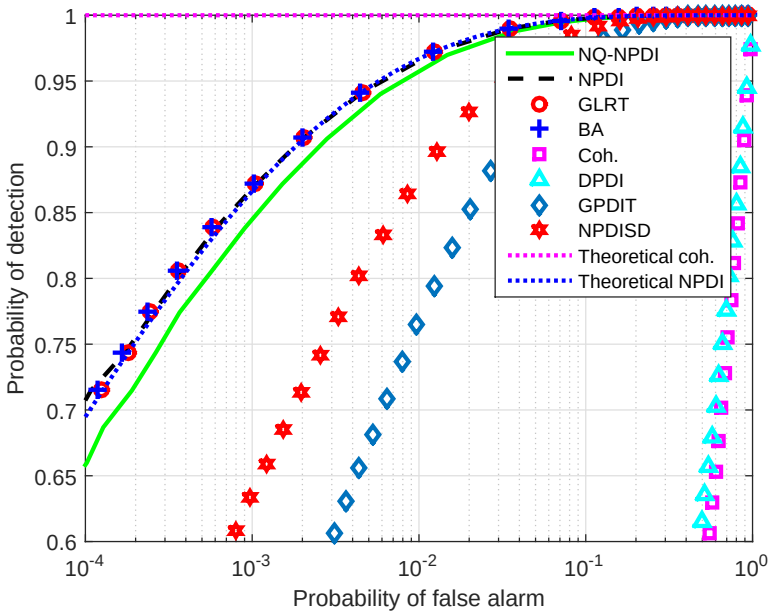

Figure 4.9: Comparison among PDI techniques assuming that ϕ_k follows a uniform distribution, $A = 0.45$, $N_{nc} = 500$ and $\sigma = 1$.

ones that were derived from the Bayesian approach and the GLRT. In this case, these techniques are well approximated by the NPDI technique since the SNR at the output of the CAF is quite small approximately -7 dB. For these values of SNR, we suggest using the NPDI technique instead of the NQ-NPDI technique.

Comparing the GLRT and the Bayesian approach for the different simulations, we can conclude that they provide an identical performance for different values of SNR, though they are different detectors. If we know the value or an approximation of A and σ and one want to obtain the optimal performance to detect weak signals with time-varying phase, we propose to use the result obtained from the GLRT approach defined in (4.7). Since it provides the same performance as the one obtained from the Bayesian approach, but it requires a lower computational load because it does not have to compute a numerical integral.

It is worth mentioning that when the techniques obtained from the GLRT and the Bayesian approach do not have the correct values of A and σ, the performance of these detectors can be between the performance of the NQ-NPDI and NPDI techniques. For instance, if we introduce an incorrect large value of A/σ^2 in the resulting detectors from the GLRT and the Bayesian approach, their performances are practically the same as the

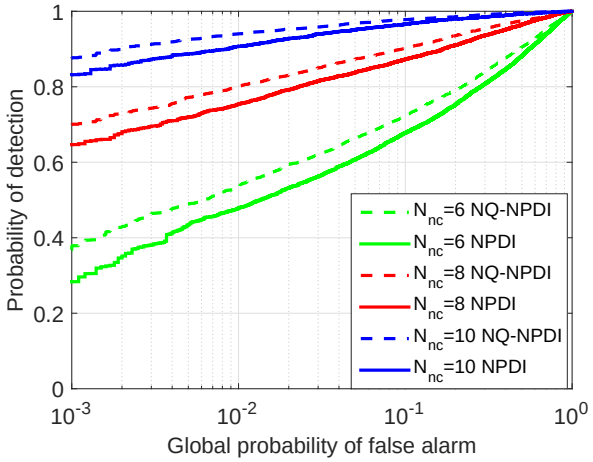

Figure 4.10: ROC comparison between the NPDI and NQ-NPDI techniques for $T_{\text{coh}} = 20$ ms, $C/N_0 = 23$ dB-Hz and using the GPS L1 signal.

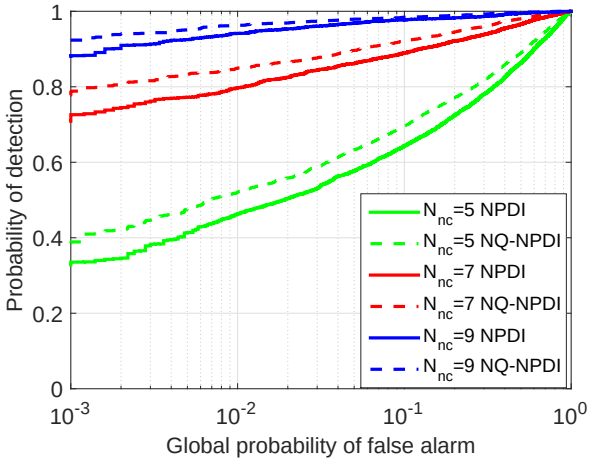

Figure 4.11: ROC comparison between the NPDI and NQ-NPDI techniques for $T_{\text{coh}} = 100$ ms, $C/N_0 = 20$ dB-Hz and using the Galileo E1BC signal.

one obtained from the NQ-NPDI technique. However, if we introduce an incorrect very small value in the detectors, the performance of the detectors is quite similar to the NPDI technique.

4.6.1.2 Comparison between the NPDI and NQ-NPDI techniques

The second part of these simulation results is based on acquiring a weak GPS L1 signal. The acquisition of the signal is performed by the application of a HS-GNSS receiver, which utilizes the double-FFT algorithm [JB06, SG12]. This algorithm provides an efficient signal acquisition using a long coherent integration time and assuming some assistance information about the Doppler of the satellite.

Figure 4.10 and 4.11 compare the ROC (i.e. the detection probability versus the global false alarm probability) of the NPDI and NQ-NPDI detectors for the GPS L1 signal (left) and Galileo E1BC (right). The results show that in both cases using a small value of N_{nc} the NQ-NPDI technique outperforms the NPDI technique in terms of signal detection. This fact occurs because the SNR at the output of the CAF is not a small number since the signal can be detected by applying a few non-coherent integrations. Therefore, the optimal detector is more accurately approximated by the NQ-NPDI technique providing a gain over the NPDI technique. This is an important result because GNSS receivers usually use the NPDI technique to acquire signals. Comparing the detection probability

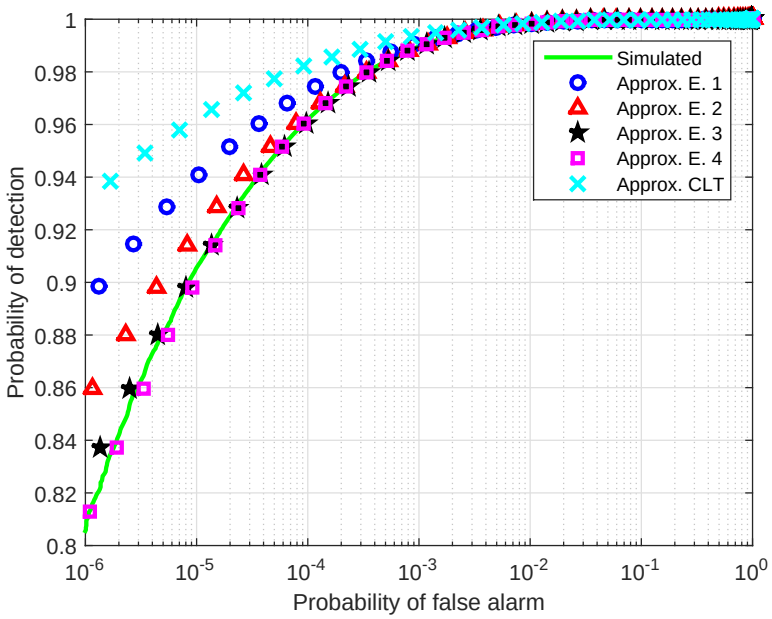

Figure 4.12: ROC curve approximations for the performance of the optimal detector using the Edgeworth series and the CLT approximation for parameters: $A = 1.7, \sigma = 1$, and $N_{nc} = 10$.

for the two techniques, we can see that, for instance, on the right figure for $N_{nc} = 7$ and detection probability of 0.85, the NQ-NPDI technique has a false alarm probability of 1e-2 while the NPDI has a value close to 3.5e-2, a value more than 3 times larger.

4.6.2 Statistical analysis of selected PDI techniques

This subsection provides the statistical characterization of the NQ-NPDI technique and the resulting technique from the Bayesian approach. This characterization is carried out by the use of the Edgeworth series described in Subsection 4.5.1 for both techniques. Moreover, for the NQ-NPDI technique, we also compare the accuracy of the Edgeworth series to the approach explained in Subsection 4.5.2 to define the detection threshold.

4.6.2.1 Statistical analysis of the Bayesian PDI technique

Simulation results are based on comparing the performance of the optimal detector in (4.16) obtained through the Monte Carlo simulations with the theoretical approximations proposed herein. Figure 4.12 illustrates ROC curves for the optimal non-coherent de-

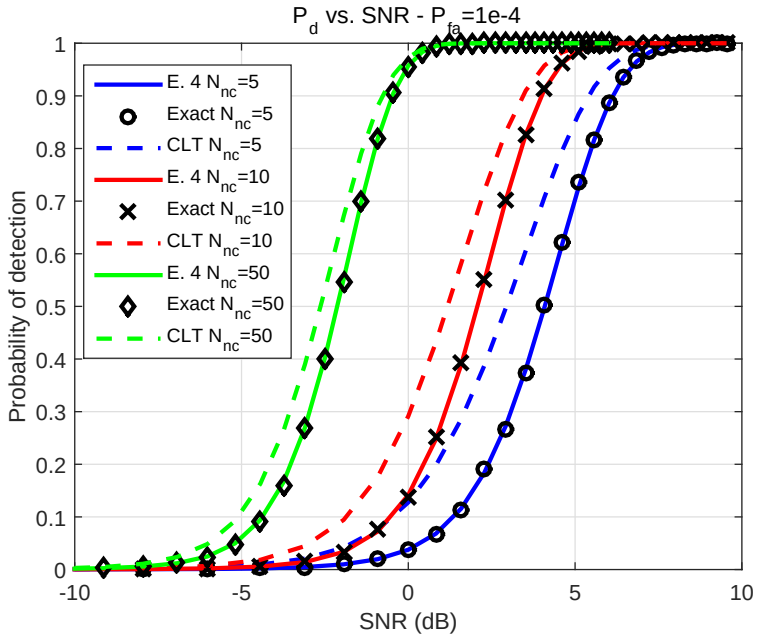

Figure 4.13: P_d vs. SNR with $N_{nc} = 5, 10, 50$ and $P_{fa} = 1e-4$ for the E.4 approximation and the optimal non-coherent detector obtained from simulations.

tector, the approximations obtained using the different Edgeworth series and the CLT approximation. The result shows that the CLT approximation is a very inaccurate approximation, particularly for small values of P_{fa}. In this figure, we can see for instance, for a detection probability of 0.94 the CLT approximation established a false alarm probability of 1.7e-6, when the empirical probability of false alarm is close to 3.5e-5. This fact causes that the CLT approximation provides a false alarm probability value approximately twenty times smaller than the empirical one. Nevertheless, the Edgeworth series approximation reduces the error offered by the CLT approximation. The more coefficients we add to the series, the smaller the error between the simulated ROC curve and the theoretical one. From this result, we can conclude that the E.4 approximation of the Edgeworth series defined in the Table 4.1 is the most accurate approximation and it allows us to predict the performance of the optimal detector even for small values of P_{fa}, which are the most common values used in the receivers.

Figure 4.13 shows the P_d vs. SNR for the optimal non-coherent detector, the E.4 approximation obtained from the Edgeworth series and the CLT. The result shows that the E.4 approximation is a very good fit and it is able to predict the detection probability of the optimal detector for any value of N_{nc} and SNR. This is an important result since it provides us prior knowledge about the P_d of this detector. The CLT approximation offers

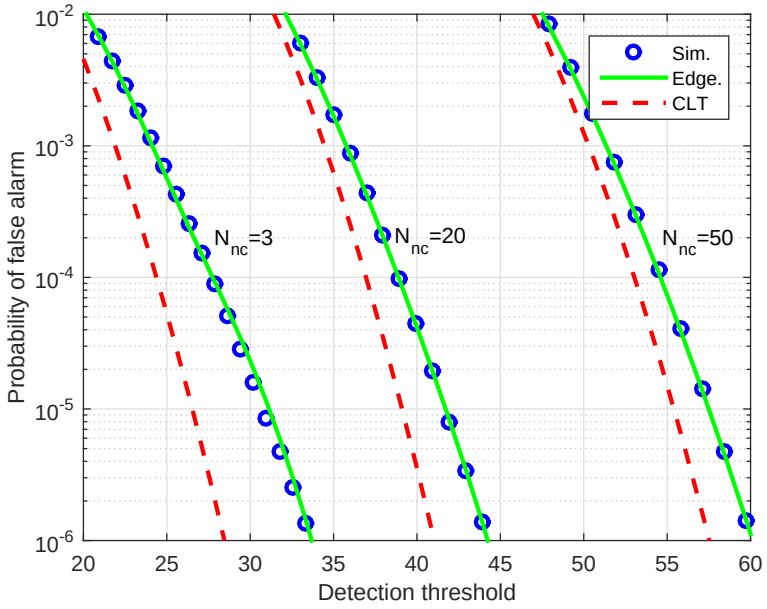

Figure 4.14: P_{fa} vs. detection threshold with $N_{nc} = 3, 20$ and 50 for the E.4 and CLT approximations and the optimal non-coherent detector obtained from simulations.

a considerably error for small values of N_{nc}. However, the larger the N_{nc}, the better the accuracy of the CLT approximation is. This occurs because the statistics of the optimal non-coherent detector tends to be Gaussian for large values of N_{nc}.

Figure 4.14 illustrates the error between the P_{fa} of the optimal detector with the E.4 and CLT approximations. The use of the Edgeworth series is preferable since it is a more effective approximation than the CLT, particularly at the tail region. The Edgeworth series allow us to set an extremely accurate detection threshold to distinguish if the signal is present or absent. The error introduced by the CLT is really significant, especially for small values of P_{fa}, which are typically implemented in receivers to avoid false alarm problems.

4.6.2.2 Statistical analysis of the NQ-NPDI technique

This subsection presents the results of the statistical characterization of the NQ-NPDI technique. The first simulation is based on comparing the approximated and empirical ROC curves of the NQ-NPDI technique for $N_{nc} = 10$, $A = 1.7$ and $\sigma = 1$ in Figure 4.15. In this figure, we have also added the empirical and theoretical ROC curves of the NPDI technique. From this figure, the result illustrates that the Edgeworth series

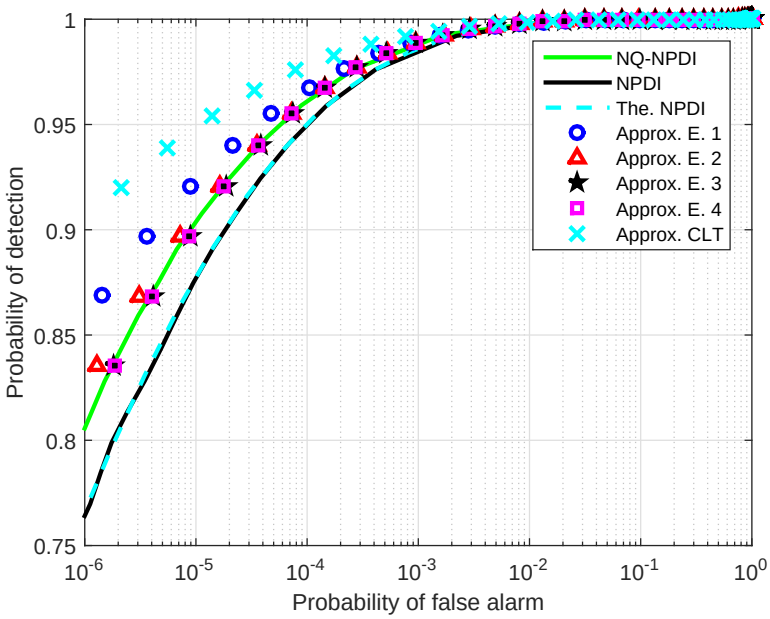

Figure 4.15: ROC curve approximations for the performance of the NQ-NPDI technique using the Edgeworth series and the CLT approximation for parameters: $A = 1.7, \sigma = 1$, and $N_{nc} = 10$. 'The. NPDI" represents the theoretical ROC curve of NPDI technique.

becomes necessary to predict the performance of the NQ-NPDI technique. The CLT approximation provides an inaccurate approximation with respect to the simulated ROC curve, in particular for small values of false alarm probability. Nonetheless, the error of the CLT approximation is reduced by applying the Edgeworth series. The larger the number of coefficients used in this series, the smaller the error between the empirical and approximated ROC curve. In this case, the approximations E.3 and E.4 provide a perfect math with the empirical curve.

Figure 4.16 shows the P_d vs. SNR for the NQ-NPDI and NPDI techniques, the E.4 approximation obtained from the Edgeworth series, the CLT approximation and the theoretical performance of the NPDI technique. The result shows that the E.4 approximation is an excellent fit of the empirical detection probability of the NQ-NPDI technique. We can observe that the CLT approximation provides a significant error with respect to the empirical detection probability. Moreover, as we previously discussed, we can see that the NQ-NPDI technique provides a signal detection gain over the NPDI technique.

Figure 4.17 illustrates the false alarm probability of the NQ-NPDI metric, the CLT approximation, the Edgeworth approximation and the new approximation proposed herein

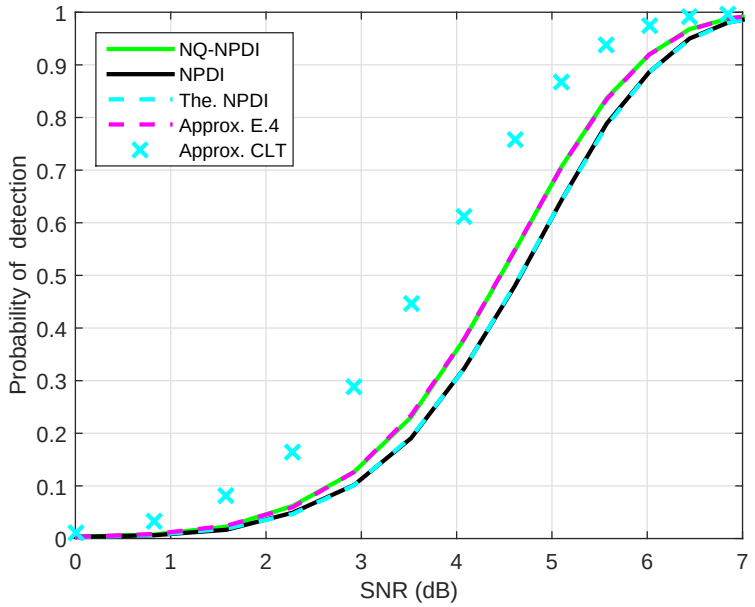

Figure 4.16: P_d vs. SNR with $N_{nc} = 10$ and $P_{fa} = 1e-8$ for the E.4 approximation, the CLT and the NQ-NPDI technique obtained from simulations; and the theoretical and empirical detection probability of the NPDI technique.

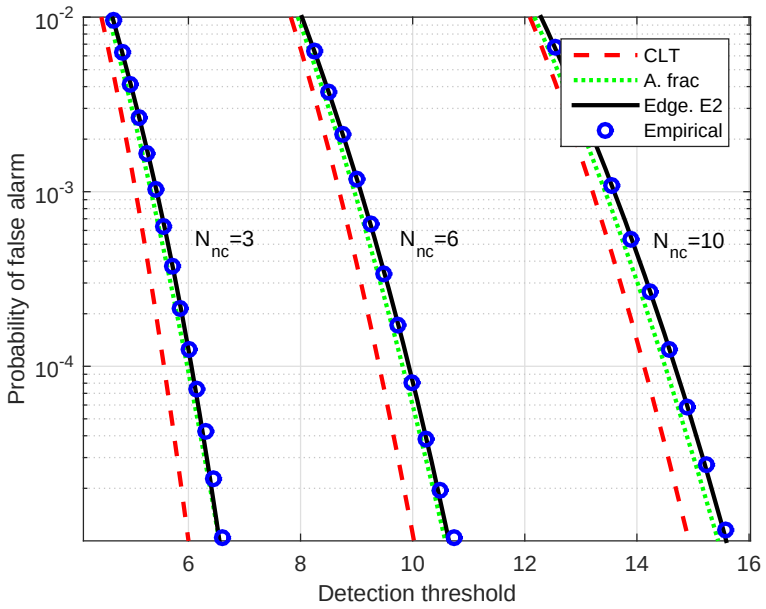

Figure 4.17: Empirical and approximated P_{fa} of the NQ-NPDI technique for $N_{nc} = 3$, 6 and 10 (in the legend, A. frac. is the approximation using the fractional exponent).

by introducing the fractional exponent $\beta = 2/3$ for different numbers of N_{nc}. The CLT approximation provides a significant error with respect to the empirical value of false alarm probability, especially for small values of this probability. The false alarm probability value obtained analytically from applying the fractional exponent is much more accurate than the CLT in the tail region. However, the Edgeworth series E.2 approximation even offers a bit better accuracy than the approximation that uses the fractional exponent. From this result, we can conclude that the Edgeworth series approximation allows us to define a more accurate detection threshold for the NQ-NPDI technique, though the Edgeworth approximation used was not the longest.

4.7 Conclusions

Based on the GLRT and the Bayesian approach, this chapter has derived the optimal PDI technique for HS-GNSS receivers in presence of data bits and variations in the carrier phase. Although the resulting PDI techniques from these approaches are different, they provide similar performance in terms of signal detection. Due to this fact, we propose to use the result from the GLRT approach defined in (4.7), as long as an approximation of the received amplitude of the signal and the noise power were known. This is because the result from the GLRT approach requires less complexity in terms of computational load than the result from the Bayesian approach since it does not need to compute a numerical integral.

If neither the amplitude nor the noise power are known, two approximations of the technique defined in (4.7) can be used leading to the traditional NPDI and NQ-NPDI techniques. Contrary to the traditional belief that the NPDI technique is the best option to acquire weak GNSS signals with time-varying random phase and data bits, this chapter proves that the NQ-NPDI is the most promising technique.

In addition, we have carried out a novel statistical analysis of the NQ-NPDI technique and the result from the Bayesian approach by using the Edgeworth series. These analyses have led to find closed-form approximations of the detection and false alarm probabilities of these techniques. Simulation results have proven that the approximation of the Edgeworth series allows us to predict the performance of the detector and set an accurate signal detection threshold for both techniques.

Chapter 5

Optimal PDI technique for the reacquisition of weak GNSS signals

As we have analysed in the previous chapters, several PDI techniques have been proposed in the literature to detect weak signals at the acquisition stage. However, less attention has been paid to the problem of reacquiring weak signals. A reacquisition must be carried out when the receiver has just lost the signal from one satellite owing to, for instance, strong attenuation caused by an obstacle in the path between the transmitter and the receiver. If the receiver loses the signal, it has to re-detect the signal in order to obtain the position of the user. However, the problem of detecting weak GNSS signals in the reacquisition is less complex than in the first acquisition since in case of reacquisition an accurate estimation of the Doppler frequency is available [VD09] and hence one of the most problematic impairments to extend the coherent integration duration for signals with data are the unknown bits.

Despite the fact that some strategies have been proposed to detect weak GNSS signals, which have been analysed in the previous chapters, the optimal PDI technique for the reacquisition remains still unknown. This occurs because PDI techniques are designed for the first acquisition of the receiver, which has to mitigate the uncertainty of the Doppler frequency. For this reason, the purpose of this chapter is to derive the optimal PDI technique by applying the detection theory tools for the reacquisition of weak GNSS signals. More precisely, the Bayesian approach and the GLRT are used to formulate the detection problem and two PDI techniques are obtained, which require a significant amount of computational resources. We also present lower-complexity approximations of these two PDI techniques. Finally, the performance of the techniques proposed herein is

compared to the PDI techniques used in previous work in terms of ROC curves, revealing a clear gain in favour of our techniques.

5.1 Signal Model

The acquisition of a satellite provides a coarse estimation of code-delay and Doppler frequency, which are obtained from the value that maximizes the CAF [GC16]. The accuracy of theses estimations can be improved performing a finer search of Doppler frequency and code-delay in the CAF. Then, the incoming signal is tracked by correlating it with a local replica, which contains accurate estimations of Doppler frequency and code delay. This process is usually carried out for a long period of time. However, the tracking of the signal can be lost due to, for example, the attenuation caused by an obstacle between the satellite and the receiver. In this situation, the HS-GNSS receiver tries to reacquire the received signal from the satellite. To do so, a local replica, which includes the estimations of code-delay and Doppler frequency obtained in the tracking stage before losing the signal, is correlated again with the received signal for different time instants, which becomes [Bor09b]

$$x_k = I_k + jQ_k = Ad_k e^{j\phi} + w_k, \tag{5.1}$$

where $I_k = \mathbb{R}(x_k)$, $Q_k = \Im(x_k)$, w_k is the noise component, the index $k = 1, ..., N_{nc}$ represents the time instant when the correlator output x_k is computed, d_k are the data bits assumed to be a random variable taking values of 1 and -1 with the same probability. The amplitude A and the phase ϕ are constant with k, and w_k is assumed independent for each k, but identically distributed. It is worth mentioning that the correlation output x_k is usually computed for several close values of the code-delay estimation since this estimation may have changed slightly due to the movement of the satellite and the receiver. Nonetheless, we omit this dependence since we can consider we are performing the analysis only for one of these values.

Combinations of several correlator outputs are needed to detect the weak GNSS signal. The best way to obtain a gain in terms of signal detection is increasing the T_{coh} (i.e. coherently combining different correlator outputs), though its duration is limited by data bits. If the coherent integration is not enough to detect the signal in harsh conditions, we must resort to apply PDI techniques, which provide signal detection improvements since they can increase the integration time by using a non-linear function. In order to known whether the satellite is present or not, the output of a PDI technique denoted

as Z_x is compared to a signal detection threshold. If the magnitude of Z_x surpasses the detection threshold the satellite is considered to be present, but if this magnitude does not surpass the detection threshold, the satellite is assumed to be absent. A block diagram representing the reacquisition process is shown in Figure 5.1. The problem of obtaining the optimal PDI technique consists in finding a function $f(x_1, ..., x_{N_{nc}})$ that allows the receiver to discriminate between the two hypotheses H_0 (the satellite is absent) and H_1 (the satellite is present) with the lower probability of false alarm and greater probability of detection:

- Under H_0: $x_k = w_k$ is a complex Gaussian noise with mean zero and variance σ^2.
- Under H_1: $x_k = Ad_k e^{j\phi} + w_k$ is the signal plus complex Gaussian noise.

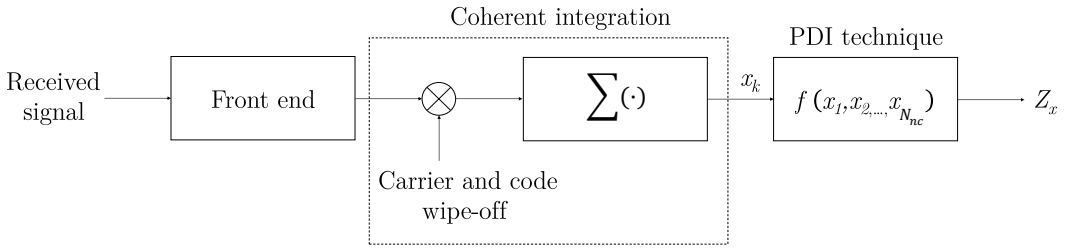

Figure 5.1: Block diagram of the GNSS signal reacquisition.

It is worth mentioning that if the phase of the signal was time-varying, the signal detection problem would be completely different, which leads to other types of solutions. Examples of this kind of signal detection problems have been analysed in Chapter 4.

5.2 Brief review of PDI techniques for HS-GNSS receivers

In this section we present a review of the most relevant PDI techniques, which will be used as a benchmark to compare the performance of the PDI techniques presented in Section 5.3. The optimal detector assuming a received signal that only contains an unknown phase during all the integration time is the coherent integration [Ric05]

$$Z_{\text{coh}}(\mathbf{x}) = \left| \sum_{k=1}^{N_{nc}} x_k \right|, \tag{5.2}$$

where $\mathbf{x} \doteq [x_1, ..., x_{N_{nc}}]^T$. However, the coherent integration is degraded, impaired in presence of frequency offset and data bits. In presence of these impairments, the most widely applied PDI technique is the NPDI, which is given by [Sch05b]

$$Z_{\text{NPDI}}(\mathbf{x}) = \sum_{k=1}^{N_{nc}} |x_k|^2 . \tag{5.3}$$

The NPDI technique is robust against the phase variations caused by data bits and frequency offset since it removes these variations by using the squared absolute value.

Alternatively, another technique to detect weak signals is the DPDI defined as follows [EB04]:

$$Z_{\text{DPDI}}(\mathbf{x}) = \left| \sum_{k=2}^{N_{nc}} x_k x_{k-1}^* \right| . \tag{5.4}$$

This technique usually offers better performance than the NPDI technique, but it experiences a performance degradation in presence of data bits. Another alternative is the NQ-NPDI technique [GC17]:

$$Z_{\text{NQ-NPDI}}(\mathbf{x}) = \sum_{k=1}^{N_{nc}} |x_k| . \tag{5.5}$$

The NQ-NPDI technique provides an improvement in signal detection performance over the NPDI technique, especially if the signal can be detected using a small number of N_{nc}, that is, $N_{nc} \leqslant 10$. Moreover, it is robust against frequency offset and data bits. An additional technique, denoted as GPDIT, combines the NPDI and DPDI techniques as [Cor07]

$$Z_{\text{GPDIT}}(\mathbf{x}) = \sum_{k=1}^{N_{nc}} |x_k|^2 + 2 \left| \sum_{k=2}^{N_{nc}} x_k x_{k-1}^* \right| . \tag{5.6}$$

The GPDIT technique outperforms the NPDI and DPDI techniques as long as the signal does not contain data bits. This occurs because the GPDIT technique consists of the DPDI term, which suffers a significant degradation in presence of data bits.

5.3 Detection strategies

This section uses the Bayesian approach and the GLRT to find the optimal PDI technique for the signal model described in Section 5.1. It should be noticed that the difference

between the detection problem analysed in this chapter and in Chapter 4 is that in Chapter 4 we consider a time-varying phase in the received signal and in this chapter we assume that this phase is constant.

5.3.1 Bayesian approach

As we have seen in Chapter 2, the Bayesian approach is often used when the LRT contains unknown parameters, to which a prior probability distribution can be assigned. Indeed, under these conditions, the Bayesian approach leads to the optimal detector [Sim95]. This approach consists in calculating the expectation of the LRT with respect to the a priori distribution of the unknown parameter. More precisely, the difficulty caused by the unknown parameter is circumvented by averaging the conditional pdf to obtain the unconditional pdf, which does not depend on the unknown parameter. The conditional pdf of the correlators outputs assuming that these outputs include data bits uniformly distributed with equal probability is written under H_1 as [GC17]

$$p(\mathbf{x}|H_1,\phi) = \frac{1}{(\pi\sigma^2)^{N_{nc}}}\exp\left(-\sum_{k=1}^{N_{nc}}\frac{1}{\sigma^2}(I_k^2+Q_k^2+A^2)\right) \prod_{k=1}^{N_{nc}}\cosh\left(\frac{2A}{\sigma^2}(I_k\cos(\phi)+Q_k\sin(\phi))\right). \tag{5.7}$$

Under H_0, the pdf of $\mathbf{x}$ can be expressed as follows,

$$p(\mathbf{x}|H_0) = \frac{1}{(\pi\sigma^2)^{N_{nc}}}\exp\left(-\sum_{k=1}^{N_{nc}}\frac{1}{\sigma^2}(I_k^2+Q_k^2)\right). \tag{5.8}$$

The Bayesian approach is based on a ratio of the two pdfs above given by

$$L_B(\mathbf{x}) = \frac{\int p(\mathbf{x}|H_1,\phi)p(\phi)d\phi}{p(\mathbf{x}|H_0)} = \frac{p(\mathbf{x}|H_1)}{p(\mathbf{x}|H_0)} \lessgtr \tilde{\gamma}_B, \tag{5.9}$$

where $p(\phi)$ is the prior pdf of ϕ and $\tilde{\gamma}_B$ is the detection threshold. First, to apply the Bayesian approach we obtain an expression of the ratio between the two pdfs: $p(\mathbf{x}|H_1,\phi)$ and $p(\mathbf{x}|H_0)$. After removing some irrelevant constants, the ratio can be written as

$$L'_B(\mathbf{x},\phi) = \prod_{k=1}^{N_{nc}}\cosh\left(\frac{2A}{\sigma^2}(I_k\cos(\phi)+Q_k\sin(\phi))\right). \tag{5.10}$$

Second, we eliminate the phase information in (5.10) using the prior information. The prior pdf of ϕ is assumed to be a uniform random variable from $-\pi$ to π. The resulting

Bayesian approach is given by the following expression:

$$L''_B(\mathbf{x}) = \frac{1}{2\pi}\int_{-\pi}^{\pi}\prod_{k=1}^{N_{nc}}\cosh\left(\frac{2A}{\sigma^2}c_k(\phi)\right)d\phi \tag{5.11}$$

with

$$c_k(\phi) = I_k\cos(\phi) + Q_k\sin(\phi). \tag{5.12}$$

Note that the larger the value of N_{nc}, the larger the number of multiplicative terms in the integral. Since in this detection problem the phase of the received signal is considered constant, we need to apply the properties of the product of cosh functions to solve this integral, that is, $\cosh(x)\cosh(y) = (\cosh(x+y)+\cosh(x-y))/2$. Proceeding in this way the integral can be rewritten as a series of integrals, where each one contains the cosh of a certain combination of sums and subtractions of the terms $c_k(\phi)$ as

$$\begin{aligned} L''_B(\mathbf{x}) = \frac{1}{2\pi 2^{N_{nc}-1}}\Bigg(&\int_{-\pi}^{\pi}\cosh\left(\frac{2A}{\sigma^2}(c_1(\phi)+c_2(\phi)+\ldots+c_{N_{nc}}(\phi))\right)d\phi + \ldots + \\ &\int_{-\pi}^{\pi}\cosh\left(\frac{2A}{\sigma^2}(c_1(\phi)-c_2(\phi)-\ldots-c_{N_{nc}}(\phi))\right)d\phi\Bigg), \end{aligned} \tag{5.13}$$

for which a more compact expression is

$$L''_B(\mathbf{x}) = \frac{1}{2\pi 2^{N_{nc}-1}}\sum_{m=1}^{2^{N_{nc}-1}}\int_{-\pi}^{\pi}\cosh\left(\frac{2A}{\sigma^2}(a_m\cos(\phi)+b_m\sin(\phi))\right)d\phi, \tag{5.14}$$

where $2^{N_{nc}-1}$ is the number of cosh functions that appears after applying the property of the multiplication of several cosh functions. The a_m and b_m coefficients aim at encompassing all possible combinations of additions and subtractions of I_k and Q_k, respectively, excluding those that refer to others already considered but with opposite sign. By stacking the above-mentioned coefficients into vectors $\mathbf{a} \doteq [a_1,\cdots,a_{2N_{nc}-1}]^T$ and $\mathbf{b} \doteq [b_1,\cdots,b_{2N_{nc}-1}]^T$, we can compute their value as follows,

$$\mathbf{a} = \mathbf{M}\mathbf{I} \tag{5.15}$$

$$\mathbf{b} = \mathbf{M}\mathbf{Q}, \tag{5.16}$$

where $\mathbf{I} \doteq [I_1,\ldots,I_{N_{nc}}]^T$, $\mathbf{Q} \doteq [Q_1,\ldots,Q_{N_{nc}}]^T$, and $\mathbf{M}$ is a $\left(2^{N_{nc}-1}\times N_{nc}\right)$ matrix whose rows contain all the possible combinations of +1 and -1, excluding those that differ from another row in a global change of sign as

$$\mathbf{M} \doteq \begin{bmatrix} 1 & -1 & -1 & \ldots & -1 \\ 1 & 1 & -1 & \ldots & -1 \\ \vdots & \vdots & \vdots & \ddots & \vdots \\ 1 & 1 & 1 & \ldots & 1 \end{bmatrix}. \tag{5.17}$$

Now, the integral can be solved by the following procedure as

$$\begin{aligned} L''_B(\mathbf{x}) &= \frac{1}{\pi 2^{N_{nc}}} \sum_{m=1}^{2^{N_{nc}-1}} \int_{-\pi}^{\pi} \cosh\left(\frac{2A}{\sigma^2}\sqrt{a_m^2+b_m^2}\cos\left(\phi - \operatorname{atan}\left(\frac{b_m}{a_m}\right)\right)\right) d\phi \\ &= \frac{1}{\pi 2^{N_{nc}+1}} \sum_{m=1}^{2^{N_{nc}-1}} \left(\int_{-\pi}^{\pi} e^{\frac{2A}{\sigma^2}\sqrt{a_m^2+b_m^2}\cos(\phi)} d\phi + \int_{-\pi}^{\pi} e^{-\frac{2A}{\sigma^2}\sqrt{a_m^2+b_m^2}\cos(\phi)} d\phi\right) \\ &= \frac{1}{2^{N_{nc}-1}} \sum_{m=1}^{2^{N_{nc}-1}} I_0\left(\frac{2A}{\sigma^2}\sqrt{a_m^2+b_m^2}\right), \end{aligned} \tag{5.18}$$

where I_0 denotes the zero-order modified Bessel function. Finally, removing some irrelevant constants the resulting detector can be expressed as

$$Z_{\text{BAPDI}}(\mathbf{x}) = \sum_{m=1}^{2^{N_{nc}-1}} I_0\left(\frac{2A}{\sigma^2}\sqrt{a_m^2+b_m^2}\right) \lessgtr \gamma_B, \tag{5.19}$$

where γ_B is the detection threshold.

The result expressed in (5.19) is referred to as Bayesian Approach PDI (BAPDI) technique. This technique is optimum in presence of unknowns bits and an unknown constant phase. Nonetheless, the BAPDI technique depends on the ratio of A and σ^2. Despite the fact that some receivers can know this ratio in tracking stage since they use a carrier-to-noise estimator, the goal of this chapter is to derive a detector which does not depends on the parameters A and σ^2 so that it can be implemented in any receiver. To do so, we propose to apply the approximation of $I_0(x) \approx \exp(|x|)$, valid for relative large values of x. This approximation can be applied for our problem since the argument of (5.19) is not a small magnitude when the received signal has the same or similar combination of bits as one of the rows of the matrix $\mathbf{M}$. Then, by considering $I_0(x) \approx \exp(|x|)$, we get

$$\sum_{m=1}^{2^{N_{nc}-1}} \exp\left(\left|\frac{2A}{\sigma^2}\sqrt{a_m^2+b_m^2}\right|\right) \lessgtr \gamma_B. \tag{5.20}$$

Introducing the logarithm of the LRT becomes

$$\ln\left(\sum_{m=1}^{2^{N_{nc}-1}} \exp\left(\left|\frac{2A}{\sigma^2}\sqrt{a_m^2+b_m^2}\right|\right)\right) \lessgtr \ln(\gamma_B). \tag{5.21}$$

To simplify the expression above, we make use of the log-sum-exp approximation, which consists in taking the maximum of the different exponentials. This approximation is reasonable for a high SNR value at the output of the PDI technique. Such values of SNR

are usually obtained at this output because otherwise the signal could not be detected. In this situation, the largest term dominates in the sum of (5.21) as

$$\max_m \left(\left| \frac{2A}{\sigma^2} \sqrt{a_m^2 + b_m^2} \right| \right) \lessgtr \gamma'_B. \tag{5.22}$$

The larger the deviation of the argument of (5.21), the better the approximation becomes. Finally, incorporating the now irrelevant constant $\frac{2|A|}{\sigma^2}$ into the threshold, the resulting detector can be expressed as

$$Z_{\text{MBAPDI}}(\mathbf{x}) = \max_m \left(\sqrt{a_m^2 + b_m^2} \right) \lessgtr \gamma''_B. \tag{5.23}$$

The solution provided by (5.23) is referred to as Maximum BAPDI (MBAPDI) technique. The MBAPDI technique can be implemented in any HS-GNSS receiver because it does not depend on the parameters A and σ^2. It is worth mentioning that if the chosen index m corresponds to the correct sequence of bits, then the result would be the same as for the coherent detector in the hypothesis H_1, but this will not always happen due to the presence of noise. Moreover, although this happened, we would have some performance degradation with respect to the coherent detector. This is because the MBAPDI requires the use of the maximum function also in the hypothesis H_0, making the receiver choose the largest value among the different $2^{N_{nc}-1}$ samples of noise, which increases the number of false alarms.

5.3.2 Generalized likelihood ratio test

As we have discussed in Chapter 2, a common approach to design detectors with unknown parameters deals with the combination of estimation and detection. The best known joint estimation and detection approach is the GLRT, which consists of two steps. First, the ML estimate of the unknown parameters are found. Second, the unknown parameters are replaced by their ML estimates under each hypothesis and the LRT is calculated as if the estimated parameters were correct [McD95, Lev08].

Although no claims about the optimality of the GLRT can be made, it provides good results in general. Moreover, the GLRT formulation usually provides simpler expressions than the Bayesian approach, which requires the integral of products of several pdfs. This occurs because ML estimation equations sometimes result in a closed-form solution. However, this is not the case of our problem where the ML estimate of the received phase affected by bits does not admit a closed-form solution. In this situation, two options are

feasible: making an approximation of the ML equation in order to get a closed-form solution, which was done in [Bor09b] or using a one-dimensional search method to evaluate the ML estimate.

A PDI technique has been already obtained in [Sat11] using an approximation of the ML phase estimate provided in [Bor09b] and replacing it in an expression of the LRT approximated for low SNR regime. Before proceeding, we make a brief description of the work done previously by other authors and after that we present new PDI techniques based on using different approaches of the GLRT. In [Bor09b], the authors computed the ML solution of the signal phase, which contains unknown bits, from the pdf of $\mathbf{x}$ as

$$p(\mathbf{x}|H_1,\phi) = \frac{1}{(\pi\sigma^2)^{N_{nc}}}\exp\left(-\sum_{k=1}^{N_{nc}}\frac{1}{\sigma^2}(I_k^2+Q_k^2+A^2)\right) \prod_{k=1}^{N_{nc}}\cosh\left(\frac{2A}{\sigma^2}(I_k\cos(\phi)+Q_k\sin(\phi))\right). \tag{5.24}$$

The log-likelihood function for ϕ, removing the terms that are not affected by ϕ, can be expressed as

$$L(\mathbf{x},\phi) = \sum_{k=1}^{N_{nc}}\ln\left(\cosh\left(\frac{2A}{\sigma^2}(I_k\cos(\phi)+Q_k\sin(\phi))\right)\right). \tag{5.25}$$

In order to find a closed-form solution of ϕ the $\ln(\cosh(x))$ function is approximated by $x^2/2$. Thus, the closed-form expression of ϕ that approximately maximizes (5.25) is [Bor09b]

$$\hat{\phi} = \frac{1}{2}\text{atan2}\left(2\sum_{k=1}^{N_{nc}}I_kQ_k, \sum_{k=1}^{N_{nc}}I_k^2-Q_k^2\right), \tag{5.26}$$

where $\text{atan2}(x,y)$ is the four quadrant atan function.

Another way to find the value of ϕ that maximizes (5.25) is numerically by evaluating that expression, which can easily be carried out implementing a one-dimensional search. The comparison between the estimators and the CRB is shown in Figure 5.2. The result illustrates that the ML estimate obtained by a one-dimensional search method exhibits practically the same performance as the approximation in (5.26). The CRB of the phase estimate is $1/(2\text{SNR}N_{nc})$ [Rif74], where the SNR is defined as A^2/σ^2.

In [Sat11], a PDI technique was presented based on the GLRT approach. The authors used the log-LRT, which can be expressed as (5.25). They propose to approximate $L(\mathbf{x},\phi)$ defined in (5.25) for a low SNR regime applying a Taylor series of the $\ln(\cosh(x))$ function

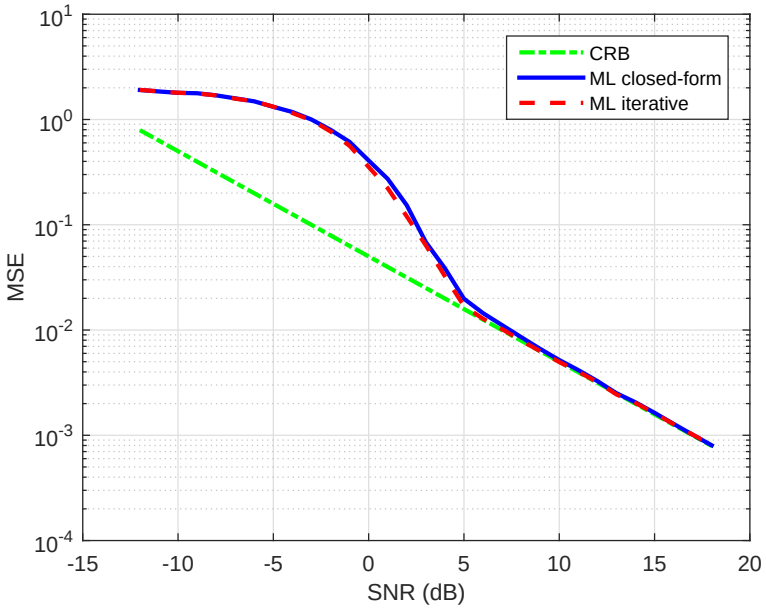

Figure 5.2: Performance comparison of the estimators and the CRB for $N_{nc} = 10$. The approximation of the ML solution expressed in (5.26) is referred to as ML closed-form and the one obtained from a one-dimensional search is indicate as ML iterative.

as $x^2/2$, which leads to

$$\sum_{k=1}^{N_{nc}} \left(\frac{2A}{\sigma^2} (I_k \cos(\phi) + Q_k \sin(\phi)) \right)^2 \lessgtr \gamma'_G. \tag{5.27}$$

Replacing the approximation of the phase estimate in (5.26) into (5.27), and making some simplifications, the NPDISD detector can be obtained as

$$Z_{\text{NPDISD}}(\mathbf{x}) = \sum_{k=1}^{N_{nc}} |x_k|^2 + \left| \sum_{k=1}^{N_{nc}} x_k^2 \right|. \tag{5.28}$$

The NPDISD detector consists of two non-coherent detectors or PDI techniques. The first detector is the conventional NPDI detector. The second detector is the squaring detector (SD), which consists in summing the squared complex correlator outputs. Despite the fact that this solution provides a good performance, an enhancement of this approach can be carried out since HS-GNSS receivers do not usually work in a very low SNR regime at the output of the coherent correlation. This occurs because the correlator outputs in HS-GNSS receivers are obtained using a long T_{coh} in general and combining few correlation outputs the signal can be detected. Then, the approximation of Taylor series used in (5.27) for low SNR values might not be the best option to obtain the best performance of the GLRT approach.

For this reason, the purpose of the following subsections is to propose several new alternatives to the GLRT in order to enhance the performance of the NPDISD technique. More precisely, we present three new approaches to obtain the best detectors using the GLRT approach in the context of HS-GNSS receivers.

5.3.2.1 GLRT (strict)

The first one boils down to the strict application of the GLRT approach. This approach is based on using the log-LRT and replacing the unknown parameter ϕ value by its ML estimation, which must be obtained from a one-dimensional search in (5.25), as

$$L(\mathbf{x}, \hat{\phi}_{\mathrm{ML}}) = \sum_{k=1}^{N_{nc}} \ln\left(\cosh\left(\frac{2A}{\sigma^2}(I_k \cos(\hat{\phi}_{\mathrm{ML}}) + Q_k \sin(\hat{\phi}_{\mathrm{ML}}))\right)\right), \tag{5.29}$$

where $\hat{\phi}_{\mathrm{ML}}$ is the ML estimate of ϕ. This approach allows us to know, which is the optimal performance of the GLRT method and how far it is from the Bayesian approach. This is an important point because the outcome of the Bayesian approach is the optimal detector under the assumed conditions. As we have seen in Subsection 5.3.1, the result of the Bayesian approach implies the computation of a matrix, whose size increases exponentially with the N_{nc} value. In fact, the computation of this matrix can become a handicap. For this reason, if the difference between the performance of the Bayesian approach and the GLRT was quite similar, the application of the GLRT could be the best option. We will continue this discussion later on in the Section 5.4 where the performance comparison of the PDI techniques is analysed.

5.3.2.2 GLRT approximation in closed-form

The second approach is based on the log-LRT in (5.29), but reducing the complexity of this method to estimate ϕ. Given the phase estimate in (5.26) exhibits almost the same performance as at ML phase estimate, while avoiding the one dimensional search, we propose to replace $\hat{\phi}_{\mathrm{ML}}$ in (5.29) with (5.26), resulting in:

$$L(\mathbf{x}, \hat{\phi}) = \sum_{k=1}^{N_{nc}} \ln\left(\cosh\left(\frac{2A}{\sigma^2}(I_k \cos(\hat{\phi}) + Q_k \sin(\hat{\phi}))\right)\right). \tag{5.30}$$

5.3.2.3 GLRT approximation for high SNR regime

The alternatives described in Subsection 5.3.2.2 and Subsection 5.3.2.1 require the knowledge of the SNR, A/σ^2. This is a drawback since this information is sometimes unknown by the receiver. For this reason, the last method that we propose avoids the need of knowing the SNR a priori. The way to obtain a detector that does not depend on the SNR is to adopt an approximation of the $\ln(\cosh(x))$ function as $|x| - \ln(2)$. This approximation gives an excellent fit for relative large values of x, which is a region appropriate to detect signals in the context of HS-GNSS receivers. After using this approximation, the PDI technique is independent of the scale factors A and σ^2. Thus, the resulting technique can be expressed as

$$L_{\mathrm{GLRT}_{a.l.}}(\mathbf{x}, \hat{\phi}) = \sum_{k=1}^{N_{nc}} \left| I_k \cos(\hat{\phi}) + Q_k \sin(\hat{\phi}) \right|. \tag{5.31}$$

This PDI technique may offer similar performance as the two previous techniques presented in Subsection 5.3.2.1 and Subsection 5.3.2.2 when the SNR at the correlator output is relatively high. Besides not requiring the knowledge of the SNR, this technique avoids the use of two non-linear functions such as the ln and cosh. It is worth mentioning that (5.31) has some resemblance to the NQ-NPDI technique described in (5.5), which was derived for time-varying phase signals. The NQ-NPDI technique offers a great performance in scenarios where the SNR is relatively high and the received signal can suffer phase changes [GC17]. However, the technique proposed in this subsection is derived for signals with constant phase. This fact suggests that in scenarios where the received signal includes a constant phase, the detector in (5.31) could provide a promising performance.

5.4 Simulation results

This section presents the simulation results based on ROC curves. These curves compare the detection performance of the PDI techniques proposed herein to the more relevant PDI techniques found in the literature. Results are obtained using Monte Carlo simulations and the σ value is normalized to 1. Theoretical ROC curves of the coherent integration and the NPDI technique are also included in the figures, which are given by [Ric05] and [Jay13], respectively.

Figure 5.3 shows the comparison among the different PDI techniques in an ideal channel containing only Gaussian noise and an unknown constant phase, but in absence of data

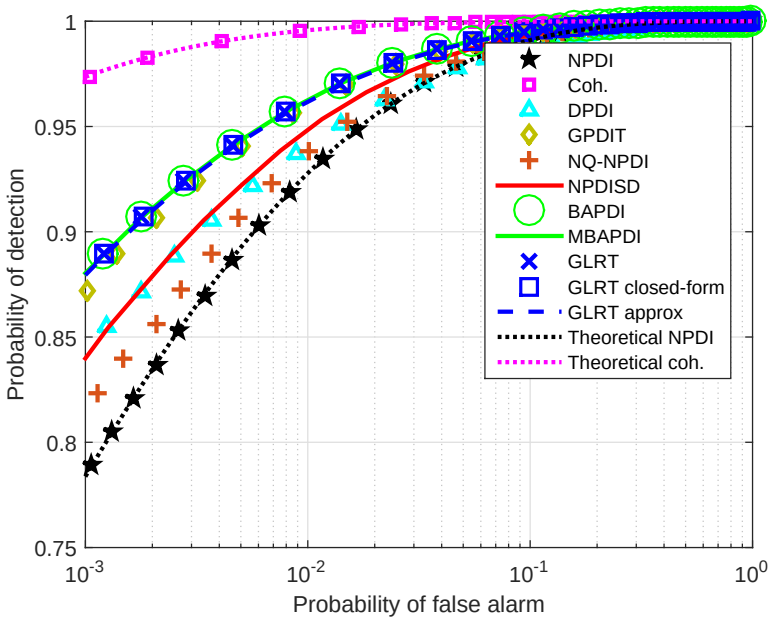

Figure 5.3: Performance comparison of the detectors in absence of bits for $N_{nc} = 6$, $A = 1.6$ and $\sigma = 1$. In the legend, GLRT, GLRT closed-form and GLRT approx refer to the techniques explained in Subsections 5.3.2.1, 5.3.2.2 and 5.3.2.3, respectively.

bits in the received signal for $N_{nc} = 6$ and $A = 1.6$. As we expected, in this situation, the optimal detector is the coherent integration since there are not effects that pose limits on its duration. The worst performing technique corresponds to the NPDI technique. The proposed five techniques, namely, BAPDI, MBAPDI, and the three obtained from the GLRT method explained in Subsections 5.3.2.1, 5.3.2.2 and 5.3.2.3, exhibit similar performance, which is also better than that of the DPDI, GPDIT, NPDISD and NQ-NPDI techniques.

Figure 5.4 shows the comparison among the different detectors in a Gaussian channel when the received signal is affected by phase changes owing to data bits using the same parameters as in Figure 5.3. The result illustrates that the DPDI, GPDIT and the coherent integration techniques suffer a strong performance degradation since they are not robust against the presence of bits. In this case, the proposed five techniques, two based on the Bayesian approach and three established from the GLRT, provide very similar performance outperforming the rest of the PDI techniques. In particular, it is interesting to pay attention to the comparison between the proposed five techniques and the NPDISD technique, which was derived by the application of the GLRT approach, but the author used an approximation for a low SNR regime. The outcome reveals a clear improvement

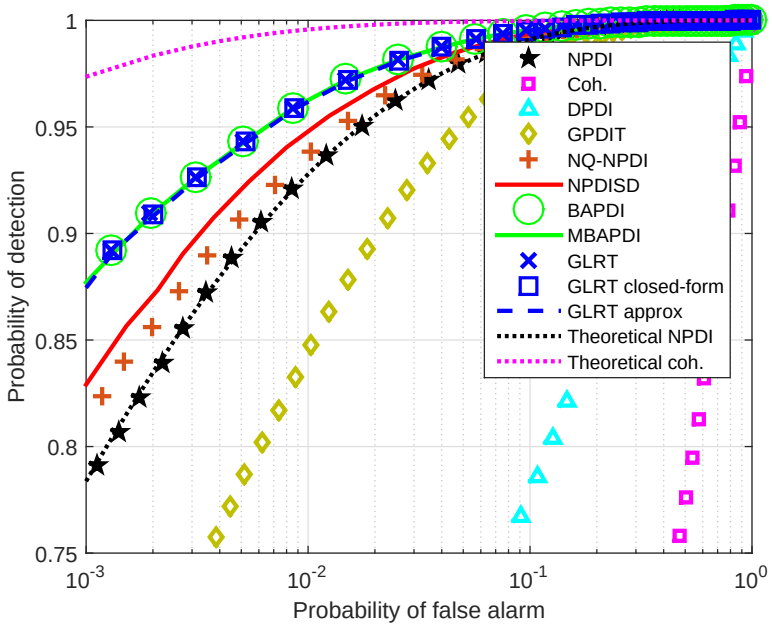

Figure 5.4: Performance comparison of the detectors in presence of data bits for $N_{nc} = 6$, $A = 1.6$ and $\sigma = 1$. In the legend, GLRT, GLRT closed-form and GLRT approx refer to the techniques explained in Subsections 5.3.2.1, 5.3.2.2 and 5.3.2.3, respectively.

in favour of the techniques proposed herein.

Figure 5.5 illustrates the comparison among the different detectors in a Gaussian channel when the received signal contains unknown data bits for $A = 1$ and $N_{nc} = 15$. This simulation reveals that although the SNR of the correlator output is lower than in Figure 5.3 and Figure 5.4, the proposed five techniques remain exhibiting the best performances. The performance difference among the five techniques and the NPDISD is smaller than in the previous simulations due to this lower SNR value. This value also causes that the technique described in Subsection 5.3.2.3, which has been derived for a relative large values of SNR, has a slight mismatch with respect to the techniques defined in Subsection 5.3.2.1 and Subsection 5.3.2.2. The MBAPDI technique also offers a very slight degradation with respect to the BAPDI because the SNR at the output of the PDI technique is slightly lower than in Figure 5.4. This effect can be seen in the zoom view, which appears in Figure 5.5.

Figure 5.6 shows the probability of detection with respect to the SNR for the different detectors in a Gaussian channel and when the received signal contains data bits. We use $N_{nc} = 5$ and set the probability of false alarm to $1e-3$. The detection threshold for

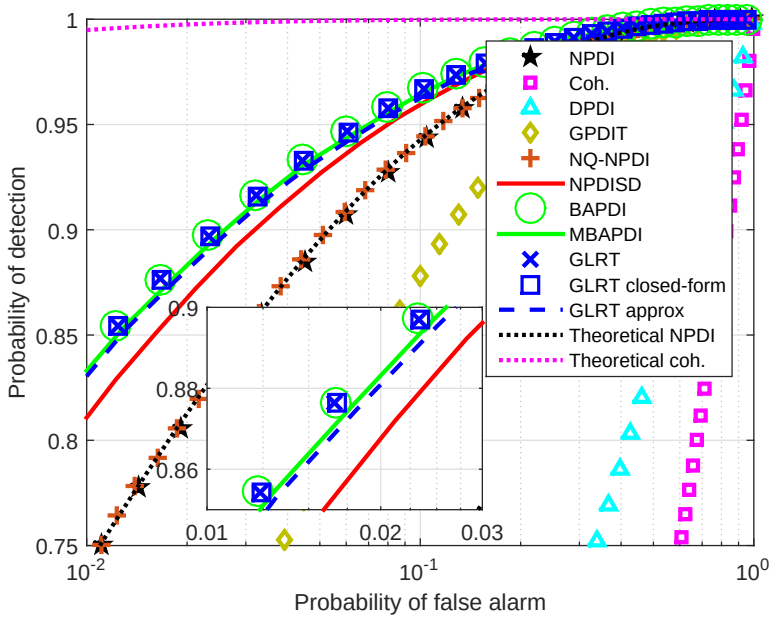

Figure 5.5: Performance comparison of the different detectors in presence of data bits for $N_{nc} = 15$, $A = 1$ and $\sigma = 1$. In the legend, GLRT, GLRT closed-form and GLRT approx refer to the techniques explained in Subsections 5.3.2.1, 5.3.2.2 and 5.3.2.3, respectively.

each PDI technique is fixed through the Monte Carlo simulations. The result illustrates that the techniques proposed in the chapter show the highest probabilities of detection. The coherent integration, DPDI and GPDIT techniques suffer a severe degradation due to the data bits. For this reason, these techniques are not useful in detection problems where the received signal have sign changes produced by the bits. The NPDI, NQ-NPDI and NPDISD techniques, which are robust against the presence of data bits, outperform the coherent integration, DPDI and GPDIT techniques, but the former group does not provide as good performance as the techniques presented in this work.

Given that the five techniques presented in the chapter offer very similar performance, exceeding that of the other techniques, for the problem at hand, the selection of the most suitable one can be based on the computational complexity. While the BAPDI is the theoretically optimal PDI technique since it has been derived from the Bayesian approach, it may present difficulties in practice because it uses a matrix, whose size grows exponentially as N_{nc} grows. Moreover, the BAPDI requires the a priori knowledge of the SNR and it needs to use the modified Bessel function, which in practice has to be evaluated numerically. The MBAPDI also suffers the disadvantage of having to evaluate a potentially large number of combinations, which introduces a large computational burden,

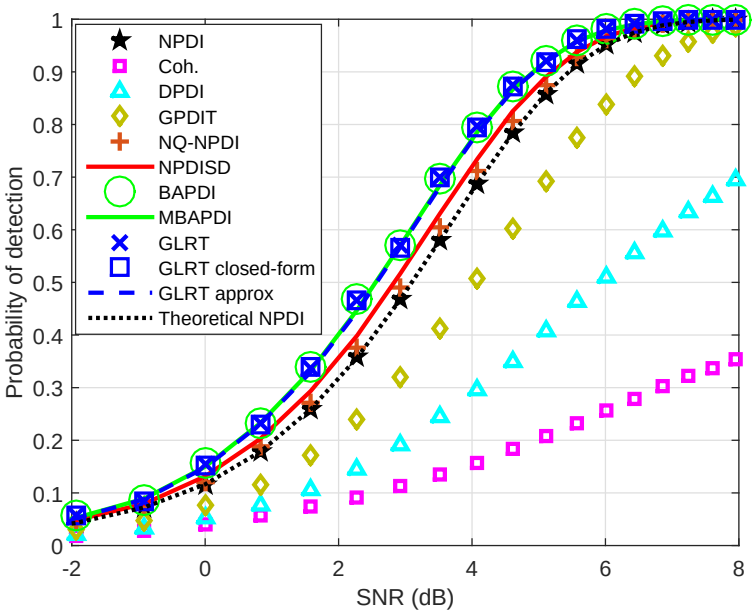

Figure 5.6: Probability of detection vs. SNR with $N_{nc} = 5$ and probability of false alarm of 1e-3 for the different detectors in presence of data bits in the received signal.

especially for large N_{nc} values. The exact GLRT presented in Subsection 5.3.2.1 requires the usage of a one-dimensional search method to estimate the phase of the received signal. This fact poses difficulties in the implementation of this technique in a HS-GNSS receiver. The GLRT approach described in Subsection 5.3.2.2 is a good option since it does not depend on large matrices nor a one-dimensional search method, but it has the drawback of requiring the knowledge of the SNR. Finally, the PDI technique presented in Subsection 5.3.2.3 becomes the best option to obtain a significant gain in terms of signal detection because its computational load is the lowest one and it does not need a priori information about the SNR.

5.5 Conclusions

In this chapter we have derived two PDI techniques by using the Bayesian approach and the GLRT for the reacquisition of weak GNSS signals. We have also proposed approximate techniques of reduced computational complexity, which can be easily implemented in HS-GNSS receivers and do not require the knowledge of the SNR. Simulation results have shown the superior performance of the techniques proposed in the chapter with respect

to other PDI techniques, while the former group provides very similar performance. For a balanced trade-off between computational burden and performance, we can conclude that the most suitable technique for the reacquisition of GNSS signals is the one based on the approximation of the GLRT approach for high SNR regime and on the use of the approximate ML phase estimate.

Chapter 6

C/N_0 estimators for high-sensitivity snapshot GNSS receivers

In recent years, the use of PDI techniques has been considered for the design of HS-GNSS receivers in order to offer the possibility of acquiring weak signals. Nevertheless, the application of PDI techniques makes it difficult to obtain reliable information about the C/N_0 of the received signal. The reason is that PDI techniques apply non-linear combinations of several consecutive CAFs, which affect to the relationship between the signal level and the noise level at the output of this technique. The measurement of C/N_0 becomes necessary since the C/N_0 provides highly desirable information about the quality of the received GNSS signal. This measurement is often used at many stages of GNSS receivers. For instance, at the acquisition stage the knowledge about the C/N_0 offers a-priori information that can lead to establishing the optimum signal detection threshold to distinguish whether the signal from the satellite is present or not [Sch05a]. At the tracking stage, it is also useful to mitigate near-far interferences [LR05] and to avoid loss-of-lock problems [Kap05]. In particular, at the PVT stage, the C/N_0 value is used by some positioning algorithms, such as the weighted least square method [HW12].

The C/N_0 estimators most commonly implemented in GNSS receivers are the Narrow-band Wide-band Power Ratio (NWPR) and Signal-to-Noise Power Ratio (SNPR) [Gro05, Bhu14, Fal11]. In general, these estimators provide accurate estimates when the signal can be detected using only coherent integrations. But, if the use of the coherent integration is not enough to acquire the signal, the accuracy of the estimators may not be acceptable. For this reason, in indoor conditions where the use of PDI techniques is mandatory to acquire weak signals, we must resort to other alternatives, which use the output of a PDI

technique to estimate the C/N_0.

Obtaining a C/N_0 estimate from a PDI technique is far from being a trivial task since the C/N_0 estimator depends on the pdfs of the metric used by the PDI technique under the presence and absence of the signal satellite. Moreover, most pdfs of these metrics are not known in closed-form, a fact that makes the derivation of an expression for estimating the C/N_0 even more difficult. The most widely PDI technique implemented is namely NPDI technique, which involves the sum of central and non-central chi-square distributions when the signal is absent and present, respectively [Sch05b]. Alternately, the DPDI often results to be a good option to acquire weak signals, though the pdf of this metric is not known in closed-form neither in the absence nor presence of a signal [EB04]. An additional technique referred to as GPDIT deals with the combination of the NPDI and DPDI techniques, which can offer some improvements in terms of signal detection [Cor07]. However, the pdfs of this combination of random variables is completely unknown. Finally, an additional alternative corresponds to the NQ-NPDI technique, which requires the computation of the sum of Rician variables in the presence of the signal and Rayleigh variables in its absence.

In this context, the purpose of this chapter is to formulate closed-form expressions for the C/N_0 estimates that can be obtained with each of the PDI techniques mentioned above. These estimators are derived through the application of a theoretical approach that is based on analyzing the distributions of each PDI technique. The idea is to use the output of the PDI technique not only to acquire the satellites, but also to estimate the C/N_0, thus allowing the estimators to be easily implemented in HS-GNSS snapshot receivers. Finally, a performance comparison between the estimators derived herein and conventional C/N_0 estimators is carried out, revealing an important gain in favor of the former group in terms of estimation accuracy.

6.1 Signal model

In this section, we are only focus on the signal model of the acquisition stage, which will be useful to derive the C/N_0 estimator in Section 6.2.2. The CAF containing the tentative values of the code-delay τ and the Doppler frequency f_d as $\tilde{\tau}$ and $\tilde{f}_d$ respectively, is expressed, in absence of data bit transition, as

$$x(\tilde{\tau}, \tilde{f}_d) = d\tilde{A}e^{j\phi}\text{sinc}(\Delta f T_{\text{coh}})B(\Delta\tau) + \omega = Ae^{j\phi} + \omega, \tag{6.1}$$

where A is the amplitude obtained from computing the CAF with phase ϕ, d is the value of the data navigation bits taking value of 1 or -1, $\Delta\tau = \tau - \tilde{\tau}$ is the time-delay offset between the local replica and the received GNSS signal, $\Delta f = f_d - \tilde{f}_d$ is the residual frequency offset, T_{coh} is the coherent integration time, $B(\Delta\tau)$ is the circular autocorrelation function of a GNSS signal and ω is AWGN after computing the CAF with zero-mean and variance σ^2.

In general, the CAF allows the receiver to distinguish between whether the satellite is present or not by using a detection threshold in outdoor environments. Nevertheless, in some scenarios such as urban or indoor environments, the satellite is not detected because the signal level after computing the CAF is below the noise level. In this condition, the best option to acquire the satellite signal consists in increasing the coherent integration time. Although it gives a considerable gain in terms of signal acquisition, it cannot be increased without bounds since frequency offsets, data bits, and phase noise effects limits its duration. The impairment caused by the frequency offset can be mitigated computing the CAF with a greater number of evaluated Doppler frequencies, though it requires a greater computational load. Moreover, in some GNSS signals such as Galileo E1BC the impairment created by the bits can be circumvented because they are composed by a known pilot sequence. In this situation, one of the most problematic impairment of HS-GNSS receivers nowadays is the phase noise of the receiver clock.

6.1.1 Phase noise

The GNSS receiver clock introduces a time-varying phase error in the received signal. This error is usually referred to as phase noise and one of its main problems is that limits the duration of the T_{coh} [PS10]. The phase noise can be modeled using a two-state model, which was developed in [Hwa92] and later implemented in [Bru06]. The model of the phase noise, W_{PN}, is represented in Figure 6.1, where u_b and u_d are two

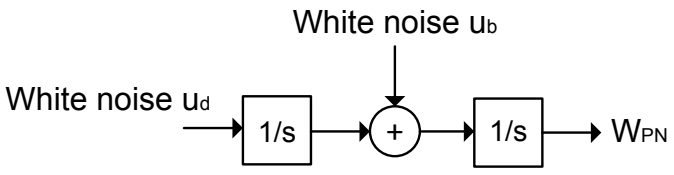

Figure 6.1: Clock error modeling.

independent Gaussian noise components with zero mean and variance S_f/T_s and S_g/T_s,

	h_0 $[s]$	h_{-2} $[1/s]$
TCXO	9.43e-20	3.8e-21
CSAC	7.2e-21	2.7e-27

Table 6.1: Clock parameters.

respectively. The coefficients S_g and S_f are the spectral amplitudes of the noise, which can be approximated as

$$S_f \approx \frac{h_0}{2}, \tag{6.2}$$

$$S_g \approx 2\pi^2 h_{-2}. \tag{6.3}$$

The parameters h_0 and h_{-2}, which depend on the quality of the receiver clock, represent the white frequency noise and the random walk frequency noise, respectively. In this chapter, we focus on two typical clocks used in GNSS receivers: Temperature Compensated Crystal Oscillator (TCXO) and Chip Scale Atomic Clock (CSAC). The TCXO clock usually introduces a greater amount of noise than a CSAC clock. An example of TCXO and CSAC clocks parameters are given in [Bru06], as shown in the Table 6.1.

6.1.2 PDI techniques

The phase noise limits the duration of the coherent integration since it causes the cancellation of the desired signal if the CAF is computed by accumulating samples during an excessively long interval. In this situation, when the receiver needs to accumulate more energy than what is possible in a coherent manner, PDI techniques, which combines non-linearly different CAFs, must be used.

The objective of all PDI techniques focuses on the discrimination between two hypotheses: the satellite is absent under H_0 ($A = 0$) or the satellite is present under hypothesis H_1 ($A \neq 0$). The maximum value of the output of a PDI technique is compared to a detection threshold to perform the distinction between the two hypotheses. If the satellite is declared present, it is possible to estimate its C/N_0 from using the techniques explained in the following section.

The most relevant techniques to acquire weak GNSS signals are the NPDI, NQ-NPDI, DPDI, and GPDIT techniques. These techniques are widely explained and analyzed in

Chapters 3 and 4. We derive one estimator for each one of these techniques.

6.2 C/N_0 estimators

This section is divided into two parts. The first one describes the most traditional estimators implemented in the literature. The second one presents four C/N_0 estimators that are specially designed for HS-GNSS snapshot receivers. These estimators only use the output of one of the PDI technique, which has been used to detect the weak signal, to carry out the estimation of the C/N_0.

6.2.1 Traditional estimators

This section describes the two more common C/N_0 estimators proposed in the literature, the NWPR and the SNPR. These estimators require the use of specific metrics to estimate the C/N_0, which are different from those obtained at the output of the PDI technique implemented to acquire a weak GNSS signal. This fact makes that the NWPR and the SNPR estimators are not really suitable for estimating C/N_0 in a HS-GNSS snapshot receiver.

6.2.1.1 Narrow-band wide-band power ratio

The conventional NWPR involves evaluating the ratio between the signal wideband power to its narrowband power as [Fal11]

$$\mathrm{NP} = \frac{\mathrm{NBP}}{\mathrm{WBP}}, \tag{6.4}$$

where WBP is a wideband measurement considering the noise bandwidth of $1/T_{\mathrm{coh}}$ as

$$\mathrm{WPB} = \max_{\tilde{\tau},\tilde{f}_d} \left(Z_{\mathrm{NPDI}}(\mathbf{x}) \right), \tag{6.5}$$

where $Z_{\mathrm{NPDI}}(\mathbf{x})$ is defined in (3.1). The NBP is a narrowband measurement assuming the noise bandwidth of $1/(N_{nc}T_{\mathrm{coh}})$ as

$$\mathrm{NPB} = \max_{\tilde{\tau},\tilde{f}_d} \left(\left| \sum_{k=1}^{N_{nc}} x_k(\tilde{\tau}, \tilde{f}_d) \right|^2 \right). \tag{6.6}$$

The accuracy of NP can be improved by performing an average of the metric computed within M consecutive integration intervals, which are hereafter indexed with the subscript m,

$$\hat{\mu}_{NP} = \frac{1}{M} \sum_{m=1}^{M} \mathrm{NP}_m, \tag{6.7}$$

where the duration of each integration interval is determined by $T_{\mathrm{coh}} N_{nc}$ seconds. The mean in (6.7) is then used to ultimately estimate the C/N_0 as

$$\widehat{C/N}_0 = 10 \log \left(\frac{1}{T_{\mathrm{coh}}} \frac{\mu_{NP} - 1}{N_{nc} - \mu_{NP}} \right), \tag{6.8}$$

where μ_{NP} is replaced for its estimation.

6.2.1.2 Signal-to-noise power ratio technique

The SNPR technique estimates the C/N_0 assuming that all of the time interval of the used signal has been integrated coherently [Bhu14]. Basically, it is based on comparing the signal level with the mean of the noise, both obtained from the NBP metric. The signal level corresponds to the subtraction between the narrowband measurement in (6.6) and the mean of the noise (μ_{NBP}) since the narrowband measurement contains information about signal and noise. The mean of the noise is calculated from all noise samples provided to compute the CAF for the incorrect trial values of code-delay and Doppler frequency as

$$\mu_{NBP} = \mathrm{E}\left[\left(\left| \sum_{k=1}^{N_{nc}} x_k(\tilde{\tau}, \tilde{f}_d) \right|^2 \right) \right] \text{ except for } \tilde{\tau} \text{ and } \tilde{f}_d \text{ that} \max_{\tilde{\tau}, \tilde{f}_d} \left(\left| \sum_{k=1}^{N_{nc}} x_k(\tilde{\tau}, \tilde{f}_d) \right|^2 \right). \tag{6.9}$$

The SNPR expression is given by

$$\mathrm{SNPR} = \frac{\mathrm{NBP} - \mu_{NBP}}{\mu_{NBP}}. \tag{6.10}$$

Finally, the C/N_0 can be expressed as

$$\widehat{C/N}_0 = 10 \log \left(\frac{\mathrm{SNPR}}{N_{nc} T_{\mathrm{coh}}} \right). \tag{6.11}$$

The resulting estimator offers a good performance as long as the signal level after computing the NBP metric did not suffer a self-cancellation, which could be caused by the impairments that limit the coherent integration time.

6.2.2 C/N_0 estimation from a PDI technique

This subsection explains the procedure to estimate the C/N_0 from different PDI techniques. The approach applied in this chapter is based on estimating the SNR at the output of the coherent correlation, which is directly related to the C/N_0 measure and the T_{coh} as

$$C/N_0 = 10\log\left(\frac{\text{SNR}}{T_{\text{coh}}}\right), \tag{6.12}$$

where $\text{SNR} = A^2/\sigma^2$. The T_{coh} is a known parameter since it is chosen by the receiver. Thus, we only need to estimate SNR to obtain the C/N_0 measurement. The estimation of SNR is carried out by solving a system of two equations, which contains information about the hypotheses H_0 and H_1. More precisely, these equations are obtained from the knowledge of the means of the PDI metric used under H_0 and H_1. The mean under H_0 can be estimated from all the noise samples provided from the CAF for the different incorrect trial values of code-delay and Doppler frequency. The mean measure under H_1 is estimated from the maximum value of the output of a PDI technique. We assume that the value of Δf and $\Delta\tau$ in (6.1) are close to zero when the received signal is acquired. Thus, the term $A\text{sinc}(\Delta_f T_{\text{coh}})B(\Delta\tau)$ can be approximated by A. This process is applied for all PDI techniques. However, the problem is that each PDI metric has a different mean under H_0 and H_1, which are analyzed in the following subsections.

6.2.2.1 C/N_0 estimation from the NPDI technique

The NPDI metric follows a central Chi-square under H_0 and a non-central Chi-square under H_1. The mean of the NPDI metric under these hypotheses is given by

$$\mu_{N|H_0} = N_{nc}\sigma^2 \tag{6.13}$$

$$\max\left(Z_{\text{NPDI}}(\mathbf{x})\right) \approx \mu_{N|H_1} = N_{nc}\sigma^2 + N_{nc}A^2, \tag{6.14}$$

where $\mu_{N|H_0}$ and $\mu_{N|H_1}$ are the mean of the NPDI metric under H_0 and H_1, respectively. The mean $\mu_{N|H_0}$ is computed from all of the samples of the NPDI output without using the maximum sample nor the samples around it. This selection of samples excludes those samples affected by a possible correlation peak obtained from the satellite signal so that purely noise samples are effectively selected. The parameter $\mu_{N|H_1}$ corresponds to the maximum value of the output of the NPDI technique. Solving the system of equations,

we get

$$\widehat{\mathrm{SNR}} = \frac{\mu'_{N|H_1}}{N_{nc}} - 1 \tag{6.15}$$

where $\mu'_{N|H_1}$ is $\mu_{N|H_1}/\sigma^2 = \mu_{N|H_1} N_{nc}/\mu_{N|H_0}$.

6.2.2.2 C/N_0 estimation from the NQ-NPDI technique

The NQ-NPDI metric combines the sum of independent Rayleigh and independent Rician distributions under H_0 and H_1, respectively. A pdf expression for any of the two hypotheses is not known in closed-form. However, there are closed-form expressions for the mean of the sum of several Rayleigh and Rician distributions, though they do not allow us to isolate the SNR parameter. This occurs because the mean of a Rician distribution involves the calculation of the modified Bessel function. More precisely, the mean of the NQ-NPDI metric under H_0 and H_1 can be expressed as

$$\mu_{NQ|H_0} = \frac{\sigma N_{nc}\sqrt{\pi}}{2} \tag{6.16}$$

$$\max\left(Z_{\text{NQ-NPDI}}(\mathbf{x})\right) \approx \mu_{NQ|H_1} = \frac{\sigma N_{nc}\sqrt{\pi}}{2} L_{1/2}\left(\frac{-A^2}{\sigma^2}\right), \tag{6.17}$$

where $L_{1/2}$ denotes a Laguerre polynomial of 1/2, which is given by

$$L_{1/2}(x) = e^{x/2}\left[(1-x)I_0\left(\frac{-x}{2}\right) - xI_1\left(\frac{-x}{2}\right)\right], \tag{6.18}$$

where $I_0(x)$ and $I_1(x)$ are the modified Bessel functions of the first kind with order zero and one, respectively. From (6.16) and (6.17), we obtain an expression only affected by SNR as

$$\mu'_{NQ|H_1} = \frac{N_{nc}\sqrt{\pi}}{2} e^{-\mathrm{SNR}/2}\left[(1+\mathrm{SNR})I_0\left(\frac{\mathrm{SNR}}{2}\right) + \mathrm{SNR}\, I_1\left(\frac{\mathrm{SNR}}{2}\right)\right], \tag{6.19}$$

where $\mu'_{NQ|H_1} = \mu_{NQ|H_1}/\sigma = \mu_{NQ|H_1} N_{nc}\sqrt{\pi}/(2\mu_{NQ|H_0})$.

One way to estimate the SNR is applying an iterative algorithm. However, the implementation of an iterative algorithm is not usually desirable because it takes more time and has a greater computational load than the application of a formula. Then, in this case, the SNR estimation requires using approximations to find a simple expression. The $I_0(x)$ and $I_1(x)$ functions can be approximated by the term $e^x/\sqrt{2\pi x}$ for relative large values of x. We choose this kind of approximation because in HS-GNSS receivers, the value of SNR at the output of the CAF is often a relative large number since it is obtained using a T_{coh}

as long as possible. This SNR value is different from the C/N_0 of the received signal since the former depends on T_{coh} used in the CAF. The longer the T_{coh} used to compute the CAF, the larger the magnitude of the SNR at the output of the CAF. Although the SNR is a relative large number, the signal is difficult to be detected without the application of a PDI technique because in a snapshot receiver, the signal must be distinguished among a large number of noise samples.

Figure 6.2 illustrates the comparison among the $I_0(x)$, $I_1(x)$, and $e^x/\sqrt{2\pi x}$ functions. The result shows that $e^x/\sqrt{2\pi x}$ is an excellent fit of these two Bessel functions, especially for large values of x. Introducing the approximation of $I_0(x)$ and $I_1(x)$ functions and

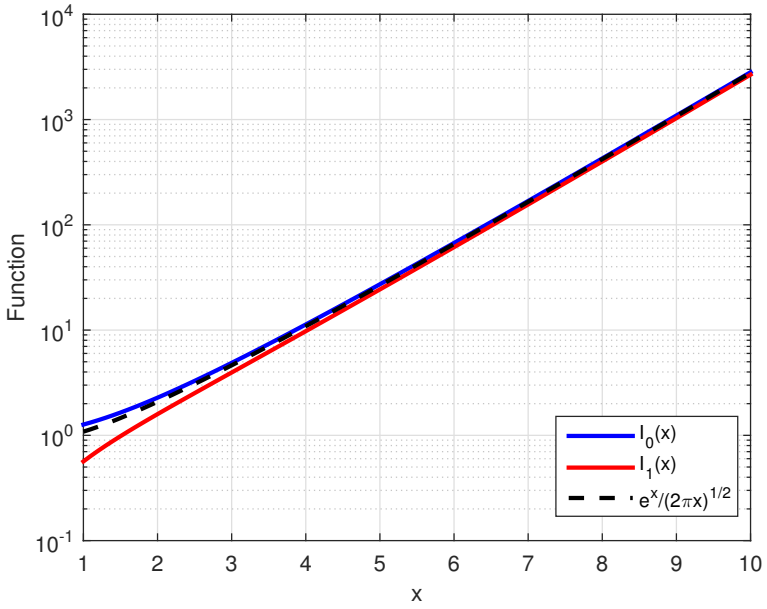

Figure 6.2: Comparison of the $I_0(x)$ and $I_1(x)$ functions with the approximation $e^x/\sqrt{2\pi x}$.

simplifying the expression, the result is

$$\mu'_{NQ|H_1} \approx \frac{N_{nc}}{2}\left(\frac{1+2\text{SNR}}{\sqrt{\text{SNR}}}\right). \tag{6.20}$$

Using this approximation, the SNR value can be estimated from a simple quadratic equation as

$$4\text{SNR}^2 + \left(4 - \left(\frac{2\mu'_{NQ|H_1}}{N_{nc}}\right)^2\right)\text{SNR} + 1 \approx 0. \tag{6.21}$$

The expression above contains two solutions, but only the following solution is correct since it provides a large enough SNR value, which belongs to the range of values where the approximation in (6.20) offers an accurate fit.

$$\widehat{\mathrm{SNR}} = \frac{-\left(4-\left(\frac{2\mu'_{NQ|H_1}}{N_{nc}}\right)^2\right)+\sqrt{\left(4-\left(\frac{2\mu'_{NQ|H_1}}{N_{nc}}\right)^2\right)^2-16}}{8}. \tag{6.22}$$

The other possible solution gives a very small value of SNR, which does not make sense owing to the approximation introduced in (6.20) for large values of SNR. This fact occurs because the term $(\mu'_{NQ|H_1})^2$ is usually a large number compare to the rest of terms in (6.21).

6.2.2.3 C/N_0 estimation from the DPDI technique

The distribution of the DPDI metric is not known in closed-form neither under H_0 nor H_1. More precisely, these distributions are far from being trivial to obtain since they are composed by the absolute value of several sums of two multiplied consecutive CAFs. In this situation, we must resort to approximate the distribution of the DPDI metric in order to estimate the SNR. Invoking the central limit theorem, the distribution of the DPDI can be approximated by a Rayleigh and Rician distribution under H_0 and H_1, respectively. Since the term inside the absolute value in the DPDI defined in (3.4) asymptotically converges to a Gaussian distribution as the N_{nc} value grows. In this case, the mean of the DPDI metric under H_0 and H_1, denoted as $\mu_{D|H_0}$ and $\mu_{D|H_1}$, respectively, can be approximated as

$$\mu_{D|H_0} \approx \frac{\sigma_D\sqrt{\pi}}{2} \tag{6.23}$$

$$\max\left(Z_{\mathrm{DPDI}}(\mathbf{x})\right) \approx \mu_{D|H_1} \approx \frac{\sigma_D\sqrt{\pi}}{2} L_{1/2}\left(\frac{-A_D^2}{\sigma_D^2}\right), \tag{6.24}$$

where $\sigma_D = \sqrt{N_{nc}-1}\sigma^2$ and $A_D = (N_{nc}-1)A^2$. Exploiting the expressions above and approximating the modified Bessel functions $I_0(x)$ and $I_1(x)$ by $e^x/\sqrt{2\pi x}$, which exhibit an excellent fit for large values of x, we obtain

$$\mu'_{D|H_1} \approx \frac{1}{2}\left(\frac{1+2(N_{nc}-1)\mathrm{SNR}^2}{\mathrm{SNR}}\right), \tag{6.25}$$

where $\mu'_{D|H_1}$ is $\mu_{D|H_1}/\sigma^2$ and σ^2 is obtained from (6.23). The estimation of SNR is obtained from a quadratic equation as

$$2(N_{nc}-1)\mathrm{SNR}^2 - 2\mu'_{D|H_1}\mathrm{SNR} + 1 \approx 0. \tag{6.26}$$

The expression above contains two solutions. Nevertheless, the unique possible solution corresponds to the following equation as

$$\widehat{\mathrm{SNR}} = \frac{2\mu'_{D|H_1} + \sqrt{4(\mu'_{D|H_1})^2 - 8(N_{nc}-1)}}{4(N_{nc}-1)}. \tag{6.27}$$

The other possible solution gives a too small SNR value, which is incorrect since the approximation of the modified Bessel functions introduced in (6.25) only makes sense for relatively large values of SNR.

6.2.2.4 C/N_0 estimation from the GPDIT technique

The pdf of the GPDIT metric is difficult to be obtained because it is composed of the sum of two correlated random variables. However, this fact does not preclude the estimation of the C/N_0 from this PDI technique. Exploiting that the mean of the GPDIT metric corresponds to the sum of the mean of the NPDI metric and twice the mean of the DPDI metric, the C/N_0 estimation can be obtained. The mean of the GPDIT metric under H_0 and H_1 denoted as $\mu_{G|H_0}$ and $\mu_{G|H_1}$, respectively, is given by

$$\mu_{G|H_0} \approx N_{nc}\sigma^2 + \sigma^2\sqrt{\pi(N_{nc}-1)} \tag{6.28}$$

$$\max\left(Z_{\mathrm{GPDIT}}(\mathbf{x})\right) \approx \mu_{G|H_1} \approx N_{nc}\sigma^2 + N_{nc}A^2 + \sigma^2\sqrt{\pi(N_{nc}-1)}L_{1/2}\left(-(N_{nc}-1)\mathrm{SNR}^2\right), \tag{6.29}$$

From (6.28) and (6.29), we introduce the approximation of the modified Bessel functions $I_0(x)$ and $I_1(x)$ by $e^x/\sqrt{2\pi x}$, which leads to

$$\mu'_{G|H_1} \approx N_{nc} + N_{nc}\mathrm{SNR} + \left(\frac{1 + 2(N_{nc}-1)\mathrm{SNR}^2}{\mathrm{SNR}}\right), \tag{6.30}$$

where $\mu'_{G|H_1}$ corresponds to $\mu_{G|H_1}/\sigma^2$ and σ^2 is obtained from (6.28). The SNR can be estimated by solving the following quadratic equation as

$$(3N_{nc}-2)\mathrm{SNR}^2 + (N_{nc} - \mu'_{G|H_1})\mathrm{SNR} + 1 \approx 0. \tag{6.31}$$

The SNR estimator is given by the following solution:

$$\widehat{\mathrm{SNR}} = \frac{-(N_{nc} - \mu'_{G|H_1}) + \sqrt{(N_{nc} - \mu'_{G|H_1})^2 - 4(3N_{nc}-2)}}{2(3N_{nc}-2)}. \tag{6.32}$$

The other possible solution from (6.31) provides an incorrect SNR value because it does not belong to the range of values where the approximation applied in (6.30) has good accuracy.

6.3 Simulation results

Simulations are based on a HS-GNSS snapshot receiver, which uses the Double FFT algorithm [SG12]. This receiver implements an efficient snapshot acquisition exploiting some assistance information about the Doppler of the satellites. The objective of these simulations is to compare the performance of the C/N_0 estimators studied in the literature to the ones presented herein. Moreover, we emphasize that the proposed estimators are specially designed for a snapshot receiver, i.e., only exploiting the output of a PDI technique. Simulations are performed using a Galileo E1BC signal and applying two different long coherent integration times such as 100 milliseconds and 1 second.

We compute the NWPR method for two cases: $M = 1$ and $M \neq 1$. The former would correspond to the approach applied typically in a snapshot receiver, where the output of the NPDI technique, applied to acquire the signal, is also used to estimate the C/N_0. In the latter, this is the approach usually implemented in tracking architectures. In both cases, the results of the intermediate coherent correlations obtained from the snapshot receiver are required. For the case of $M = 1$, these correlations are needed to compute the NBP metric and for the case of $M \neq 1$ they are needed to compute the NBP and WBP metrics. Although these correlations are not usually stored by default in a snapshot receiver, it is possible to do so, but at the expense of requiring more memory resources. Despite this fact, simulations of these approaches are really useful since they allow us to compare the performance of the estimators proposed herein for a snapshot receiver with the performance of the NWPR method.

Figure 6.3 illustrates the estimators' performance in terms of estimated C/N_0 vs. real C/N_0 in an AWGN channel using a $T_{\text{coh}} = 100$ ms and $N_{nc} = 10$. Two sets of parameters are considered for the NWPR: i) $T_{\text{coh}} = 100$ ms, $N_{nc} = 10$ and $M = 1$, which is labelled as NWPR in the figure and is representative of a snapshot implementation; ii) $T_{\text{coh}} = 4$ ms, $N_{nc} = 25$ and $M = 10$, which is labelled as NWPRt and is illustrative of a tracking architecture. In both cases, the total integration time to perform the estimation corresponds to 1 second. In this scenario, the estimations provided by all techniques are really accurate. However, the estimation from the NQ-NPDI technique suffers a small accuracy degradation (less than 1 dB) for low values of C/N_0 since the approximation introduced in (6.20) is less effective in this region. The result shows that the closed-form expression derived herein allows the snapshot receiver to estimate the C/N_0 regardless when any of the NQ-NPDI, NPDI, DPDI or GPDIT techniques is used for the signal detection. This fact is really important since for estimating the C/N_0 using the NWPR

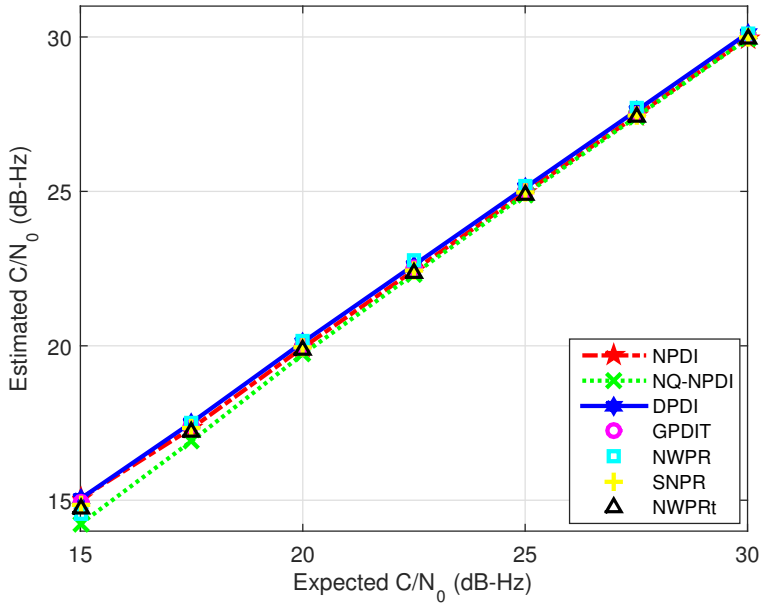

Figure 6.3: The C/N_0 estimates for $T_{\text{coh}} = 100$ ms and $N_{nc} = 10$ for all cases, except for NWPRt with $T_{\text{coh}} = 4$ ms, $N_{nc} = 25$ and $M = 10$.

or SNPR techniques requires the computation of additional intermediate correlation values that are not necessary for detection in a snapshot receiver, whereas the use of the proposed estimators make it possible to obtain the C/N_0 as a byproduct of the acquisition process.

Figure 6.4 shows in a box plot the comparison of the different techniques in an AWGN channel for $C/N_0 = 20$ dB-Hz, using the same parameters as Figure 6.3. In this channel, all techniques offer similar performance except for the NWPR technique, which exhibits a larger variance. Nevertheless, the median obtained by all of the estimators is very near to 20 dB-Hz. This happens because in this scenario it is possible to coherently integrate during 1 second since there is no presence of phase noise.

Figures 6.5 and 6.6 compare the performance of the estimators in the presence of an AWGN channel with the same parameters as Figures 6.3 and 6.4, but adding phase noise from a TCXO clock. This type of clock allows for coherent integrations up to few hundreds of milliseconds. Figure 6.5 shows the estimators' performance comparing estimated C/N_0 vs. real C/N_0. Recall that, the SNPR and NWPR techniques need a coherent integration as long as the non-coherent integration in the other techniques. As a result, they offer an inaccurate estimation of the C/N_0 owing to the signal self-cancellation caused by the

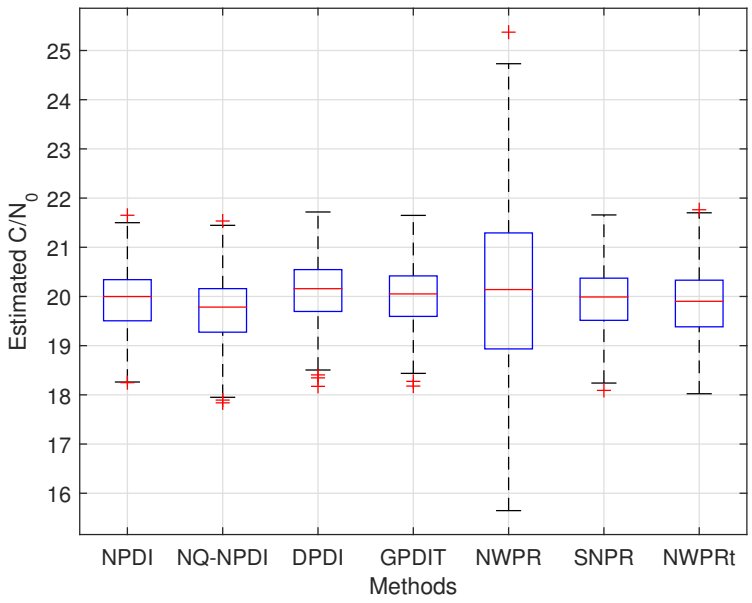

Figure 6.4: Box plot comparison for $C/N_0 = 20$ dB-Hz using the same parameters as Figure 6.3. The central red line of each box illustrates the median of the distribution. The top and bottom edges of each box provide the 75th and 25th percentiles, respectively. The whiskers extend to the most inaccurate C/N_0 estimation without considering outliers and the outliers are plotted as individual points by applying the $'+'$ symbol.

phase noise in the correlation process. The worst technique in these circumstances is the NWPR. The rest of the techniques provide a precise estimation since they are integrating only 100 ms coherently to compute the PDI metric. In this situation, the proposed estimators become the best option to estimate the C/N_0 in a snapshot receiver since they have less computational than the NWPRt technique.

Figure 6.6 shows the box plot for the case of $C/N_0 = 20$ dB-Hz. The proposed techniques and the NPRWt exhibit accurate estimations, though with a small negative bias because the phase noise causes a small reduction of the signal component of the CAFs. However, in this case, most of the estimations offered by the SNPR and NWPR are quite inaccurate since they provide errors larger than 3 dB and 10 dB, respectively.

Figure 6.7 shows a box plot in presence of an AWGN channel. The parameters of the simulation are $T_{\text{coh}} = 1$ s and $N_{nc} = 10$ except for NWPRt, which uses a $T_{\text{coh}} = 4$ ms, $N_{nc} = 250$ and $M = 10$. The simulation is performed using a $C/N_0 = 10$ dB-Hz. In this figure, in absence of phase noise, all of the estimators can accurately estimate the C/N_0,

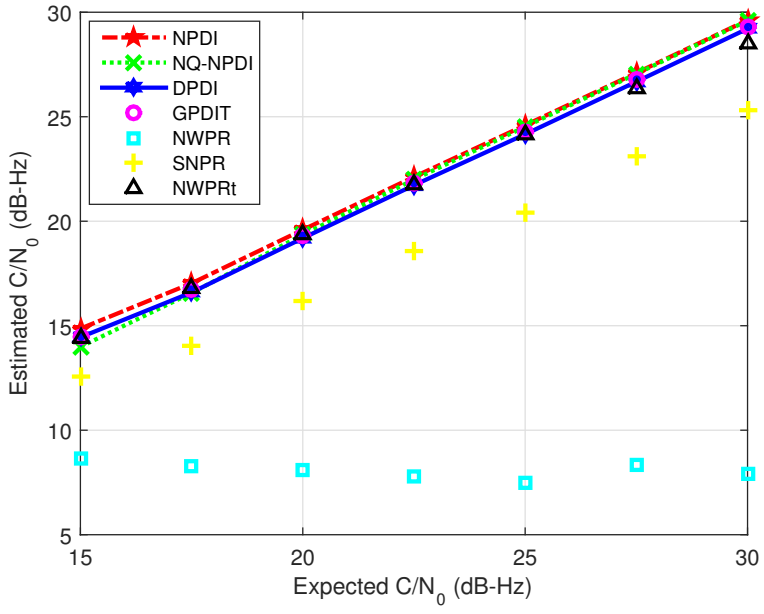

Figure 6.5: The C/N_0 estimates for $T_{\text{coh}} = 100$ ms and $N_{nc} = 10$ except for NWPRt with $T_{\text{coh}} = 4$ ms, $N_{nc} = 25$ and $M = 10$ in the presence of phase noise introduced by a TCXO.

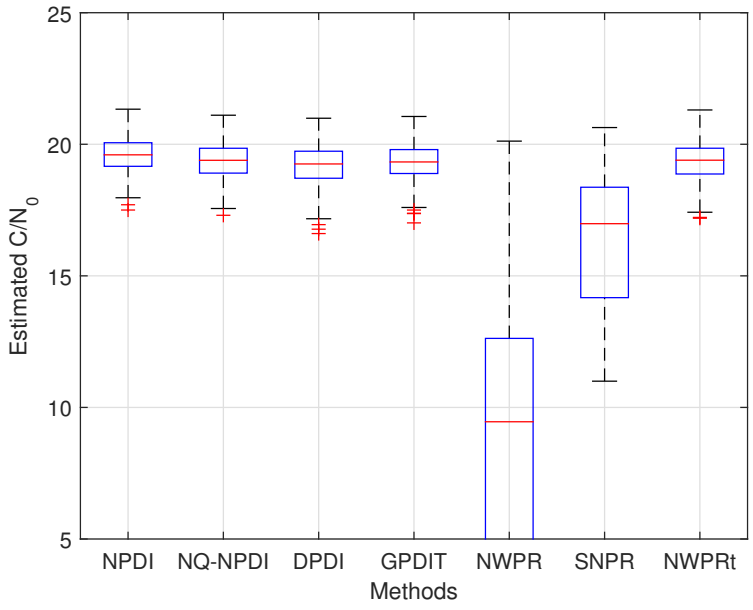

Figure 6.6: Box plot comparison for $C/N_0 = 20$ dB-Hz in an AWGN channel and with the presence of phase noise introduced by a TCXO clock.

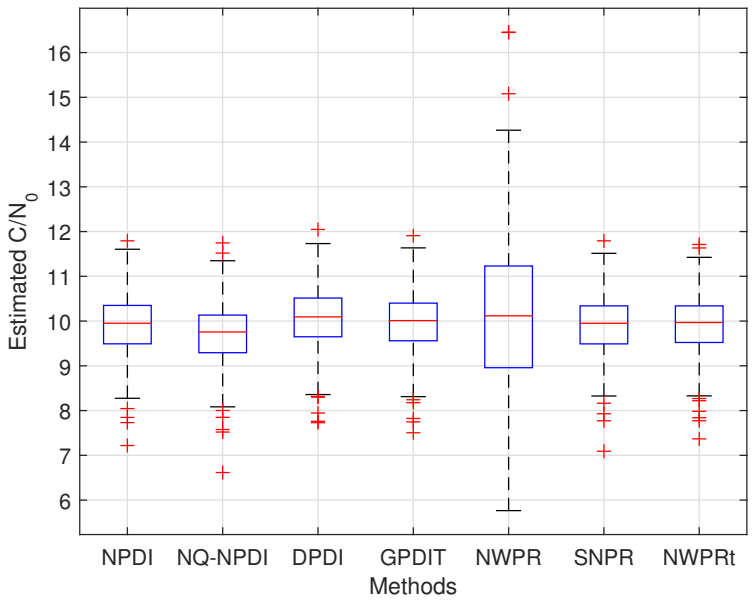

Figure 6.7: Box plot comparison for $C/N_0 = 10$ dB-Hz in an AWGN channel.

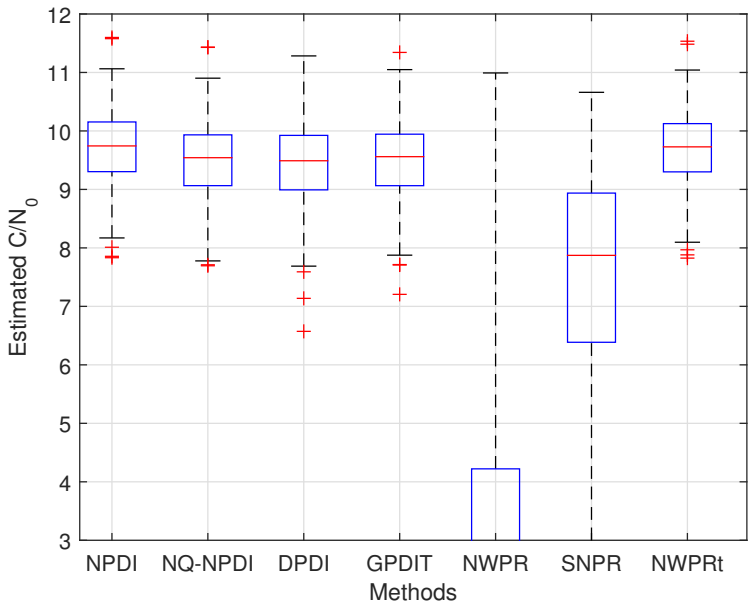

Figure 6.8: Box plot comparison for $C/N_0 = 10$ dB-Hz in an AWGN channel with the presence of phase noise introduced by a CSAC clock.

with the NWPR technique providing the larger variance. The rest of the estimator offer a similar accuracy. This result is similar to the one obtained in Figure 6.4, since, in this

case, it is feasible to integrate coherently 10 seconds because there is not any impairment that limits the coherent integration time.

Figure 6.8 shows a box plot in presence of an AWGN channel with phase noise introduced by a CSAC clock using the same parameters as Figure 6.7. Given that a TCXO clock is not stable enough to allow the receiver to integrate coherently during 1 second, we have used a CSAC. In this case, only our proposed estimators and the NWPRt offer an accurate C/N_0 estimation while the NWPR and SNPR techniques completely fail providing most of the estimations with errors larger than 7 dB and 2 dB, respectively. Given that the NWPRt involves the computation of additional intermediate results in the acquisition process, it turns out that the proposed techniques are the most appropriate ones in this low C/N_0 scenario.

6.4 Conclusions

We have proposed new methods to estimate the C/N_0 based only on the output of detection techniques combining coherent and non-coherent integrations, which are especially suitable for snapshot receivers. Four simple closed-form expressions have been derived to estimate the C/N_0. Each expression applies to one of the PDI techniques, namely NPDI, NQ-NPDI, DPDI or GPDIT. These expressions allow the receiver to estimate the C/N_0 without the need to compute additional correlations or metrics beyond those needed for the signal detection itself. Two conventional estimators taken from the literature have been used as a benchmark. The estimators proposed offer a much more accurate C/N_0 estimation than the benchmarks, especially in the presence of phase noise. Moreover, the proposed estimators offer similar performance to a modification of one of the conventional estimators, but this latter comes with an increased computational load due to the need of obtaining correlation values that are not required by the acquisition stage.

Chapter 7

Problems of high-order BOC signals

With the upcoming full operability of the Galileo system, the trend of next-generation GNSS receivers moves towards providing positioning services that use high-order BOC signals. These signals provide a significant enhancement in terms of positioning accuracy with respect to conventional BPSK signals. This improvement is owing to the increase of the Gabor bandwidth, which leads to a reduction of the CRB of the time-delay estimate. However, high-order BOC signals present several disadvantages. The most important drawback is the presence of secondary lobes in the autocorrelation function that are very little apart from each other and whose amplitude is very similar to the main correlation peak. This causes the CAF of high-order BOC signals to be ambiguous due to the difficulties to distinguish the main correlation peak, particularly in scenarios with low C/N_0 such as deep urban canyons. The acquisition of a secondary peak, also referred to as false lock problem, leads to an incorrect estimation of the time-delay, introducing a bias of some meters in the user's position [Bor14a, GM16].

We focus in this chapter on two problems related to the correlation peaks of high-order BOC signals. On the one hand, we address the problem of mitigating the false lock probability for conditions of weak signal reception at the acquisition stage. To do so, we propose to use a PDI technique to detect the weak GNSS signal and we suggest using the output of this PDI technique to avoid the false lock problem by applying an estimator.

On the other hand, this chapter also tackles the problem of refining the Doppler frequency estimation provided in the acquisition stage for high-order BOC signals in post-correlation. The refinement of Doppler frequency must be done because the estimation obtained from the acquisition stage is not usually accurate enough to track the signal in the tracking stage. The characteristic multi-peaked of high-order BOC correlations can

lead to a more accurate estimation of the Doppler frequency in post-correlation than the conventional BPSK correlation. This is because the secondary peaks of high-order BOC correlations contain enough energy and it can be used to improve the Doppler frequency estimation provided by the acquisition stage. We propose a new technique to refine the coarse Doppler frequency estimation provided by the acquisition stage, especially for high-order BOC signals.

7.1 Mitigation of false locks in the acquisition of high-order BOC signals

This section deals with the mitigation of the false lock probability for high-order BOC signals. We start analysing the most relevant work carried out by previous authors in this topic, which is usually addressed in the tracking stage. The most common techniques to circumvent this problem in the tracking stage are bump jumping, double optimization multi-correlator-based estimator and BPSK methods, which are described in the following subsections.

Although many people have tackled the false problem in the tracking stage, less attention has been paid to the problem of the main peak detection or false locks at acquisition stage. In latter stage, the code-delay estimation obtained from high-order signals is often biased since it is obtained from a secondary peak. This fact causes that the tracking of the signal starts in a secondary peak making the first estimates of the user's position biased. In this chapter, after the review of the techniques to solve the false lock problem, we propose a method to solve the unambiguous estimation problem of weak high-order BOC signals in the acquisition stage. First, we propose to acquire the weak GNSS signal by using the NPDI or DPDI technique. Then, we suggest applying the LS and ML approaches to solve the false lock problem.

7.1.1 Brief review of mitigation of false lock techniques

7.1.1.1 Bump jumping

One of the most common method used to reduce the false lock problem is the bump jumping, which was proposed in [Fin99]. The bump jumping works with five correlation points at tracking stage: very early, early, prompt, late and very late [Blu07a]. This

technique decides if the main correlation peak is being tracked or not by comparing the magnitude of the peak currently being followed by the prompt to the magnitude of the adjacent peaks, which are followed by the very early and very late correlators.

This technique adopts three counters, each associated with the very early, prompt or very late correlator, to detect the false lock. The magnitudes of the very early, prompt and very late correlators are compared each time instant. Whenever the very late correlator contains the largest magnitude, the counter of the very late is increased one and the very early counter is decremented one, when the very early is the largest magnitude the opposite occurs. If the prompt surpasses both the very early and late, the former is increased one and the latter counters are decreased one. A false lock is detected, whether the very early and very late counters reach a threshold before the prompt counter. Then, the prompt is changed by the counter that reaches the threshold. The counters are reset when a threshold is reached and cannot have a value lower than zero.

7.1.1.2 Double optimization multi-correlator-based estimator

The double optimization multi-correlator-based estimator is a technique to circumvent the unambiguous estimation of high-order BOC autocorrelations exploiting several correlator outputs at the tracking stage [GM16, GM14]. The number of correlation outputs can be chosen by the receiver. This technique is based on minimizing a ML cost function comparing the received correlators outputs with an ideal autocorrelation function. This minimization allows the receiver to obtain an accurate estimation of the time-delay, which leads to identify the main correlation peak. Moreover, the performance of the technique can be improved by combining several consecutive cost functions. Thereby, the effect of the noise component in the correlator outputs is reduced permitting the receiver to provide a more reliable decision about which is the main correlation peak.

7.1.1.3 Full BPSK methods

The full BPSK methods is a family of techniques whose objective is to transform the autocorrelation of a BOC signal in an unambiguous one. Several of these techniques are included in [Loh08, Bur06]. The most known technique consists in transforming the autocorrelation of the received signal from BOC to BPSK [Hei04]. To do so, one of the two lobes of the BOC signal spectrum is shifted towards the middle of frequency band. This lobe contains a similar spectrum as a conventional BPSK signal. Then, the resulting

signal is correlated with a local BPSK reference obtaining an autocorrelation of a BPSK signal. The same process can be applied to the other lobe. The correlation provided by the two lobes is combined non-linearly to obtain a gain in terms of signal detection. The resulting correlation becomes an unambiguous triangle. This method allows the receiver to obtain an unambiguous estimation of the time-delay, but it is less accurate than the one offered by the BOC signals. Moreover, although the two lobes of the signal are exploited, some degradation in terms of signal detection is suffered since the two lobes must be combined non-linearly, which is less effective than a coherent combination.

7.1.1.4 Double estimator technique

The Double estimator technique is based on circumventing the ambiguity of the BOC signal in the tracking stage by using three tracking loops: a DLL for the time-delay, a PLL for the carrier and a sub-carrier lock loop (SLL) for tracking the sub-carrier component [Blu07a]. The main idea of this technique is to use two estimates of the time-delay, one from the DLL and another from the SLL. The estimate obtained from the SLL is very accurate but ambiguous whereas the estimate obtained from the DLL is unambiguous but less accurate. Assuming that the noise level in the latter is sufficiently low, it can be used to solve the ambiguity of the measure based on the subcarrier. More precisely, the time-delay estimate of this technique is provided by using a rounding operation, in which the DLL time-delay estimate is applied to circumvent the SLL time-delay ambiguity.

7.1.2 Signal model

The conventional approach to acquire the satellites in view consists in computing the CAF for a given coherent integration time. Considering that there is no bit transition, the CAF can be expressed as

$$x(\tilde{\tau}, \tilde{f}_d) = d\tilde{A}e^{j\phi}\text{sinc}(\Delta f T_{\text{coh}})B(\Delta\tau) + \omega, \tag{7.1}$$

where $\tilde{A}$ is the signal amplitude with phase ϕ, d is the value of the data navigation bit taking value of 1 or -1, $\Delta\tau = \tau - \tilde{\tau}$ is the time-delay offset between the local replica and the received GNSS signal, $\Delta f = f_d - \tilde{f}_d$ is the residual frequency offset, T_{coh} is the coherent integration time, $B(\Delta\tau)$ is the autocorrelation function of the GNSS signal and ω is AWGN after computing the CAF with zero-mean and variance σ^2.

A PDI technique, defined as Z_x, is applied by the use of a non-linear function of

several consecutive CAFs computed in different time instants. PDI techniques allow the receiver to accumulate the enough energy to be able to detect weak signals. The goal of the metric of the PDI technique is to discriminate between two hypotheses. Under H_0 the satellite is not in view (*i.e.* $\tilde{A} = 0$) and under H_1 the satellite is in view (*i.e.* $\tilde{A} \neq 0$). The discrimination between the two hypotheses is performed comparing the maximum value of the metric of the PDI technique with a threshold. The satellite is declared in view, if the maximum value of this metric exceeds the threshold. More details about the definition of a detection threshold can be found in Subsection 2.2.2.

7.1.3 PDI techniques

As we have seen in Chapters 3 and 4, there are many PDI techniques to acquire weak GNSS signals. The approach that we propose in this chapter to reduce the false lock probability could be applied for all of them. However, as in this chapter we want to focus on the false lock problem, we will only use two PDI techniques to acquire the weak GNSS signal: the NPDI and the DPDI, which are the most used nowadays.

The most common technique used to perform non-coherent integrations is the NPDI as

$$Z_{\text{NPDI}}(\mathbf{x}) = \sum_{k=1}^{N_{nc}} |x_k(\tilde{\tau}, \tilde{f}_d)|^2. \tag{7.2}$$

The NPDI technique removes carrier impairments such as frequency offset and data bits by using the squared absolute value. The drawback of the NPDI technique is that it suffers from the squaring loss effect. That is, the mean of the noise is increased with respect to the coherent integration. Thereby, this technique offers a lower detection gain than the coherent integration in an AWGN channel, but the former can be applied to detect signals in presence of frequency offset and data bits.

Alternatively, the DPDI method can be implemented, which is defined as

$$Z_{\text{DPDI}}(\mathbf{x}) = \left| \sum_{k=2}^{N_{nc}} x_k(\tilde{\tau}, \tilde{f}_d) x_{k-1}^*(\tilde{\tau}, \tilde{f}_d) \right|. \tag{7.3}$$

The idea behind this technique is to eliminate the uncertainty of the frequency offset without increasing the mean of the noise. This is achieved by multiplying one CAF with the next CAF conjugated. By doing so, the noise components of 2 consecutively CAFs are uncorrelated, while the signal components are highly correlated. Using this approach

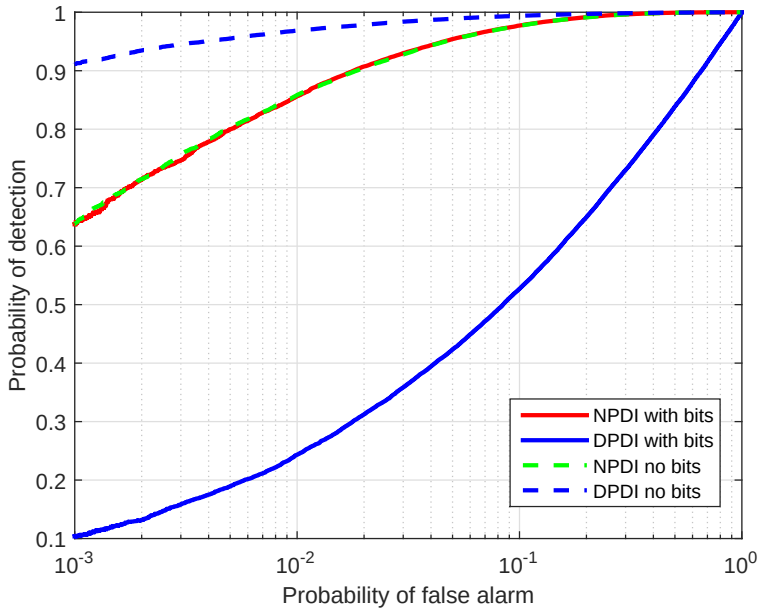

Figure 7.1: Example of ROC curves for the NPDI and DPDI techniques with $C/N_0 = 20$ dB-Hz, $T_{\text{coh}} = 100$ ms, $N_{nc} = 20$.

the mean of the noise is not increased, and therefore in an AWGN channel, the DPDI technique provides a gain over the NPDI method in terms of signal detection as long as there is no presence of data bits.

A performance comparison between the NPDI and DPDI techniques is shown in Figure 7.1. This figure illustrates the ROC curves of these techniques in presence and absence of bits. As we can be observed, the NPDI is insensitive to the presence of data bits, whereas the performance of the DPDI technique suffers a strong degradation due to data bits. However, if there is no presence of data bits, the DPDI illustrates a clear gain in signal detection over the NPDI.

7.1.4 Mitigation of false lock probability

The acquisition of the main peak is a challenging problem because the secondary peaks of its autocorrelation have practically the same energy as the main peak. The conventional approach used at acquisition stage, that is, to estimate the time-delay as the position of the maximum of the correlation, might not be a good solution to solve this problem in certain conditions. These conditions include when the correlation function is impacted by

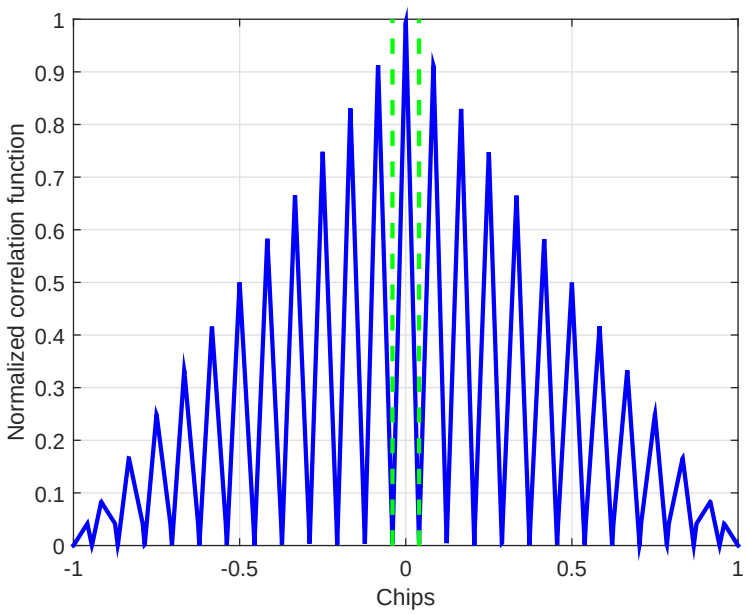

Figure 7.2: Definition of the false lock region in the autocorrelation of a $\text{BOC}_{\cos}(15,2.5)$ signal.

the sampling frequency used, AWGN and distortions introduced by the receiver front-end.

Before proceeding, we define that a false lock is present when the estimation of the code-delay belongs to a secondary peak. On the contrary, if the estimation of the code-delay is the main correlation peak, there is no false lock. This region is delimited in Figure 7.2, which shows the absolute value of the $\text{BOC}_{\cos}(15,2.5)$ autocorrelation signal as a representative case of high-order BOC modulations. Taking into account this figure, we assume that a false lock is present when the estimated code-delay is outside the region defined between the two green lines in Figure 7.2.

To solve the problem of unambiguous estimation at the acquisition stage, we propose to use the ML and LS approaches. Although, these estimators have been already implemented in [GM14] and [GM16], they have been applied for the tracking stage, where only use coherent correlator outputs obtained from this stage. In [GM16], it is also mentioned that it is possible to combine theses correlator outputs to improve the performance of the technique. However, in this document, we use these estimators to solve the problem at acquisition where PDI techniques must be used first to detect the weak GNSS signal. After that, the ML or LS estimator are applied to solve the problem of unambiguous estimation. We propose to use the output of the PDI technique not only to detect the

satellite signal but also to mitigate false lock problem. This approach allows the receiver to start the tracking of the signal in the main correlation peak. This is an advantage with respect to the techniques implemented in tracking stage, since they usually need some time to correct the false lock problem, which causes that the first position estimations of the user can be biased.

The ML and LS estimators exploit the fact that the autocorrelation function of high-order BOC signals is known. Taking into account this information the correct peak can be acquired and the probability of false lock can be improved in certain conditions where the usage of the maximum of the correlation is not the optimum approach. In this sense, the procedure is as follows: the NPDI or DPDI technique is used to acquire a weak signal. Then, a coarse estimation of the code delay τ and the Doppler frequency f_d is obtained as $\hat{\tau}$ and $\hat{f}_d$, respectively. From these estimations, we define the vector $\mathbf{z}$ containing a set of $2Q+1$ samples as follows:

$$\mathbf{z} \doteq [Z_x(\mathbf{x}, \hat{\tau} - Q, \hat{f}_d), \ldots, Z_x(\mathbf{x}, \hat{\tau} + Q, \hat{f}_d)]^T, \tag{7.4}$$

where $Z_x(\mathbf{x}, \hat{\tau} - Q, \hat{f}_d), \ldots, Z_x(\mathbf{x}, \hat{\tau} + Q, \hat{f}_d)$ is the output of the NPDI method or the DPDI method for the estimation of the Doppler frequency $\hat{f}_d$ and for the $2Q+1$ samples of the correlation function contained around $\hat{\tau}$ in $\pm$ 1 chip; Q is the number of samples contained in one side of the correlation function during 1 chip, that is, the ratio between the sampling frequency and the chip rate of the BOC signal. The samples of the expected correlation with an unknown code delay τ are known in advance and can be stacked in vector form as,

$$\mathbf{b}(\tau) \doteq [B(\tau - Q), \ldots, B(\tau + Q)]^T. \tag{7.5}$$

One way to estimate the code-delay that is more robust against the false lock problem consists in finding the value of the delay that provides the best fit between the measured correlation and the expected one. This value of the delay is obtained as the argument that minimizes the following non-linear least square cost function:

$$J(\tau, \varphi) = ||\mathbf{z} - \varphi\mathbf{b}(\tau)||^2, \tag{7.6}$$

where φ is the unknown amplitude. This function depends on two unknown parameters τ, φ and it can be solved by separation of variables. To do so, the unknown amplitude is replaced by $\hat{\varphi} = (\mathbf{b}(\tau)^T\mathbf{b}(\tau))^{-1}\mathbf{b}(\tau)^T\mathbf{z}$ [Kay98]. After that, the problem can be solved by using an iterative algorithm because an analytical solution does not exist in a closed-form.

Another approach consists in applying the ML estimator assuming that the output of the NPDI and DPDI techniques were Gaussian. By doing so, the cost function can be

reformulated as follows:

$$F(\tau, \varphi) = (\mathbf{z} - \varphi\mathbf{b}(\tau))^T \mathbf{\Sigma}^{-1} (\mathbf{z} - \varphi\mathbf{b}(\tau)), \tag{7.7}$$

where the $((2Q + 1) \times (2Q + 1))$ covariance matrix $\mathbf{\Sigma}$ is non-diagonal matrix owing to the colored noise generated at post-correlation level. This matrix is given by the autocorrelation of the BOC signal [Gus16]. This cost function can be minimized by the same procedure used to minimize the cost function in (7.6), but substituting the unknown amplitude by the following expression that contains the covariance matrix $\hat{\varphi} = (\mathbf{b}(\tau)^T \mathbf{\Sigma}^{-1} \mathbf{b}(\tau))^{-1} \mathbf{b}(\tau)^T \mathbf{\Sigma}^{-1} \mathbf{z}$.

It should be added that this estimator is not strictly the ML for the NPDI and DPDI techniques because the noise produced by these techniques is not Gaussian. Nonetheless, the noise of the NPDI metric follows Chi-square distribution under hypothesis H_0, but when the number of N_{nc} is large the noise tends to be Gaussian by the central limit theorem. On the other hand, the pdf of the DPDI metric is not known in a closed-form. Therefore, the minimization of the cost function in (7.7) for the DPDI method might be far from being the optimal ML estimator. However, this estimator has a good performance for the DPDI method as we will see later on.

7.1.5 Simulation results

Simulations have been performed using a $\text{BOC}_{\cos}(15,2.5)$ signal as a representative case of a high-order BOC signal. The sampling frequency used is 50 MHz, which is the maximum value of a good USRP nowadays [Res12]. The frequency search space is within -500 Hz to 500 Hz because we assume that we have some assisted information about the Doppler frequency of the satellite and we assume that there is no presence of data bits in the received signal. The coherent time used is 10 ms and the steps of the search frequency are every 50Hz.

In this subsection, the probability of false lock at acquisition is assessed for three different methods: the conventional approach used at acquisition stage (to estimate the time-delay as the position of the maximum of the correlation), the ML estimator, and the LS estimator. It is clear that the performance of the three methods is affected by the noise level of the received signal because it distorts the correlation function. Moreover, the performance of the conventional approach used at acquisition stage is limited by the sampling frequency or the space between the samples of the correlation function. This happens because sometimes the maximum of the correlation is sampled in a secondary

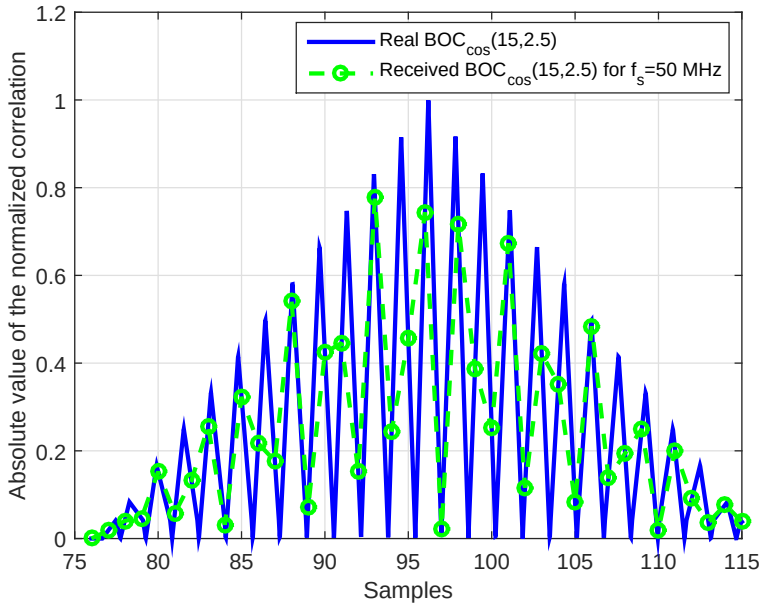

Figure 7.3: Example of a false lock due to the sampling frequency.

peak instead of a main peak. An example of the false lock owing to the sampling frequency is shown in Figure 7.3.

Figure 7.4 shows the comparison among the conventional approach used at acquisition stage (referred to as "max" in the plot), the ML estimator, and the LS estimator in an AWGN channel. The simulation includes an unknown random time-delay at the received signal, which follows a uniform distribution. We have a high probability of false lock owing to the sampling frequency by applying the conventional approach used at acquisition stage, though we have a high C/N_0. Nevertheless, this effect can be mitigated by using the ML and LS estimators as proposed in this work. These estimators are able to provide small values of false lock probability for small values of C/N_0. For instance, using a total integration of 200 ms, we can obtain a false lock probability smaller than 0.1 for a C/N_0 value of 30 dB-Hz. For the particular case considered in the simulation, the best method from the ones assessed to reduce the probability of false lock is the ML estimator, which offers and improvement over the LS estimator. Moreover, the larger the number of N_{nc}, the better performance the method offers. This is because we are increasing the total integration time and it allows the receiver to reduce the effect of the noise. Comparing the estimators applied over the NPDI and DPDI techniques, we can see that these estimators have better performance by using the DPDI method in terms of probability of false lock.

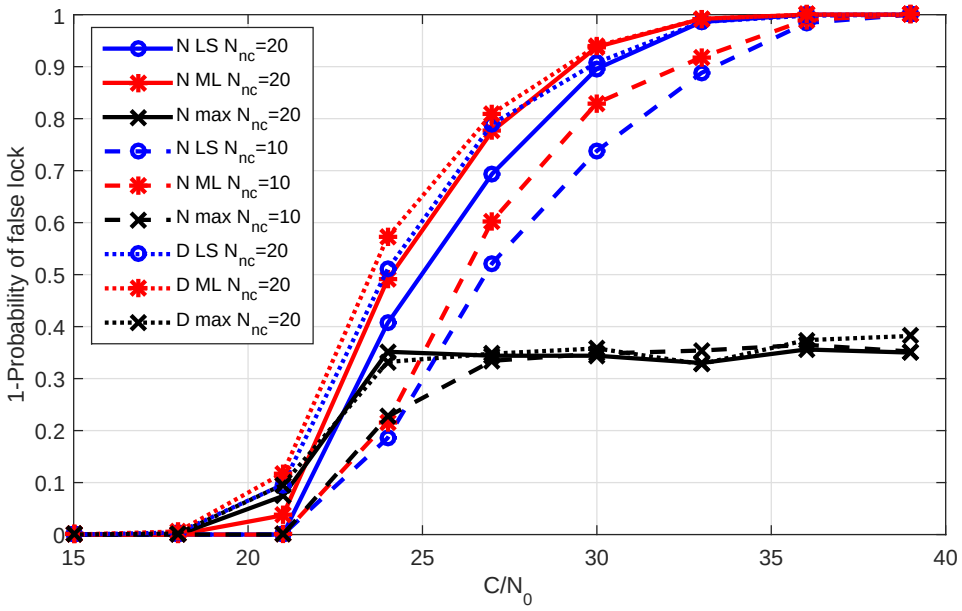

Figure 7.4: Comparison between the conventional approach used at acquisition stage, ML, and LS for a $P_{FA} = 0.05$ ("N" means NPDI, "D" means DPDI).

7.1.6 Conclusions

The probability of false lock obtained by applying the conventional approach used at acquisition stage is limited by the sampling frequency. This approach is not able to mitigate the false lock problem, though the received signal arrives with high C/N_0. We have proposed two estimators the ML and the LS to solve the problem of false locks. These estimators reduce the probability of false lock with respect to the conventional technique used at acquisition stage. The most promising technique corresponds to the ML. In addition, the application of these estimators after using the DPDI method provides a gain over the application of these estimators after using the NPDI method in terms of probability of false lock.

7.2 Fine frequency estimation for high-order BOC signals

The main task of the acquisition stage of a GNSS receiver is to obtain a coarse estimation of the time-delay and the Doppler frequency for each satellite in view. After that, these

estimations are tracked and refined to accurately follow any possible variation of time and frequency at the tracking stage. Nevertheless, many times the coarse estimation of Doppler frequency provided by the acquisition stage is not accurate enough to pass directly to the tracking stage. In that situation, the accuracy of the Doppler frequency estimation must be improved before starting the tracking stage.

According to the estimation theory, the ML estimator of the Doppler frequency is the value that maximizes the magnitude of the CAF. Nonetheless, it is not possible to apply this estimator in practice to find an accurate estimation of the Doppler frequency since this estimator has a high computational complexity. Then, we must resort to other alternatives to get a precise estimation of the Doppler frequency [Tan13].

One way to obtain a fine Doppler frequency estimation is by the use of a FLL. However, the FLLs need a particular architecture using filters, numerical control oscillators and some additional data. Moreover, the FLLs are usually integrated inside the tracking loop and more and more GNSS receivers are using an open-loop architecture, which do not have a tracking loop. Another approach is used [Tan13]. This method estimates the Doppler frequency by application of a formula, but it only works properly when the receiver uses a specific Doppler frequency step to acquire the signal. An additional technique was proposed in [Tan12], which improves the Doppler frequency estimation based only on the CAF obtained from the acquisition stage by using a LS estimator in post-correlation.

In this chapter, a new technique to refine the Doppler frequency referred to as Multilag Least Squares (MLS) is proposed. The proposed technique herein exploits the characteristic multi-peaked of high-order BOC signals to increase the accuracy of the Doppler frequency estimation. The CRB and a conventional least square found in the literature are used as a benchmark to compare the performance of the MLS estimator. Moreover, we analyze how affects the sampling frequency used to acquire the signal in the performance of the estimators. Before proceeding, we introduce some notation and definitions that will be used throughout the chapter.

7.2.1 Signal model

The CAF computed to acquire one satellite in view assuming that there is absence of bit transition can be written as follows:

$$x(\tilde{\tau}, \tilde{f}_d) = d\tilde{A}e^{j\phi}\text{sinc}(\Delta f T_{\text{coh}})B(\Delta\tau) + \omega, \tag{7.8}$$

where $\tilde{A}$ is the amplitude obtained from computing the CAF with phase ϕ, d is the value of the data navigation bits taking value of 1 or -1, $\Delta\tau = \tau - \tilde{\tau}$ is the time-delay offset between the local replica and the received GNSS signal, $\Delta f = f_d - \tilde{f}_d$ is the residual frequency offset, T_{coh} is the coherent integration time, $B(\Delta\tau)$ is the circular autocorrelation function of a GNSS signal and ω is AWGN after computing the CAF with zero-mean and variance σ^2. The $\text{sinc}(\Delta f T_{\text{coh}})$ term provides the losses of coherent integration because of the residual Doppler frequency between the received signal and the local replica. After performing the CAF, its absolute value is computed as

$$Z(\tilde{\tau}, \tilde{f}_d) = |x(\tilde{\tau}, \tilde{f}_d)|. \tag{7.9}$$

In order to detect if the satellite is in view or the satellite is not in view, the maximum magnitude of (7.9) is compared to a signal detection threshold. The satellite is not in view if the maximum magnitude of (7.9) does not exceed the detection threshold. Nevertheless, if the maximum magnitude of (7.9) exceeds the signal detection threshold the satellite is considered in view and a coarse estimation of the τ and f_d is obtained as $\hat{\tau}$ and $\hat{f}_d$.

In acquisition stage, the accuracy of the $\hat{\tau}$ is usually given by the sampling frequency, denoted as f_s, used at the receiver. This occurs because the receivers compute the CAF in frequency domain using FFT and IFFT operations. The accuracy of $\hat{f}_d$ is comprised between the range $[-f_{st}/2,\ f_{st}/2]$, where f_{st} is the search step of Doppler frequency used in the local replica to compute the CAF. The f_{st} is chosen taking into account a trade-off between the complexity in terms of computational burden at the receiver and the accuracy in the estimation of Doppler frequency. A typical value of f_{st} to mitigate the coherent integration losses is $1/(2T_{\text{coh}})$. However, many times the estimation $\hat{f}_d$ is not precise enough to track the signal in the tracking stage. For this reason, a more accurate estimation of f_d must be done before starting the tracking stage.

7.2.2 Least squares estimator

As we have already mentioned, the degradation produced in the CAF by the residual Doppler frequency between the received signal and the local replica is affected by a sinc function. This method exploits this fact to refine the coarse Doppler frequency estimation obtained in the acquisition stage [Tan12]. More precisely, the method consists in finding the Doppler frequency value that provides the best fit between the theoretical sinc function and the measured one. To do so, let us define the received or the measured sinc function in a vector $\mathbf{g}$ containing a set of 3 samples: the maximum value of the CAF in (7.8) and

the two adjacent values of the CAF in the frequency domain for the estimation of $\hat{\tau}$ as

$$\mathbf{g} \doteq \begin{bmatrix} Z(\hat{\tau}, \hat{f}_d - f_{st}) \\ Z(\hat{\tau}, \hat{f}_d) \\ Z(\hat{\tau}, \hat{f}_d + f_{st}) \end{bmatrix}. \tag{7.10}$$

We define the vector $\mathbf{t}(f_d)$ containing also 3 samples of the theoretical sinc function with an unknown Doppler frequency:

$$\mathbf{t}(f_d) \doteq \begin{bmatrix} |\mathrm{sinc}((f_d - \hat{f}_d - f_{st})T_{\mathrm{coh}})| \\ |\mathrm{sinc}((f_d - \hat{f}_d)T_{\mathrm{coh}})| \\ |\mathrm{sinc}((f_d - \hat{f}_d + f_{st})T_{\mathrm{coh}})| \end{bmatrix}. \tag{7.11}$$

It is worth mentioning that we only take three points to define the vectors $\mathbf{g}$ and $\mathbf{t}(f_d)$ because we want to guarantee that the three chosen points are located in the main lobe of the sinc function. We do not take more points of the sinc function since the rest of the points contain almost no signal and in presence of noise, they may cause a worsening of the fine Doppler estimation of f_d.

Figure 7.5 shows an illustrative plot of the expected theoretical sinc function, the measured sinc function obtained from the acquisition stage, and the Doppler frequency of the received signal. The fine Doppler frequency estimation of f_d is carried out by minimizing the following non-linear LS cost function:

$$J(\alpha, f_d) = ||\mathbf{g} - \alpha\mathbf{t}(f_d)||^2, \tag{7.12}$$

where α is the unknown amplitude due to the propagation effects of the received signal. The non-linear LS, which is affected by two unknown parameters f_d and α, can be minimized by separation of variables in two steps [Kay98]. Firstly, the non-linear LS is minimized with respect to α so that the cost function depends only on f_d. The unknown amplitude that minimizes the function J is $\hat{\alpha} = (\mathbf{t}(f_d)^T\mathbf{t}(f_d))^{-1}\mathbf{t}(f_d)^T\mathbf{g}$. Replacing this expression in (7.12), we get

$$J(\hat{\alpha}, f_d) = ||\mathbf{g} - (\mathbf{t}(f_d)^T\mathbf{t}(f_d))^{-1}\mathbf{t}(f_d)^T\mathbf{g}\mathbf{t}(f_d)||^2. \tag{7.13}$$

Secondly, the problem now reduces to minimize (7.13). The cost function must be minimized by the application of an a one-dimensional search method since there is no analytical solution in closed-form for f_d. In our simulation, we use simple for loop to estimate the value of f_d.

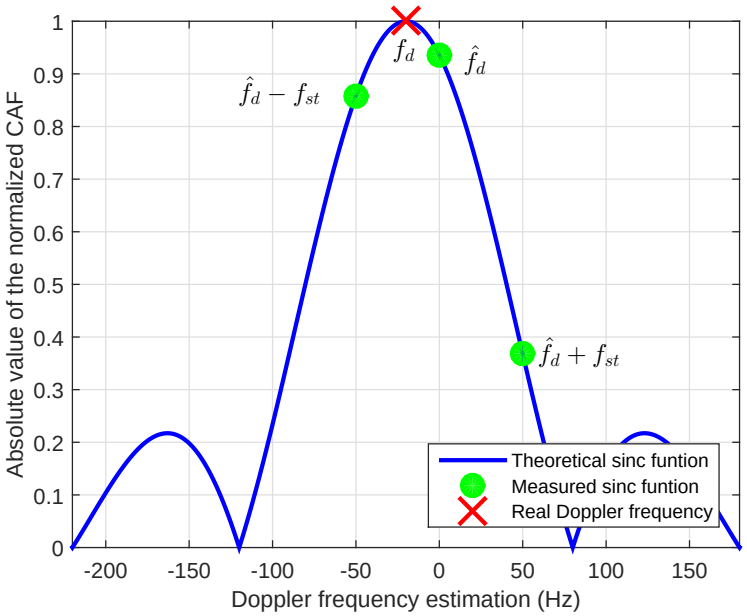

Figure 7.5: Illustrative plot of the CAF in frequency domain.

7.2.3 Multilag least squares estimator

In this subsection, we propose a novel contribution for estimating the f_d in the acquisition stage referred to herein as MLS estimator, especially for high-order BOC signals. We want to exploit the fact that the ideal CAF in time domain of a high-order BOC signal contains a considerable number of secondary peaks. Moreover, the received signal is always impacted by the sampling frequency used and this causes that many times the high-order BOC signals are not sampled in the maximum of the CAF since the signal arrives with an unknown random time-delay. One example of the ideal CAF of a $\text{BOC}_{\cos}(15,2.5)$ signal in time domain and the received CAF using a $f_s = 50$ MHz, which is the maximum value of a USRP nowadays [Res12], is shown in Figure 7.6. The received CAF often exhibits some high peaks with practically the same magnitude, which may be a useful tool to estimate f_d of a more effective way in terms of accuracy than the estimator explained in Subsection 7.2.2.

The method explained in Subsection 7.2.2 only uses the maximum value of the CAF and the two adjacent values of the CAF in frequency domain. Nonetheless, we propose to use the different high peaks of the CAF in time domain (including the highest peak) and each high peak with their two adjacent values of the CAF in frequency domain. This approach can be solved by minimizing the distance between two matrices. The method

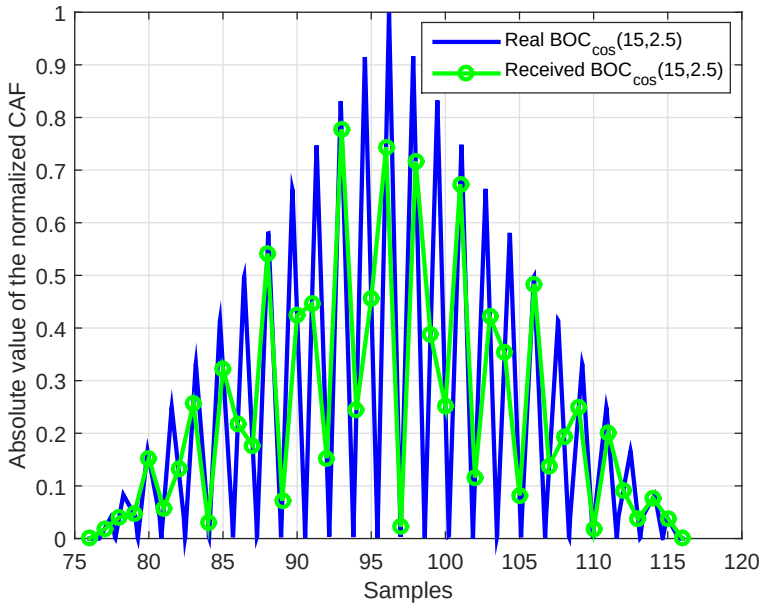

Figure 7.6: Illustrative plot of the ideal CAF of a $\text{BOC}_{\cos}(15,2.5)$ signal in time domain and the received CAF using a $f_s = 50$ MHz (without taking into account the noise and the Doppler effect).

proposed herein deals with the estimation of Doppler frequency by finding the best fit between the theoretical sinc functions and the different measured sinc functions. Before proceeding, we denote the magnitude of the second highest peak of the CAF in time domain as α_2 with argument τ_2 and the magnitude of the thirst highest peak of the CAF in time domain as α_3 with argument τ_3 and so on. Thereby, let us define the $K \times 3$ matrix $\mathbf{G}$, with K the number of chosen high peaks of the CAF in time domain, containing the different measured sinc functions from each high peak as

$$\mathbf{G} \doteq \begin{bmatrix} Z(\hat{\tau}, \hat{f}_d - f_{st}) & Z(\hat{\tau}, \hat{f}_d) & Z(\hat{\tau}, \hat{f}_d + f_{st}) \\ Z(\hat{\tau}_2, \hat{f}_d - f_{st}) & Z(\hat{\tau}_2, \hat{f}_d) & Z(\hat{\tau}_2, \hat{f}_d + f_{st}) \\ Z(\hat{\tau}_3, \hat{f}_d - f_{st}) & Z(\hat{\tau}_3, \hat{f}_d) & Z(\hat{\tau}_3, \hat{f}_d + f_{st}) \\ \vdots & \vdots & \vdots \\ Z(\hat{\tau}_K, \hat{f}_d - f_{st}) & Z(\hat{\tau}_K, \hat{f}_d) & Z(\hat{\tau}_K, \hat{f}_d + f_{st}) \end{bmatrix}. \tag{7.14}$$

The cost function can be expressed by the Frobenius distance as

$$H(\boldsymbol{\alpha}, f_d) = ||\mathbf{G} - \boldsymbol{\alpha} \cdot \mathbf{t}(f_d)^T||_F^2, \tag{7.15}$$

where the vector $\boldsymbol{\alpha} = [\alpha, \alpha_2, \alpha_3, \cdots, \alpha_K]^T$ have all the unknown amplitudes, one unknown

amplitude for each chosen high peak and $\mathbf{t}(f_d)$ is defined in (7.11). The estimation of f_d is the value that minimize the cost function. To minimize this problem, we apply separability of variable because the vector $\boldsymbol{\alpha}$ is linearly dependent over $\mathbf{t}$. Then, we must replace $\hat{\boldsymbol{\alpha}} = \frac{\mathbf{G}\cdot\mathbf{t}(f_d)}{||\mathbf{t}(f_d)||^2}$ by $\boldsymbol{\alpha}$ in (7.15). Thus,

$$H(\hat{\boldsymbol{\alpha}}, f_d) = \left|\left|\mathbf{G} - \frac{\mathbf{G}\cdot\mathbf{t}(f_d)}{||\mathbf{t}(f_d)||^2}\mathbf{t}(f_d)^T\right|\right|_F^2. \tag{7.16}$$

After that, the fine estimation of f_d is found by applying a one-dimensional search method since there is not any analytical solution in closed-form. In this case, we also use a simple for loop to minimize the cost function.

7.2.4 Cramer-Rao bound

Theoretical lower bounds become necessary for evaluating the performance of the proposed estimators in the Subsections 7.2.2 and 7.2.3. The CRB, which expresses a lower bound on the variance of any unbiased estimator, provides a benchmark to compare the performance of the LS and MLS estimators. The CRB is defined by:

$$\text{var}(\hat{f}_d) \geqslant \text{CRB}(f_d) = -\left[E\left[\frac{\partial^2}{\partial f_d^2}\ln p_r(\mathbf{r}; f_d)\right]\right]^{-1}, \tag{7.17}$$

where $E[\cdot]$ is the expected operator, $\mathbf{r}$ is a vector containing the M_{ch} samples of the received signal defined in (2.12) and $p_r(\mathbf{r}; f_d)$ is the probability density function of the received signal. The CRB of the Doppler frequency estimation in an AWGN channel is given by [Rif74]

$$\text{var}(\hat{f}_d) \geqslant \frac{6}{(2\pi)^2\text{SNR}T_s^2 M_{ch}(M_{ch}^2 - 1)}, \tag{7.18}$$

where SNR is referred to the signal-to noise ratio of the received signal at pre-correlation level and $T_s = 1/f_s$. Assuming that $M_{ch} = f_s T_{\text{coh}} >> 1$ the CRB is written as follows:

$$\text{var}(\hat{f}_d) \geqslant \frac{6}{(2\pi)^2\text{SNR}f_s T_{\text{coh}}^3}. \tag{7.19}$$

Typically, the SNR is not a parameter used in GNSS since it depends on the receiver front-end bandwidth denoted as B_w. The parameter usually utilized to analyze the performance of techniques is the C/N_0, which is not affected by the receiver bandwidth. The relationship between the SNR at pre-correlation level and the C/N_0 is given by

$$\text{SNR} = \frac{C}{N_0 B_w}, \tag{7.20}$$

where B_w is assumed ideally to be flat over the whole digital bandwidth. The CRB in (7.19) is the bound for the estimation of f_d because it takes into account the C/N_0 from the received signal. However, often in post-correlation, we do not get a C/N_0 as high as in pre-correlation since the received CAF many times exhibits some high peaks, but none of them match with the real peak of the CAF (Figure 7.6). This fact causes a degradation at post-correlation in terms of C/N_0, which is due to the sampling frequency and the unknown random code-delay of the received signal.

7.2.5 Simulation results

Simulations are carried out by the use of $\text{BOC}_{\cos}(15,2.5)$ signals, as a particular case of high-order BOC modulations, using a coherent time of 10 ms. We consider a frequency search range from -500 Hz to 500 Hz since we assume knowing the assisted information about the Doppler frequency from the satellite and the steps of the search frequency are every 50 Hz. The implemented receiver computed the CAF in frequency domain by using the FFT and IFFT operations. Moreover, simulations are performed in an AWGN channel and including an unknown random time-delay at the received signal, which follows a uniform distribution.

To measure the performance of the LS and MLS estimators, the mean square error (MSE) is used

$$f_{\text{MSE}} = E\left[\left(f_d - \hat{f}_d\right)^2\right], \tag{7.21}$$

which is computed by averaging 3000 Monte Carlo iterations for each value of C/N_0.

Figure 7.7 shows the MSE of the LS estimator, MLS estimator and CRB for a $f_s = 50$ MHz. In this case, we use $K = 3$ for the MLS estimator. The rationale for that will be explained later on. The result shows that the MLS estimator is the best estimator because it provides an improvement over the LS estimator in terms of accuracy in Doppler frequency estimation. The MLS estimator allows us to recover a part of the energy lost in the CAF by the unknown random difference between the time-delay of the received signal and the local replica. Therefore, the usage of several peaks from the CAF leads to a frequency estimation more accurate than only using the main peak from the CAF. However, the MLS estimator is not able to reach the CRB value.

In order to find the optimum number of chosen high peaks of the CAF in time domain K, we carry out an extensive number of simulations with different values of K. Figure

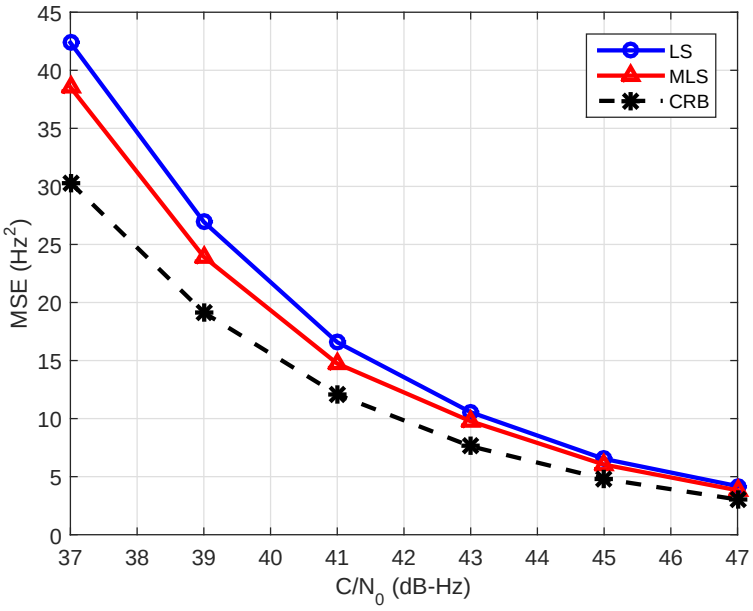

Figure 7.7: MSE of the MLS and LS estimators using a $f_s = 50$ MHz.

7.8 shows the division between the MSE using the MLS estimator with $K = 3$, $K = 5$, and $K = 10$ and the MSE of the LS estimator. The result shows that it makes little difference when the value of K is changed for values such as 3 or 5. Nevertheless, the MLS estimator always provides the best performance for $K = 3$ using a $f_s = 50$ MHz. The larger the number of K, the more degradation the MLS suffers. Moreover, although we do not use the optimal value of K, the MLS estimator might provide an improvement over the LS estimator.

Figure 7.9 shows the comparison among the LS estimator, the MLS estimator and the CRB for different values of f_s. In this simulation, we analyze the effect of the sampling frequency used in the receiver, which affects to the separation among the samples of the CAF in the acquisition stage. This fact causes that the precision in the Doppler frequency estimation must be different since this estimation depends on the magnitudes of the chosen samples from the CAF. The larger the magnitudes of the chosen samples, the more accurate the estimation tends to be since less degradation we have at post-correlation level in terms of C/N_0.

We choose several values of f_s, such as 40 MHz, 62 MHz and 100 MHz, to perform the simulation. In this case, the results show that the most accurate estimation of the Doppler frequency is provided using 100 MHz. Intuitively, one can think the larger the

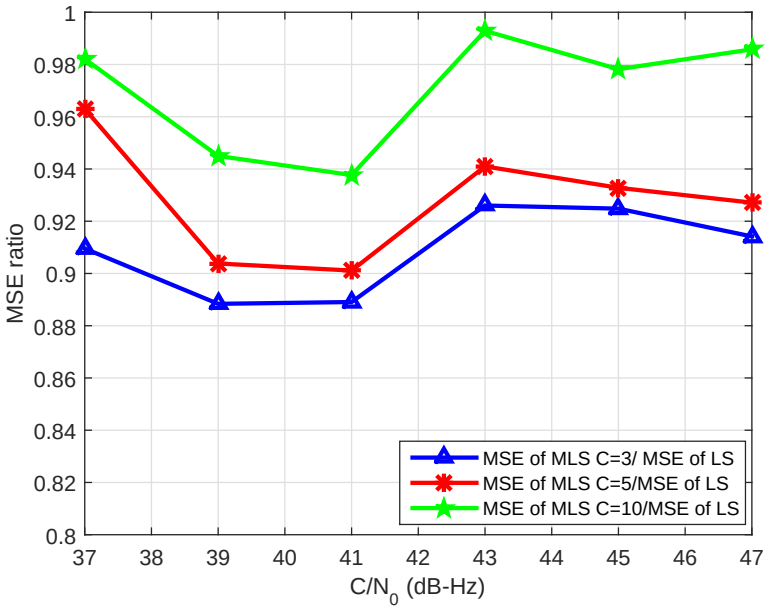

Figure 7.8: The division between the MSE applying the MLS estimator with $K = 3$, $K = 5$, and $K = 10$ and the MSE of the LS estimator using a $f_s = 50$ MHz.

f_s, the more accurate the estimation of the Doppler frequency is because the separation among the samples in the CAF is smaller, which usually allows the receiver to select samples with a large magnitude. Nevertheless, this is not always true, as it can be seen for the case of $f_s = 40$ MHz and $f_s = 62$ MHz. This happens because the separation among the samples of the received signal using a $f_s = 62$ MHz is really similar to the distance between the peaks in the CAF of the $\text{BOC}_{\cos}(15,2.5)$ signal. More precisely, the distance between the peaks of a BOC correlation is given by $1/(2f_{sub})$, where f_{sub} is sub-carrier frequency. In particular, the f_{sub} of a $\text{BOC}_{\cos}(15,2.5)$ signal is $15 \cdot 1.023$ MHz. In this situation, using a $f_s = 62$ MHz, we have approximately two samples equidistant for each peak of the correlation. The CAF of the $\text{BOC}_{\cos}(15,2.5)$ signal is sampled in all the different peaks of the correlation function of the same way, but any secondary peak cannot outperform the magnitude of the main peak (without presence of noise). However, using the $f_s = 40$ MHz, this effect does not happen because the separation among the samples of the received signal is not equidistant compare to the distance between the peaks of the $\text{BOC}_{\cos}(15,2.5)$ correlation and, in this case, the magnitude of a secondary peak can outperform the value of the main peak.

This fact causes that the value of $f_s = 40$ MHz usually provides larger magnitudes in the CAF than using the $f_s = 62$ MHz. For this reason, the estimation of the Doppler

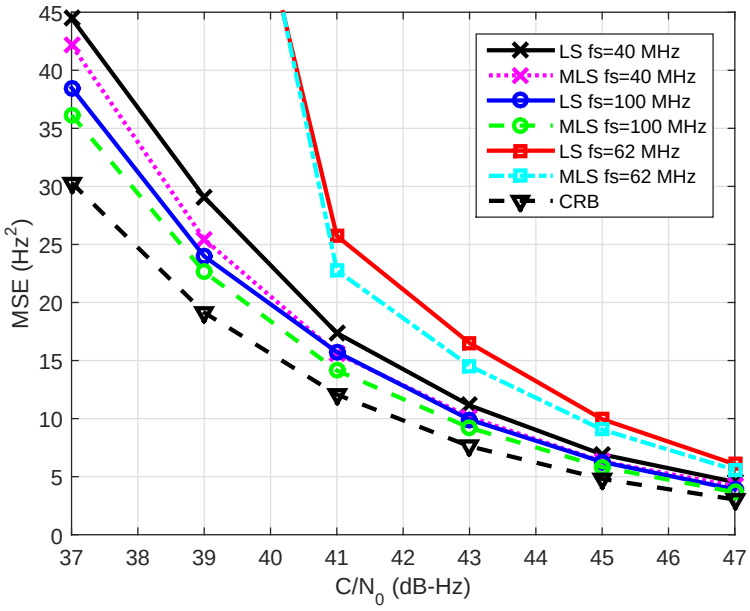

Figure 7.9: Comparison between the MLS and LS estimators using f_s = 40, 62 and 100 MHz.

frequency can be more accurate using f_s = 40 MHz than using f_s = 62 MHz. Moreover, this also causes that the MSE of the estimators using f_s = 62 MHz needs a larger C/N_0 value to provide accurate estimations of the Doppler frequency since using this sampling frequency, the receiver is more prone to suffer wrong detections. In addition to this, the proposed MLS estimator improves the performance of the LS estimator for the different values of sampling frequency.

7.2.6 Conclusions

A new technique has been proposed, which is so-called multilag least squares estimator, to refine the Doppler frequency estimation obtained in the acquisition stage. This technique exploits the secondary peaks provided by the CAF of a high-order BOC signal to get an accurate estimation of the Doppler frequency. The MLS estimator outperforms the LS estimator proposed in the literature. The optimum number of chosen high peaks of the CAF is 3 to obtain the most accurate estimation of Doppler frequency using a sampling frequency of 50 MHz. Moreover, the advantage of the MLS estimator is that it can be applied in any receiver since it only uses the CAF generated in the acquisition stage. In addition, we have analyzed the dependence between the sampling frequency used to

acquire the signal and the accuracy to estimate the Doppler frequency. The values of f_s that offer the most accurate estimations of the Doppler frequency are the ones that provide a separation among the samples of the received signal which is not equidistant with the distance between the peaks of the $\mathrm{BOC}_{\cos}(15,2.5)$ correlation.

Chapter 8

Conclusions and future work

This thesis has tackled several problems of processing weak GNSS signals, such as the detection at the acquisition stage, the determination of their signal quality and the mitigation of potential false lock. The main problem of this thesis has dealt with the detection of weak signals, which arrive at the receiver highly attenuated owing to the presence of obstacles in the path between the satellite and the receiver. The acquisition of these signals becomes a challenge since they are usually below the noise level. The receiver must counteract the effect of the noise by accumulating the received signal for a long period of time in order to detect it. However, the optimal detector depends on the impairments that limit the duration of the accumulation of the received signal such as data bits, frequency offset and phase noise. We have found the most promising techniques including all and several of the impairments. Moreover, this thesis has addressed the problem of estimating the C/N_0 from a weak GNSS signal. The C/N_0 estimates are very important in many applications of HS-GNSS receivers such as the determination of a detection threshold or the mitigation of near-far problems. Finally, this thesis has proposed accurate estimators of the Doppler frequency and time-delay for high-order BOC signals. The conclusions of the thesis are drawn in this section, alongside the open issues pending for future work.

8.1 Conclusions

In Chapter 2, the main features of the GNSSs and the fundamentals of the signal detection theory have been described. More precisely, the architecture and the signals implemented in the GPS and Galileo system have been explained to show the difference between the

two systems and the advantages and drawbacks of using BOC signals. In addition to this, we have described the main stages of GNSS receivers: acquisition, tracking and PVT, and we have introduced more details in the acquisition stage, which is the stage where the main issues of this thesis have been addressed. Finally, the detection tools required to find optimal detectors to improve the acquisition of HS-GNSS receivers have been provided.

In Chapter 3, in order to understand the evolution of GNSS signal acquisition, the state of the art of PDI techniques for GNSS has been provided. This survey has shown that the NPDI is the most widely implemented technique in practice, since it allows the receiver to detect weak signals and there are known expressions for its detection and false alarm probabilities. Moreover, we have seen other alternatives such as the DPDI and GPDIT techniques, which offer better detection probability than the NPDI technique in an AWGN channel. The most relevant techniques of this chapter have been benchmarked for low C/N_0 levels in presence of phase noise introduced by a TCXO and OCXO receiver clocks and frequency offset. We have concluded that the most promising technique in presence of frequency offset is the GPDIT and the technique most robust against the presence of phase noise is the NPDI. Moreover, the TCXO limits the coherent correlation interval to about 100 ms, whereas the receiver can implement coherent integration times as long as 1 second when use an OCXO.

In Chapter 4, we have addressed the problem of finding the optimal detector to acquire weak GNSS signals. We have considered a scenario with a received signal which includes the presence of data bits and a time-varying phase. Based on the GLRT and the Bayesian approach, we have obtained two different PDI techniques, which offer very similar performance. Given that the PDI technique obtained from the GLRT is less complex than the one obtained from the Bayesian approach, we have concluded that the result from the GLRT is a better option. However, the resulting PDI techniques from the Bayesian approach and the GLRT have the drawback of requiring the SNR of the received signal. In order to circumvent this problem, we have proposed approximations of these techniques that do not depend on the SNR value leading to the NPDI and NQ-NPDI techniques. Contrary to the traditional belief that the NPDI technique is the best option to acquire weak GNSS signals, which include the presence of data bits and a time-varying phase, in this chapter it has been shown that the NQ-NPDI is the most promising technique. Finally, we have proposed closed-form expressions for the detection and false alarm probabilities of the NQ-NPDI technique and the optimal detector obtained from the Bayesian approach. We have drawn the conclusion that the use of the Edegworth series provides a very accurate approximation of the probabilities of these techniques.

In Chapter 5, we have tackled the problem of reacquiring weak GNSS signals. The Bayesian approach and the GLRT have been applied to find the optimal detector for weak GNSS signals. We have proposed five new techniques the BAPDI and MBAPDI obtained from the Bayesian approach and three other obtained from the GLRT. All of these techniques outperform the conventional PDI techniques proposed in the literature. However, the former group provides practically the same performance. Due to this fact, the chapter has drawn conclusions on which is the best technique to reacquire weak GNSS signals in practice considering a trade-off between performance and complexity. The best technique for the reacquisition of GNSS signals is the one based on the approximation of the GLRT approach for high SNR regime.

In Chapter 6, we have proposed new C/N_0 estimators based only on the output of PDI techniques, which are especially designed for snapshot receivers. Four simple closed-form expressions have been derived to estimate the C/N_0. Each expression applies to one of the most relevant PDI techniques, namely NPDI, NQ-NPDI, DPDI or GPDIT. We have suggested using the output of the PDI technique not only to acquire the satellites, but also to estimate the C/N_0. The C/N_0 estimators proposed herein have shown to be very accurate and easy to implement in a HS-GNSS receiver. Moreover, these estimators exhibit much more accurate C/N_0 estimates than the benchmarks, particularly if there is the presence of phase noise.

In Chapter 7, we have focused on two problems of high-order BOC signals. On the one hand, we have mitigated the problem of false locks at the acquisition stage for weak high-order BOC signals. We have suggested using the ML and LS estimators, which outperform the conventional approach used in literature to estimate the time-delay of the received signal. The proposed estimators have shown to be able to provide a small value of probability of false lock, though the received signal arrives with a low C/N_0 value. On the other hand, we have tackled the problem of refining the Doppler frequency estimation provided in the acquisition stage for high-order BOC signals. We have proposed a new estimator that exploits the energy of the secondary peaks of the autocorrelation of high-order BOC signals to obtain an accurate estimation of the Doppler frequency. This estimator improves the performance of the conventional estimator proposed in the literature.

8.2 Future work

The open issues addressed for future work are described in this section.

- Considering the GNSS detection problem including multipath effects in the received signal. The introduction of this effect in the model could provide a new class of PDI techniques.
- Performing a statistical characterization of the PDI techniques derived in Chapter 5, which allow us to obtain closed-form expressions of their false alarm and detection probabilities.
- Obtaining closed-form expressions for the C/N_0 estimate of the techniques proposed in Chapter 5.
- Finding algorithms to mitigate the false lock probability of high-order BOC signals without having to use a one-dimensional search method.
- Applying the detection tools to the problem of GNSS spoofing. Thereby, we could find optimal techniques to detect spoofing attacks.

Bibliography

[AR08] J. A. Avila-Rodriguez, G. W. Hein, S. Wallner, J. Issler, L. Ries, L. Lestarquit, A. Latour, J. Godet, F. Bastide, T. Pratt, *et al.*, "The MBOC modulation: the final touch to the Galileo frequency and signal plan", *Navigation*, Vol. 55, nº 1, pags. 15–28, 2008.

[Ban85] S. Bancroft, "An algebraic solution of the GPS equations", *IEEE Transactions on Aerospace and Electronic Systems*, Vol. AES-21, nº 1, pags. 56–59, Jan 1985.

[Bei12] ICD BeiDou, "Beidou navigation satellite system signal in space interface control document open service signal B1I", 2012.

[Bet15] J. W. Betz, *Engineering Satellite-Based Navigation and Timing: Global Navigation Satellite Systems, Signals, and Receivers*, John Wiley & Sons, 2015.

[Bhu14] M. Z. H. Bhuiyan, S. Söderholm, S. Thombre, L. Ruotsalainen, M. Kirkko-Jaakkola, H. Kuusniemi, "Performance evaluation of carrier-to-noise density ratio estimation techniques for beidou B1 signal", *2014 Ubiquitous Positioning Indoor Navigation and Location Based Service (UPINLBS)*, pags. 19–25, Nov 2014.

[Blu07a] P. Blunt, *Advanced global navigation satellite system receiver design*, PhD Thesis, University of Surrey (United Kingdom), 2007.

[Blu07b] P. Blunt, R. Weiler, S. Hodgart, M. Unwin, "Demonstration of BOC (15, 2.5) acquisition and tracking with a prototype hardware receiver", *ENC GNSS, May*, 2007.

[Bor07] Dennis M. Borre, K., N. Bertelsen, P. Rinder, S. Jensen, *A software-defined GPS and Galileo receiver: a single-frequency approach*, Springer Science & Business Media, 2007.

[Bor08] D. Borio, L. L. Presti, "Data and pilot combining for composite GNSS signal acquisition", *International Journal of Navigation and Observation*, Vol. 2008, 2008.

[Bor09a] D. Borio, D. Akos, "Noncoherent Integrations for GNSS Detection: Analysis and Comparisons", *IEEE Transactions on Aerospace and Electronic Systems*, Vol. 45, nº 1, pags. 360–375, Jan 2009.

[Bor09b] D. Borio, G. Lachapelle, "A non-coherent architecture for GNSS digital tracking loops", *Annals of telecommunications-annales des télécommunications*, Vol. 64, nº 9-10, pags. 601–614, 2009.

[Bor14a] D. Borio, "Double phase estimator: new unambiguous binary offset carrier tracking algorithm", *IET Radar, Sonar Navigation*, Vol. 8, nº 7, pags. 729–741, Aug 2014.

[Bor14b] D. Borio, "Non-coherent squaring detector and its application to bi-phased signals", *IET Radar, Sonar Navigation*, Vol. 8, nº 4, pags. 327–335, April 2014.

[Bru06] T. S. Bruggemann, D. G. Greer, R. A. Walker, "Chip Scale Atomic Clocks: Benefits to Airborne GNSS Navigation Performance", *International Global Navigation Satellite Systems Society Symposium*, 2006.

[Bur06] A. Burian, E. S. Lohan, M. Renfors, "BPSK-like methods for hybrid-search acquisition of galileo signals", *2006 IEEE International Conference on Communications*, Vol. 11, pags. 5211–5216, June 2006.

[Cha11] J. Chandrasekhar, C. R. Murthy, "Robust GNSS signal detection in the presence of navigation data bits", *2011 IEEE International Conference on Acoustics, Speech and Signal Processing (ICASSP)*, pags. 4344–4347, May 2011.

[Com11] European Commission, "European GNSS (Galileo) Open Service. Signal in Space Interface Control Document", 2011.

[Cor03] G.E. Corazza, R. Pedone, "Maximum likelihood post detection integration methods for spread spectrum systems", *Wireless Communications and Networking (WCNC)*, Vol. 1, pags. 227–232, March 2003.

[Cor07] G.E. Corazza, R. Pedone, "Generalized and average likelihood ratio testing for post detection integration", *IEEE Transactions on Communications*, Vol. 55, nº 11, pags. 2159–2171, Nov 2007.

[Cra46] H. Cramér, *et al.*, *Mathematical methods of statistics.*, Princeton university press, 1946.

[Cur12] J.T. Curran, G. Lachapelle, C.C. Murphy, "Digital GNSS PLL Design Conditioned on Thermal and Oscillator Phase Noise", *IEEE Transactions on Aerospace and Electronic Systems*, Vol. 48, nº 1, pags. 180–196, Jan 2012.

[Dan54] H. E. Daniels, "Saddlepoint approximations in statistics", *The Annals of Mathematical Statistics*, pags. 631–650, 1954.

[EB04] H. Elders-Boll, U. Dettmar, "Efficient differentially coherent code/Doppler acquisition of weak GPS signals", *IEEE Eighth International Symposium on Spread Spectrum Techniques and Applications*, pags. 731–735, Aug 2004.

[ER15] D. Egea-Roca, G. Seco-Granados, J. A. López-Salcedo, C. Moriana, M. J. Pasnikowski, E. Domínguez, E. Aguado, D. Lowe, D. Naberzhnykh, F. Dovis, *et al.*, "Signal-level integrity and metrics based on the application of quickest detection theory to multipath detection", *ION GNSS+*, 2015.

[ER17] D. Egea-Roca, G. Seco-Granados, J. A. López-Salcedo, "Comprehensive overview of quickest detection theory and its application to GNSS threat detection", *Gyroscopy and Navigation*, Vol. 8, nº 1, pags. 1–14, 2017.

[Fal11] E. Falletti, M. Pini, L. L. Presti, "Low complexity carrier-to-noise ratio estimators for GNSS digital receivers", *IEEE Transactions on Aerospace and Electronic Systems*, Vol. 47, nº 1, pags. 420–437, January 2011.

[Fin99] P. Fine, W. Wilson, "Tracking algorithm for GPS offset carrier signals", *Institute of Navigation, National Technical Meeting'Vision 2010: Present and Future', San Diego, CA*, pags. 671–676, 1999.

[GC16] D. Gómez-Casco, J. A. López-Salcedo, G. Seco-Granados, "Generalized integration techniques for high-sensitivity GNSS receivers affected by oscillator phase noise", *IEEE Statistical Signal Processing Workshop (SSP)*, 2016.

[GC17] D. Gómez-Casco, J. A. López-Salcedo, G. Seco-Granados, "Optimal fractional non-coherent detector for high-sensitivity GNSS receivers robust against residual frequency offset and unknown bits", *2017 14th Workshop on Positioning, Navigation and Communications (WPNC)*, pags. 1–5, Oct 2017.

[GM14] J. A. Garcia-Molina, M. Navarro-Gallardo, G. Lopez-Risueño, M. Crisci, "Unambiguous tracking of high-order BOC signals in urban environments: Channel considerations", *IEEE 7th ESA Workshop on Satellite Navigation Technologies and European Workshop on GNSS Signals and Signal Processing (NAVITEC)*, pags. 1–6, 2014.

[GM16] J. A. Garcia-Molina, M. Navarro-Gallardo, G. Lopez-Risueño, M. Crisci, "Robust unambiguous estimation of high-order BOC signals: The dome approach", *Navigation*, Vol. 63, nº 4, pags. 511–520, 2016.

[Gro05] P. D. Groves, "GPS signal-to-noise measurement in weak signal and high-interference environments", *Navigation*, Vol. 52, nº 2, pags. 83–94, 2005.

[Gus16] A. Gusi, P. Closas, J. A. Garcia-Molina, "Sampling frequency impact on false lock of high order BOC signals in open-loop processing", *2016 8th ESA Workshop on Satellite Navigation Technologies and European Workshop on GNSS Signals and Signal Processing (NAVITEC)*, pags. 1–5, Dec 2016.

[Ham03] R. Hamila, E. S. Lohan, M. Renfors, "Subchip multipath delay estimation for downlink WCDMA system based on teager-kaiser operator", *IEEE Communications Letters*, Vol. 7, nº 1, pags. 1–3, Jan 2003.

[Har15] H. Harde, M. R. Shahade, D. Badnore, "Indian regional navigation satellite system", *International Journal of Research in Science & Engineering (IJRISE)*, 2015.

[Hei04] V. Heiries, D. Roviras, L. Ries, V. Calmettes, "Analysis of non ambiguous BOC signal acquisition performance acquisition", *ION GNSS*, 2004.

[HW12] B. Hofmann-Wellenhof, H. Lichtenegger, J. Collins, *Global positioning system: theory and practice*, Springer Science & Business Media, 2012.

[Hwa92] P. Y. C. Hwang, R. G. Brown, *Introduction to Random Signals and Applied Kalman Filtering*, Wiley, 1992.

[Jay13] C. Jayaram, C. R. Murthy, "Noncoherent integration for signal detection: Analysis under model uncertainties", *IEEE Transactions on Aerospace and Electronic Systems*, Vol. 49, nº 4, pags. 2413–2430, October 2013.

[JB06] D. Jiménez-Baños, N. Blanco-Delgado, G. López-Risueño, G. Seco-Granados, A. Garcia-Rodriguez, "Innovative techniques for GPS indoor positioning using a snapshot receiver", *ION GNSS*, 2006.

[Kap05] E. Kaplan, C. Hegarty, *Understanding GPS: principles and applications*, Artech house, 2005.

[Kay98] S. M. Kay, "Fundamentals of statistical signal processing: Detection theory, vol. 2", 1998.

[Ken68] G. Kendall, *et al.*, *The advanced theory of statistics*, Charles Griffin, 1968.

[Lan73] G. W. Lank, I. S. Reed, G. E. Pollon, "A Semicoherent Detection and Doppler Estimation Statistic", *IEEE Transactions on Aerospace and Electronic Systems*, Vol. AES-9, nº 2, pags. 151–165, March 1973.

[Lev08] B. C. Levy, *Principles of signal detection and parameter estimation*, Springer Science & Business Media, 2008.

[Loh08] E. S. Lohan, A. Burian, M. Renfors, "Low-complexity unambiguous acquisition methods for BOC-modulated CDMA signals", *International Journal of Satellite Communications and Networking*, Vol. 26, nº 6, pags. 503–522, 2008.

[Loh13] E. S. Lohan, J. Lopez-Salcedo Salcedo, G. Seco-Granados, "Analysis of advanced post-detection integration techniques for the acquisition with pilot signals in high sensitivity-galileo receivers", *4th International Colloquium Scientific and Fundamental Aspects of the Galileo Programme. ESA Proceedings WPP. European Space Agency*, Vol. 355, 2013.

[LR05] G. Lopez-Risueno, G. Seco-Granados, "CN0 estimation and near-far mitigation for GNSS indoor receivers", *2005 IEEE 61st Vehicular Technology Conference*, Vol. 4, pags. 2624–2628 Vol. 4, May 2005.

[LS16a] S. Locubiche-Serra, J. A. López-Salcedo, G. Seco-Granados, "Statistical near-far detection techniques for GNSS snapshot receivers", *2016 IEEE International Conference on Acoustics, Speech and Signal Processing (ICASSP)*, pags. 6570–6574, March 2016.

[LS16b] S. Locubiche-Serra, G. Seco-Granados, J. A. López-Salcedo, "Doubly-adaptive autoregressive Kalman filter for GNSS carrier tracking under scintillation conditions", *2016 International Conference on Localization and GNSS (ICL-GNSS)*, pags. 1–6, June 2016.

[LS16c] V. Lucas-Sabola, G. Seco-Granados, J. A. López-Salcedo, J García-Molina, M Crisci, "Demonstration of Cloud GNSS Signal Processing", *ION GNSS*, pags. 34–43, 2016.

[LS16d] V. Lucas-Sabola, G. Seco-Granados, J. A. López-Salcedo, J. A. García-Molina, M. Crisci, "Cloud GNSS receivers: New advanced applications made possible", *2016 International Conference on Localization and GNSS (ICL-GNSS)*, pags. 1–6, June 2016.

[Mar50] J. I. Marcum, "Table of Q functions", 1950.

[Mar60] J. Marcum, "A statistical theory of target detection by pulsed radar", *IRE Transactions on Information Theory*, Vol. 6, nº 2, pags. 59–267, April 1960.

[McD95] R. N. McDonough, A. D Whalen, *Detection of signals in noise*, Academic Press, 1995.

[Mis06] P. Misra, P. Enge, "Global Positioning System: signals, measurements and performance second edition", *Massachusetts: Ganga-Jamuna Press*, 2006.

[Mus14] L. Musumeci, F. Dovis, P. F. Silva, H. D. Lopes, J. S. Silva, "Design of a very high sensitivity acquisition system for a space GNSS receiver", *ION PLANS*, pags. 556–568, 2014.

[Nav14a] Navipedia, "Galileo Signal Plan — Navipedia,", 2014, [Online; accessed 9-November-2017].

[Nav14b] Navipedia, "GNSS signal — Navipedia,", 2014, [Online; accessed 7-November-2017].

[Nur16] J. Nurmi, E. Lohan, H. Wymeersch, G. Seco-Granados, O. Nykänen, *Multi-Technology Positioning*, Springer, 2016.

[O'D09] Cillian O'Driscoll, James T. Curran, "Codeless code tracking of the Galileo E1 PRS", *Inside GNSS*, Vol. 4, nº 5, pags. 30–39, 2009.

[Paj06] E. Pajala, E. S. Lohan, T. Huovinen, M. Renfors, "Enhanced differential correlation method for the acquisition of Galileo signals", *2006 10th IEEE Singapore International Conference on Communication Systems*, pags. 1–5, Oct 2006.

[Pap02] A. Papoulis, S. Unnikrishna, *Probability, random variables, and stochastic processes*, Tata McGraw-Hill Education, 2002.

[Poo13] H. V. Poor, *An introduction to signal detection and estimation*, Springer Science & Business Media, 2013.

[Pou15] A. Pousinho, M. Toledo, T. Ferreira, J. A. López-Salcedo, S. Locubiche-Serra, G. Seco-Granados, M. Ribot, A. Jovanovic, C. Botteron, A. Farine, *et al.*, "Adaptive Tracking Techniques in Non-Stationary Environments", *in 28th International Technical Meeting of The Satellite Division of the Institute of Navigation (ION GNSS+ 2015)*, nº EPFL-CONF-214301, 2015.

[Pre09] L. L. Presti, X. Zhu, M. Fantino, P. Mulassano, "GNSS signal acquisition in the presence of sign transition", *IEEE Journal of Selected Topics in Signal Processing*, Vol. 3, nº 4, pags. 557–570, Aug 2009.

[PS10] E. Perez Serna, S. Thombre, M. Valkama, S. Lohan, V. Syrjälä, M. Detratti, H. Hurskainen, J. Nurmi, "Local oscillator phase noise effects on GNSS code tracking", *Inside GNSS*, 2010.

[Res12] Ettus Reserch, "USRP N200/N210 NetwQrked Series", *Moun- tain Viewi CA: Ettus Research*, 2012.

[Rib98] J. Riba, J. Tome, M. Lagunas, "Instantaneous open-loop frequency estimation methods for navigation receivers", *Global navigation satellite systems. European symposium*, 1998.

[Ric05] M. A. Richards, *Fundamentals of radar signal processing*, Tata McGraw-Hill Education, 2005.

[Rif74] D. Rife, R. Boorstyn, "Single tone parameter estimation from discrete-time observations", *IEEE Transactions on Information Theory*, Vol. 20, nº 5, pags. 591–598, Sep 1974.

[Sat11] S. Satyanarayana, D. Borio, G. Lachapelle, "A non-coherent block processing architecture for standalone GNSS weak signal tracking", *ION/GNSS, Portland, OR*, pags. 1777–1785, 2011.

[Sch05a] A. Schmid, A. Neubauer, "Carrier to noise power estimation for enhanced sensitivity Galileo/GPS receivers", *2005 IEEE 61st Vehicular Technology Conference*, Vol. 4, pags. 2629–2633 Vol. 4, 2005.

[Sch05b] A. Schmid, A. Neubauer, "Differential correlation for Galileo/GPS receivers", *IEEE International Conference on Acoustics, Speech, and Signal Processing (ICASSP)*, Vol. 3, pags. iii/953–iii/956, March 2005.

[Sel65] I. Selin, "Detection of coherent radar returns of unknown Doppler shift", *IEEE Transactions on Information Theory*, Vol. 11, nº 3, pags. 396–400, July 1965.

[SG12] G. Seco-Granados, J. A. López-Salcedo, D. Jimenez-Banos, G. Lopez-Risueno, "Challenges in indoor global navigation satellite systems: Unveiling its core features in signal processing", *IEEE Signal Processing Magazine*, Vol. 29, nº 2, pags. 108–131, March 2012.

[Sim95] M. K. Simon, M. M. Shihabi, T. Moon, "Optimum detection of tones transmitted by a spacecraft", 1995.

[Sim07] M. K. Simon, *Probability distributions involving Gaussian random variables: A handbook for engineers and scientists*, Springer Science & Business Media, 2007.

[Str07] C. Strässle, D. Megnet, H. Mathis, C. Bürgi, "The squaring-loss paradox", *International Technical Meeting of the Satellite Division GNSS 20th*, 2007.

[Ta10] T. H. Ta, F. Dovis, D. Margaria, L. L. Presti, "Comparative study on joint data/pilot strategies for high sensitivity Galileo E1 open service signal acquisition", *IET Radar, Sonar Navigation*, Vol. 4, nº 6, pags. 764–779, December 2010.

[Tah12] M. Tahir, L. L. Presti, M. Fantino, "A novel quasi open loop frequency estimator for GNSS signal tracking", *IEEE/ION Position, Location and Navigation Symposium*, pags. 952–960, April 2012.

[Tan12] X. Tang, E. Falletti, L. L. Presti, "Fine Doppler frequency estimation in GNSS signal acquisition process", *6th ESA Workshop on Satellite Navigation Technologies and European Workshop on GNSS Signals and Signal Processing, (NAVITEC)*, pags. 1–6, Dec 2012.

[Tan13] X. Tang, E. Falletti, L. L. Presti, "Fast nearly ML estimation of Doppler frequency in GNSS signal acquisition process", *Sensors*, Vol. 13, nº 5, pags. 5649–5670, 2013.

[VD09] F. S. Tromp V. Diggelen, *A-GPS: Assisted GPS, GNSS, and SBAS*, Artech House, 2009.

[Vil07] M. Villanti, P. Salmi, G. E. Corazza, "Differential post detection integration techniques for robust code acquisition", *IEEE Transactions on Communications*, Vol. 55, nº 11, pags. 2172–2184, Nov 2007.

[VT04] H. L. Van Trees, *Detection, estimation, and modulation theory*, John Wiley & Sons, 2004.

[Wei06] L. Weill, "Theoretical and practical sensitivity limits for assisted GNSS receivers using legacy and future gnss signals", *ION GPS/GNSS*, 2006.

[Wu14] H. B. Wu, J. L. Liu, Y. Zhang, Y. H. Hu, "An improved acquisition method for high-order BOC-modulated signals based on fractal geometry", *Advanced Materials Research*, Vol. 846, pags. 1185–1188, Trans Tech Publ, 2014.

[Yan07] C. Yang, M. Miller, E. Blasch, T. Nguyen, "Comparative study of coherent, non-coherent, and semi-coherent integration schemes for GNSS receivers", *ION Annual meeting*, pags. 572–588, April 2007.